DOCUMENT CONTROL DATA - R & D

(Security classification of title, body of abstract and indexing annotation must be entered when the overall report is classified)

1. ORIGINATING ACTIVITY (Corporate author)	2a. REPORT SECURITY CLASSIFICATION
U.S. Naval Ordnance Laboratory, White Oak Silver Spring, Md. 20910	UNCLASSIFIED
	2b. GROUP None

3. REPORT TITLE

On The TiNi (Nitinol) Martensitic Transition; Part I

4. DESCRIPTIVE NOTES (Type of report and inclusive dates)

NOL Technical Report

5. AUTHOR(S) (First name, middle initial, last name)

Frederick E. Wang

6. REPORT DATE	7a. TOTAL NO. OF PAGES	7b. NO. OF REFS
January 1, 1972	100	76

8a. CONTRACT OR GRANT NO.	9a. ORIGINATOR'S REPORT NUMBER(S)
b. PROJECT NO. MAT-03L-000/2R00-001-010	NOLTR 72-4
c.	9b. OTHER REPORT NO(S) (Any other numbers that may be assigned this report)
d.	

10. DISTRIBUTION STATEMENT

Approved for public release; distribution unlimited.

11. SUPPLEMENTARY NOTES	12. SPONSORING MILITARY ACTIVITY
	Naval Material Command Washington, D.C.

13. ABSTRACT

The experimental evidence obtained and the theory proposed thus far on the TiNi martensitic transition are summarized and reviewed. Fundamental principles involved in the various modes of investigation are described and the uniqueness of the transition is detailed.

AD 742 767

14. KEY WORDS	LINK A		LINK B		LINK C	
	ROLE	WT	ROLE	WT	ROLE	WT
Martensitic Transition						
TiNi Intermetallic Compound						

ON THE TiNi (NITINOL) MARTENSITIC TRANSITION

PART-I

Prepared by:

Frederick E. Wang

ABSTRACT: The experimental evidence obtained and the
theory proposed thus far on the TiNi martensitic
transition are summarized and reviewed. Fundamental
principles involved in the various modes of investi-
gation are described and the uniqueness of the transi-
tion is detailed.

January 1, 1972

U.S. Naval Ordnance Laboratory
White Oak, Maryland

i

January 1, 1972

ON THE TiNi(NITINOL) MARTENSITIC TRANSITION;PART-I

Ever since the discovery of the unique physical property changes associated with the TiNi transition by Buehler et al. at the U.S. Naval Ordnance Laboratory in 1962, the nature of TiNi and its transition has been the subject of an intense investigation in many laboratories. The high degree of interest in the TiNi problem is reflected in an International Symposium on "TiNi and Its Related Compounds", held at NOL(Naval Ordnance Laboratory) in 1967 and a number of research thesis written for advanced degrees as well as a score of published papers on this subject in recent years.

Through these studies, many theories have been proposed and many explanations have been offered. But, like so many unique phenomena observed before it in the field of solid state, understanding of the TiNi transition is far from complete and the investigation continues as of this writing.

Part of the difficulties associated with the understanding of the TiNi transition was that not only were there differences among investigators with regard to the interpretation of the data, but in many instances, the data themselves differed from one another. In view of this fact, no attempt has been made(nor is it possible in this short monograph) either to review every article writt'n on TiNi or to treat every explanation offered. As an alternative, I have tried not only to review the selected key investigations reported thus far, but also to explain wherever possible, the underlying principles involved in the various modes of investigation. It is hoped that in this manner the readers will be better informed and thus can better judge the different interpretations offered, Simultaneously, it must be emphasized that for any model or theory offered to be aesthetically satisfying and physically significant, it must ultimately embrace within a single unified framework, a logical explanation of all the related physical phenomena observed and the differences that exist in the data collected.

The view on the TiNi transition as offered here in a large measure represents that of my own and should be regarded as such. Followingly, the primary intention of this writing is to challenge and to stimulate further research and eventually derive a true understanding of not only the TiNi transition but also the martensitic transition as a whole.

In this Part-I of the TiNi monograph, the presentation is limited to the electronic, thermodynamic and crystallographic aspect of the TiNi transition. In Part-II, attempts will be made to relate these

understandings to the metallurgical and mechanical engineering and
therefore the practical application of the TiNi alloy --"NITINOL"
technology.

Finally, I wish to acknowledge the many helpful discussions and
encouragements I have received from Mr. William J. Buehler of this
laboratory in the course of this investigation.

Dr. James R. Holden, Mr. Ernest Heintzleman and Mrs. Mary Jo Wang
have been instrumental in proof reading the original manuscript
which led to much improvement in the final manuscript.

U.S. Naval Ordnance Laboratory   Frederick E. Wang
White Oak, Maryland 20910

ROBERT WILLIAMSON II
Captain, USN
Commander

Wayne W. Scanlon

WAYNE W. SCANLON
By direction

CONTENT

I. HISTORICAL BACKGROUND

A. Phase Diagram

Historically, investigation of the Ti-Ni system was first undertaken by Wallbaum and his co-workers[1,2] in 1938 In these works, the general features of the Ti-Ni phase diagram in the titanium concentration ranged from 0 to 50 at.% was outlined.

1. A primary solid solution of titanium in nickel exists with the solubility falling with decreasing temperature.

2. The primary solid solution of titanium in nickel forms a eutectic with a congruent melting intermediate phase, $TiNi_3$.

3. A eutectic on the titanium-rich side of $TiNi_3$ is bounded by titanium and nickel with slightly variable composition.

In 1941, Wallbaum[3] extended his previous work into the titanium-rich end of the diagram and discovered Ti_2Ni which forms a eutectic with a solid solution of nickel in β-titanium. This partial phase diagram was supplemented by the work of Long and co-workers[4](1949) who confirmed the existence of Ti_2Ni as well as a eutectic and a eutectoid below 34 at.% nickel at the titanium-rich end of the diagram. However, the temperature of the eutectoid reported by these authors was lower than that reported by Wallbaum[3]. A more accurate determination of the solid solubility of nickel in titanium was later made by Taylor and Floyd[5](1951).

Craighead, Fawn and Eastwood[6](1949) carried out a limited study of the Ti-Ni phase diagram up to approximately 11.5 at.% nickel within a limited temperature range but did not define the eutectic or eutectoid temperatures.

These studies identified three intermediate phases in the Ti-Ni system corresponding to the compositions, Ti_2Ni, $TiNi$ and $TiNi_3$. In the course of a structural investigation of these intermediate phases, Duwez and Taylor[7](1950) claimed evidence for TiNi decomposition into Ti_2Ni and $TiNi_3$. In the mean time, Margolin, Ence and Nielsen[8](1953) attributed the lower eutectic temperature obtained by Long et al[4] to oxygen and/or nitrogen contamination, and resumed investigation of the system. Using relatively high-purity sponge(99.7 wt.% Ti) and iodide(99.9 wt.% Ti) titanium, the authors determined the Ti-Ni phase diagram in the 0 to 65 at.% Ni range, above 500°C. This work confirmed the previous reports that Ti_2Ni is a peritectic compound melting at about 1230°C as shown in Fig. 1. However, this work did not confirm the earlier claim made by Duwez and Taylor[7] that TiNi decomposes into Ti_2Ni and $TiNi_3$.

Pool and Hume-Rothery[9](1954) first investigated the entire phase diagram above 850°C by means of thermal, metallurgical and X-ray methods.
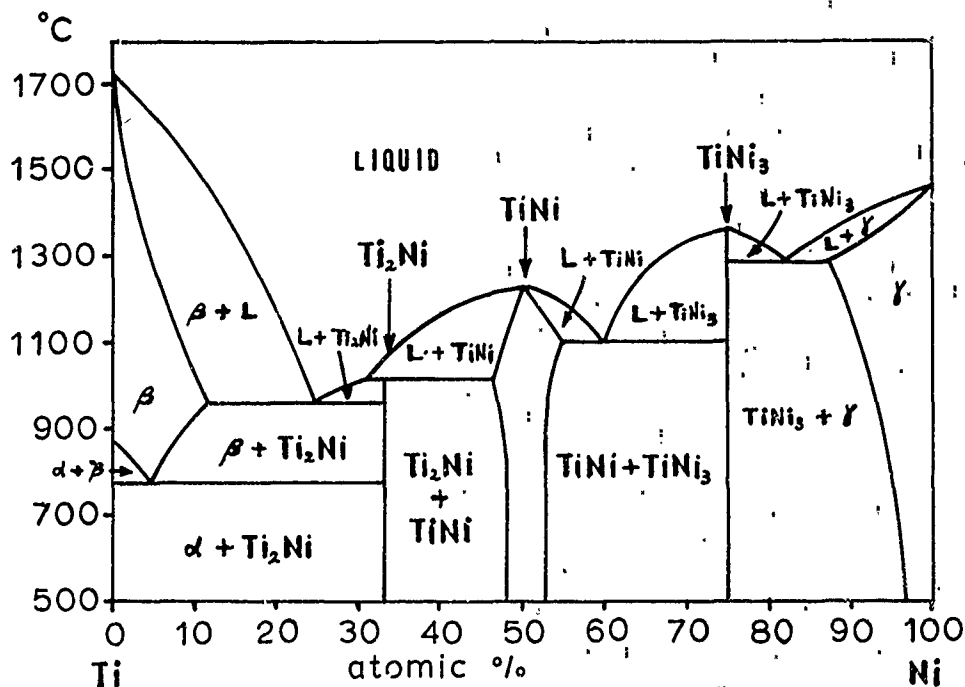
(after Margolin, Ence & Nielsen; ref. 8)

Fig. 1; The Ti-Ni phase diagram.
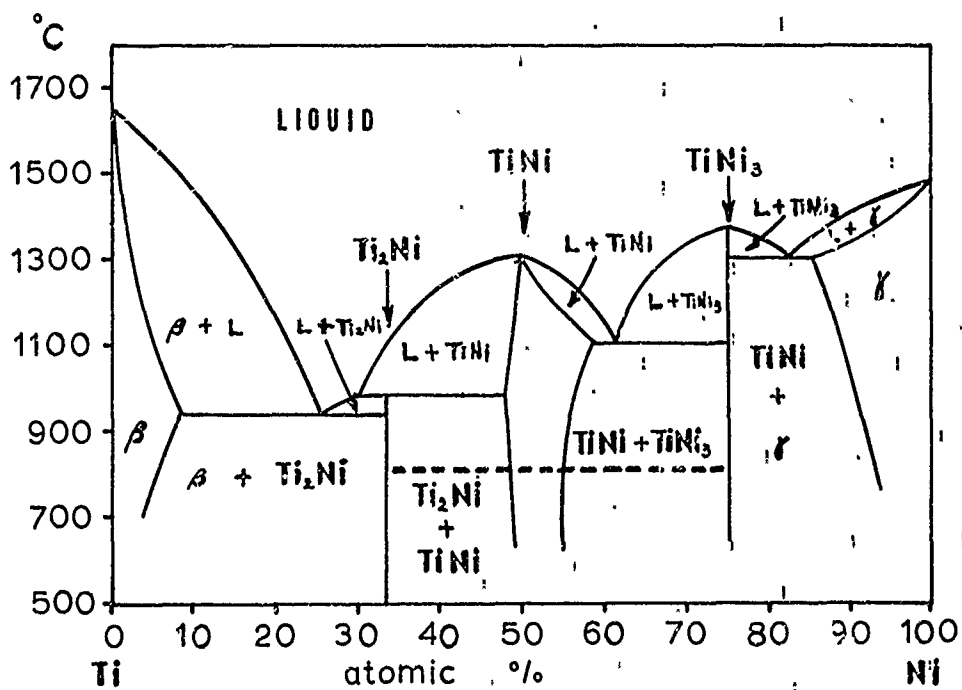
(after Pool & Hume-Rothery; ref. 9)

Fig. 2; The Ti-Ni phase diagram.

They confirmed the general features of the phase diagram reported in the previous studies but found somewhat different temperatures (Fig. 2). In their X-ray study, they found some evidence to support the possible decomposition of TiNi into Ti_2Ni and $TiNi_3$ claimed by Duwez and Taylor[7]. The characteristic temperatures determined in this work are as follows:

a. The eutectic between $TiNi_3$ and the primary solid solution of titanium in nickel exists at 1304°C.

b. The eutectic between $TiNi_3$ and TiNi exists at 1118°C.

c. Ti_2Ni is formed by a peritectic reaction at 984°C.

d. Another eutectic exists between Ti_2Ni and β-titanium at 942°C.

e. Melting points of the two congruently melting compounds, $TiNi_3$ and TiNi, are 1380°C and 1310°C respectively.

The phase diagram, according to the authors, shows that TiNi has a narrow solid solubility range on the titanium-rich side and approximately 5 at.% maximum solid solubility on the nickel-rich side at 1120°C. Further investigation of the titanium-rich end of the phase diagram was undertaken by Polonis and Parr[10] (1956). This work defined the eutectoid reaction, β = α + Ti_2Ni at 770°C and the eutectic reaction, liquid = β + Ti_2Ni at 955°C.

Because of the differences reported for the solid solubility range of TiNi and the controversy over the existence of the decomposition of TiNi into Ti_2Ni and $TiNi_3$, Purdy and Parr[11] (1961) eventually undertook yet another investigation of the Ti-Ni system. This investigation covered the composition range, 34 - 58 at.% Ni, and the temperature range, 0° - 1400°C. The results, summarized in Fig. 3, show the TiNi solid solubility range to be much narrower than that reported by other authors[8,9]. Further, no evidence was found to support the decomposition of TiNi into Ti_2Ni and $TiNi_3$. Instead, these authors found a reversible diffusionless transformation at 36°C for TiNi compositions in the range, 34.8 - 47.5 at.% Ni.

In summary, the general features of the Ti-Ni phase diagram and the existence of the three intermediate phases, Ti_2Ni, TiNi and $TiNi_3$, as confirmed by all investigators are shown in Fig. 4-a. However, the decomposition of TiNi into Ti_2Ni and $TiNi_3$ remained in dispute in spite of their efforts.

A comparison of the features of the Ti-Ni, Ti-Co and Ti-Fe phase equilibrium diagrams reported to date is given in Fig. 4. Out of a general similarity, a number of differences exists among the three systems.

B. Crystal Structures

Based on powder patterns, Laves and Wallbaum[12,13] first invest gated
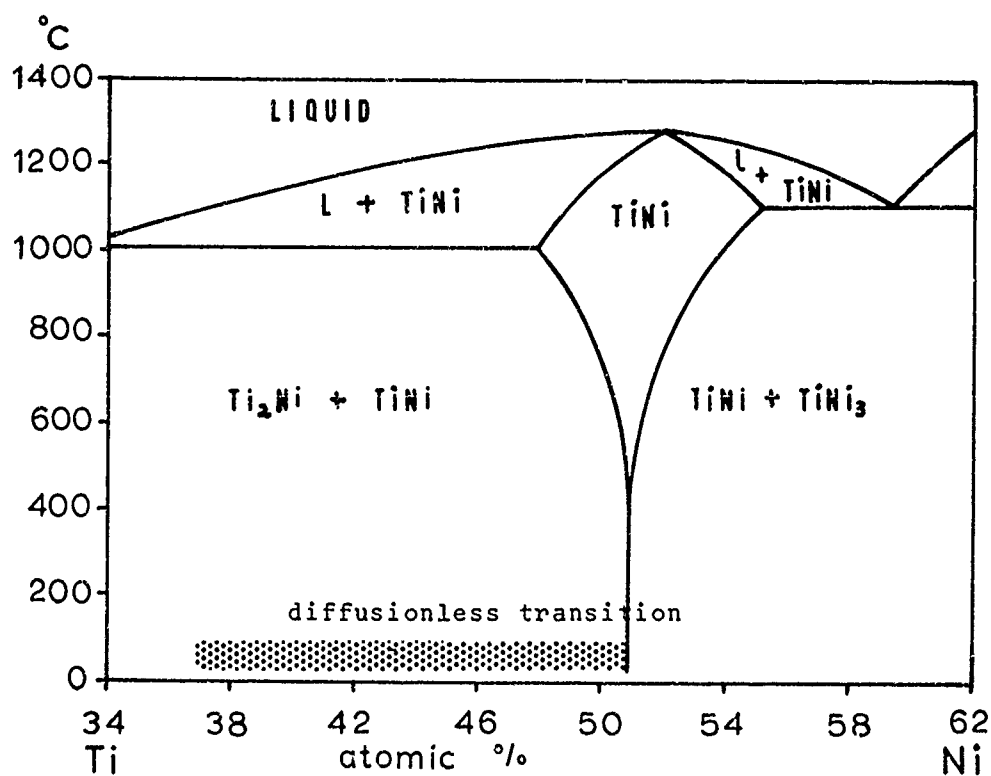
(after Purdy & Parr; ref. 11)

Fig. 3; Partial Ti-Ni phase diagram.
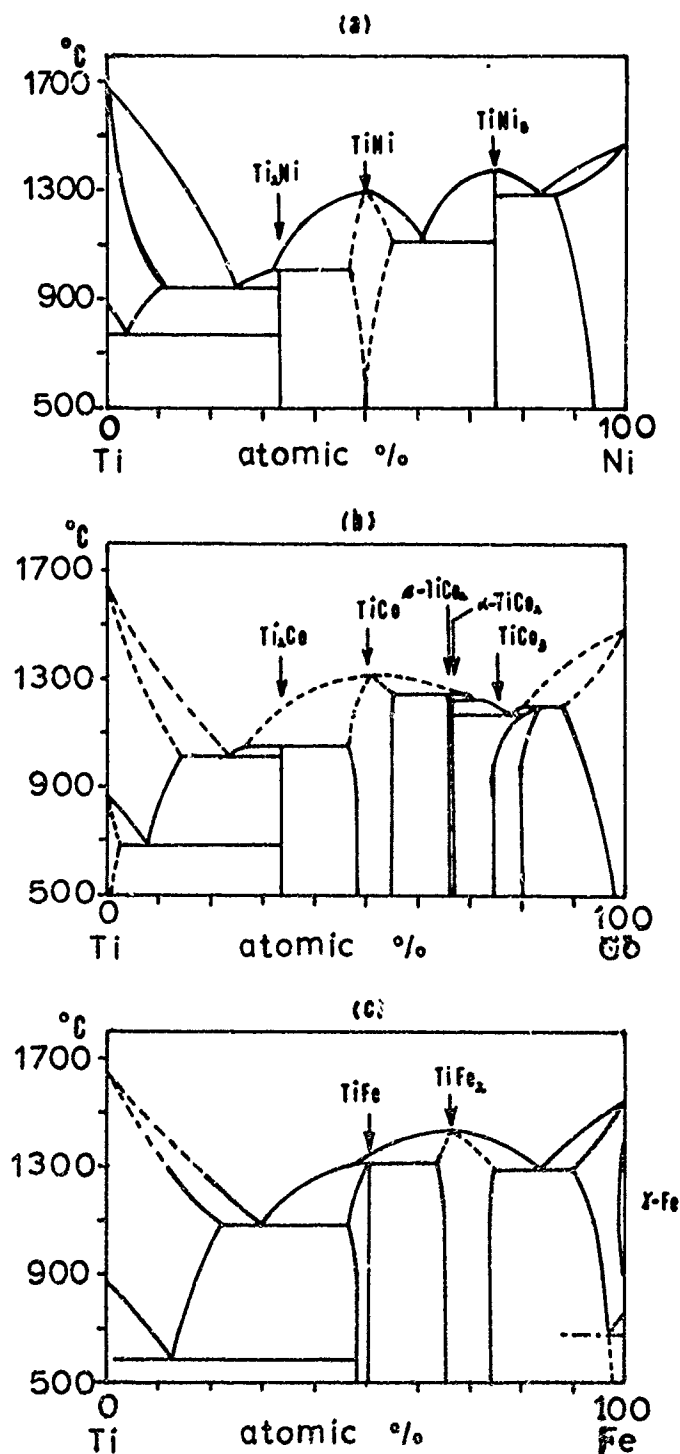
Fig. 4

Fig. 4; Comparison of the TiNi, TiCo and TiFe
phase diagrams.

5

the crystal structures of the intermediate phases, Ti_2Ni, $TiNi$ and $TiNi_3$ around 1939. These authors identified Ti_2Ni as fcc with 96 atoms per unit cell and $TiNi$ as bcc(disordered CsCl-type) with two atoms per unit cell. $TiNi_3$ was reported to be hexagonal(DO_{24}-type) with lattice constants, $a = b = 5.096$, $c = 8.304$ kX (1 kX = 1.00202 Å) and containing 16 atoms per unit cell.

The lattice parameters for Ti_2Ni and $TiNi$ as well as the refined parameters for $TiNi_3$ were later given by Duwez and Taylor[7](1950) as:

Ti_2Ni(fcc) --------- $a = 11.310$ kX

$TiNi$(bcc) -------- $a = 2.980$ kX

$TiNi_3$(hex.) ------- $a = b = 5.093$ kX
$c = 8.276$ kX

As mentioned earlier, these authors were the first ones to claim the decomposition of $TiNi$ into Ti_2Ni and $TiNi_3$. At about the same time, Taylor and Floyd[14](1950) gave more accurate parameters, $a = b = 5.1010$, $c = 8.3067$ Å for $TiNi_3$. The following year, Rostoker[15](1951) obtained a lattice parameter, $a = 11.29$ kX, for Ti_2Ni and described the structure as being of the Fe_3W_3C type, both in the pure state and in the presence of oxygen. Two years later, Margolin, Ence and Nielsen[8](1953) reported the absence of any evidence to support the decomposition of $TiNi$ into Ti_2Ni and $TiNi_3$ either in the microstructures or the X-ray powder patterns of alloys near the stoichiometric composition quenched from above and below 800°C. Following this report, Poole and Hume-Rothery[9](1954) reported the following lattice constants:

Ti_2Ni(fcc) ------- $a = 11.297(\pm 0.002)$ kX at 21°C

$TiNi$(bcc) ---------$a = 3.007(\pm 0.0005)$ kX at 22°C

$TiNi_3$(hex.) ------ $a = b = 5.09855(\pm 0.00005)$ kX
$c = 8.30197(\pm 0.00008)$ kX at 25°C.

These authors admitted implicitly for the first time that the $TiNi$ equiatomic alloy was not brittle and in fact was so ductile that filing was the only manner in which a specimen for X-ray work could be obtained. According to these authors, the alloy quenched in silicone oil from 1000°C showed 17 slightly diffuse diffraction lines of which only eight were identifiable as belonging to the CsCl type structure. Filings annealed in the same manner but rapidly cooled by withdrawing the specimen from the furnace gave a diffuse X-ray pattern with many lines not attributable to the CsCl-type structure. Further, filings annealed for two weeks at 600°C showed a considerable diffused CsCl-type pattern together with four extra lines which could be attributed to Ti_2Ni and five extremely faint lines identifiable with those of $TiNi$. Based on these observations, the authors concluded that the earlier report of Duwez and Taylor[7] on the decomposition of $TiNi$ into Ti_2Ni and $TiNi_3$ was correct.

In determining the relationship between the bonding characteristics

6

and the lattice constants in TiFe, TiCo and TiNi, Phillip and Beck[16] (1957) gave a = 3.015 Å as the lattice constant of TiNi. Stuwe and Shimomura[17](1961) while investigating the relationship between lattice parameter and composition of TiFe, TiCo and TiNi alloys found the titanium-rich side of TiNi alloy to have a lattice constant, a = 3.011 Å., but widely scattered values for alloys containing 51 to 56 at.% Ni. During an investigation of the Ti-Ni phase diagram between Ti_2Ni and TiNi, Purdy and Parr[11](1961)discovered a diffusionless transformation and identified the transformation product "π " phase as hexagonal with a = b = 4.572 and c = 4.660 Å based on the powder pattern given in Table 1. The transformation temperature for 34.8 through 47.5 at.% Ni alloys is 36°C as shown in Fig. 3. Nevertheless, these authors did not find any evidence to support the decomposition of TiNi into Ti_2Ni and $TiNi_3$ as claimed by Duwez and Taylor[7](1950). Notwithstanding these conflicting reports, Pietrokowsky and Youngkin[18] (1960) undertook an investigation of order-disorder in the TiNi CsCl-type structure. Based on the existence of one super-reflection, 100, the authors claimed TiNi to have an ordered CsCl-type structure.

Meanwhile, in the process of looking for a new structural material, Buehler and Wiley[19](1962) discovered in TiNi a highly interesting and unique physical property. This property is a drastic change in hardness and acoustic damping capacity with temperature. Below about 65°C, the alloy yields with ease to plastic deformation, and has high acoustic damping capacity; above 65°C, the alloy has a high resistance to plastic deformation and a low acoustic damping capacity. Further, this transition is associated with a perfect "memory" effect; that is if a wire or sheet of this alloy is deformed below 65°C, it will regain its original shape when heated above 65°C. These authors also openly admitted for the first time that TiNi is a ductile intermetallic compound. Following these reports of the physical changes in TiNi, Gilfrich[20](1962), through use of an X-ray powder diffractometer(with temperature control) , associated the changes in the diffraction pattern occuring at around 65°C with the decomposition of TiNi into Ti_2Ni and $TiNi_3$. These diffractometric observations were then combined with dilatometric studies of TiNi by Buehler, Gilfrich and Wiley[21](1963) who concluded that TiNi decomposes into Ti_2Ni and $TiNi_3$ in a reversible manner near room temperature. Although not fully understanding the transformation mechanism, the authors pointed out the fact that the transformation temperature is highly sensitive to factors such as composition and mode of plastic deformation.

Single crystals of TiNi in wire form were first obtained by Wang et al. [22](1965) through use of a modified "strain-anneal" method in which poly-crystalline TiNi wire was subjected to repeated fast thermal cyclings. By X-ray diffraction studies of these single crystals, Wang, Buehler and Pickart[23](1965) confirmed the existence of a diffusionless transformation near 166°C for stoichiometric TiNi. The transformation temperature dropped sharply with composition on either side of the stoichiometric composition as shown in Fig. 5. Based on the two transitions observed, one at 600°- 700°C(with diffusion) and the other at 166°C(diffusionless), these authors designated TiNi-I, TiNi-II and TiNi-III as the phases existing above 700°C, between 166 and 600°C and below 166°C respectively. These authors

POWDER PATTERN OF THE "π" PHASE

Observed Sin²θ Cu Kα	Intensity	hk·ℓ
0.1099	W	00 2
0.1143	-	*11 0
0.1405	S	11 1
0.1502	-	*20 0
0.2584	-	*20 2
0.2670	W	21 0
0.2940	W	21 1
0.3416	W	30 0
0.3675	VW	30 1
0.4375	M	00 4
0.4921	M	31 0
0.5120	MW	21 3
0.5904	VW	20 4
0.7760	M	30 4
0.7960	M	41 0
0.8353	W	40 3

* These reflections also correspond to Ti_2Ni.

(after Purdy and Parr; ref. 11)

Table 1.; Powder pattern of the "π" Phase
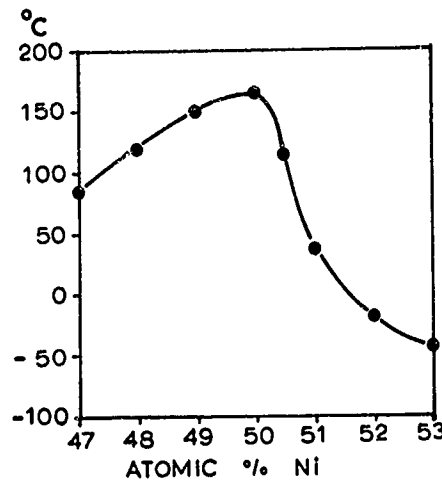
(after Wang et al.;ref.23)

Fig.5; The acoustic damping capacity change
of the near-stoichiometric TiNi alloys as a
function of the Ni atomic composition. Above
the curve, the alloy is low in damping capac-
ity,below the curve damping capacity is high.
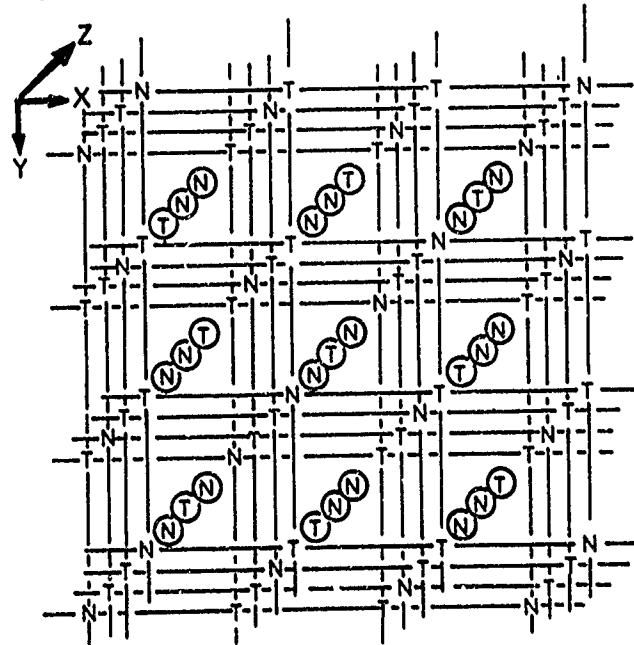
(after Wang et al.; ref. 23)

Fig.6; The short-range order of the TiNi-II
phase as proposed by Wang et al(ref. 23); the
structure is composed of two distinct linear
atomic sequences, $-(Ti-Ti-Ni)_n-$ and $-(Ni-Ni-Ti)_n-$
One type in circles and the other interconnected
with solid lines.

9

concluded that crystal structure of TiNi-II is a complex with a short-range structure(trigonal) based on -(Ti-Ni-Ni)$_n$- and -(Ni-Ti-Ti)$_n$- linear sequences(Fig. 6). The long-range structure (cubic) is a statistical distribution of short-range trigonal structures with their unique axes aligned in the four <111> cubic directions. According to these authors, the TiNi-II $\rightleftharpoons$ TiNi-III transformation is diffusionless in nature and "martensitic" in character but unique in that that 1) it is accompanied by a considerable amount of heat of transformation and 2) there is evidence for a crystallographic distortion(second order) and not a crystallographic transformation (first order). The authors also showed evidence for a 9 Å superstructural repeat(3 times the reported lattice repeat for the CsCl-type structure of TiNi) for TiNi-III.

Simultaneously, Dautovich and Purdy[24](1965) used electron transmission and diffraction methods, for the first time in an investigation of the TiNi alloys. They concluded that TiNi(51 at.% Ni) undergoes a martensitic transformation near 50°C but that the transformation is preceded by a pre-martensitic second order transformation. They reported the intermediate phase to be rhombohedral with a = 6.02 Å, α = 90.7° and the final product, martensite, to be triclinic with a = 4.60 Å b = 2.86, c = 4.11 Å, α = 90.1°, β = 90.9° and γ = 96.7°. Although an a = 9 Å repeat, identical to that observed by Wang et al.[23], was also observed in this electron diffraction study, the authors interpreted this as due to ordering of substitutional defects.

In 1952, Rostoker[25] reported the existence of Ti_4Ni_2O as fcc but listed some diffraction lines which did not correspond to a fcc structure(all odd or all even indices). However, the structure reported was confirmed later by Nevitt[26](1960). Meanwhile Yurko, Barten and Parr[27](1959) made a complete determination of the structure of Ti_2Ni and found the structure to belong to space group, Fd3m, with a = 11.32 Å. Using both X-ray and neutron diffraction techniques, Mueller and Knott[28](1963) determined and compared the structures of Ti_2Ni and Ti_4Ni_2O. Aside from a slight difference in their lattice constants (Ti_2Ni -- a = 11.3193 Å vs. Ti_4Ni_2O -- a = 11.3279 Å) and interatomic distances, the authors found the two structures to be completely identical and thus not readily differentiated by X-ray or electron diffraction methods.

The accelerated research efforts of many investigators, after the discovery of the unique physical properties of TiNi by Buehler and Wiley[19]in 1962, were presented at a symposium on "TiNi and Associated Compounds" in 1967. This symposium was held at the U.S. Naval Ordnance Laboratory where the unique properties of TiNi were first discovered. Out of this symposium, the following conclusions(including some disputes) concerning the nature of TiNi and its transformation emerged:(see NOLTR 68-16)

    1. The earlier identifications of the TiNi-I, TiNi-II and TiNi-III phases by Wang et al[23]are vindicated by the internal friction study of Hasiguti and Iwasaki[29].

    2. As pointed out by Carter[30], the short-range trigonal structure inferred earlier by Wang et al.[23], actually belongs to space group

P$\bar{3}$m1 and a simple diffusion-mechanism exists for the transformation between the B2(CsCl)-type and the P$\bar{3}$m1 structures.

3. The TiNi transition can be identified as a 'covalent' to 'metallic' electronic state transformation by various transport and thermodynamic property changes observed at and around the transition (Wang et al.[31]).

<u>Disputes:</u>

The contention by Wang et al[23] that the super-structure with a = 9 Å has the short-range P$\bar{3}$m1 structure(assigned to the TiNi-II phase) was challenged by Chandra and Purdy[32] and Scholl et al.[33], based on their electron diffraction patterns. Chandra and Purdy interpreted the diffuse streaks obtained in their electron diffraction pattern as that due to scattering by large amplitude but short-wave length phonons.

Meanwhile, Marcinkowski,Sastri and Koskimaki[34] [35](1968,1969) reinvestigated the nature of TiNi and its diffusionless transformation by transmission electron microscopy. In their first report(1968), the authors identified two independent martensites, both with monoclinic structures; M(a = 5.19, b = 4.96, c = 4.25 Å and β= 99°), M'(a = 5.19, b = 5.52, c = 4.25 Å and β= 116°). The authors also confirmed the earlier reports of Wang et al.[23] that the TiNi transition proceeds by a diffusionless shear in the <111> direction and in the (112) plane. Based solely on the electron microscopic identification of the Ti$_2$Ni and TiNi$_3$ phases, the authors claimed once more in their second paper(1969) the existence of eutectoidal decomposition of TiNi into Ti$_2$Ni and TiNi$_3$.

In order to resolve the dispute between the a = 9 Å complex structure inferred by Wang et al.[23] on one hand and the phonon-scattering interpretation suggested by Chandra and Purdy[32] on the other, Otsuka and Shimizu[36](1968) undertook yet another electron transmission microscopic study of TiNi. Based on the nature of the extra reflections observed, the authors concluded that micro-precipitates were their cause. Contrary to the work of Koskimaki et al.[35], the authors did not find Ti$_2$Ni and/or TiNi$_3$, the eutectoidal decomposition products of TiNi.

More recently, Wang et al.[37] (1969) showed by structure factor calculations, that the B2 and P$\bar{3}$m1 structures are practically indistinguishable in both their X-ray and neutron powder diffraction patterns. This calculation therefore implies that the P$\bar{3}$m1 structure advocated by Wang et al.[23] cannot be ruled out simply because the X-ray or neutron powder patterns are indexable as a B2(CsCl)-type structure.

C. Eutectoidal Decomposition of TiNi into Ti$_2$Ni and TiNi$_3$.

Prior to the discoveries of a diffusionless transformation of TiNi by Purdy and Parr[11] and the unusual mechanical behavior of TiNi by Buehler and Wiley[19], the major disagreement concerned the decomposition of TiNi into Ti$_2$Ni and TiNi$_3$(hereafter referred to as the decomposition). Without giving actual experimental evidence, Duwez

and Taylor[7] first reported the decomposition of TiNi as similar to
that of TiFe to Ti_2Fe and $TiFe_2$. These authors made no mention
whatsoever of the now recognized[9,19,26], difficulty of preparing
TiNi powder for X-ray diffraction. Further, the decomposition of TiFe
was later proven to be non-existent[38]. Nontheless, the report was sec-
onded by Pool and Hume-Rothery[9] based on an X-ray powder pattern
in which four extra lines were attributable to Ti_2Ni and five extreme-
ly faint lines were attributable to $TiNi_3$. It should be noted that
the powder pattern was obtained from a specimen which had been
annealed at 600°C for two weeks then quenched. The assumption made
here was that the process of quenching retained the structure of the
alloy matrix at 600°C at room temperature at which the pattern was
obtained. This is not necessarily true. In fact, it was proven to
be in error by Gilfrich[20] who used a controlled high temperature
X-ray powder diffractometer to obtain the powder patterns of the alloy
at various temperatures. This experiment showed that the extra lines,
attributed to Ti_2Ni or $TiNi_3$, actually appear at about 80°C (tempera-
ture varies with the history of the alloy), as shown in Fig. 7.
Moreover, the extra lines appear and disappear almost instantaneously
as the temperature is lowered and raised. However, this observation
directly contradicts Gilfrich's own conclusion that the extra lines
are due to Ti_2Ni and $TiNi_3$; for decomposition requires diffusion
which would be extremely slow if not impossible at these temperatures.
If the extra lines are due to Ti_2Ni and $TiNi_3$, they could not appear
and disappear almost instantaneously.

More recently, Koskimaki et al.[35] , based exclusively on an electron
transmission microscopic study, claimed once more the eutectoidal
decomposition of TiNi. The identification of Ti_2Ni by these authors
was based on the lattice constants and symmetry observed. However,
the lattice constants and symmetry alone cannot 'prove' the existence
of Ti_2Ni and subsequently the 'decomposition'. This is because
Mueller and Knott[28] have shown by neutron diffraction that Ti_2Ni and
Ti_4Ni_2O are crystallographically identical, and an extended period
of annealing could produce oxidation of TiNi to Ti_4Ni_2O.

To summarize, it can be said that the evidence presented by various
investigators in support of 'decomposition' is insufficient. Against
these reports and claims, Margolin et al.[8] reported a fruitless
search for any evidence to substantiate the 'decomposition'. Purdy
and Parr[11], who first discovered the diffusionless transformation in
TiNi near room temperature, also disclaimed 'decomposition'. Further,
in the only single crystal study of TiNi, Wang et al.[23] could find
no evidence for 'decomposition.' Therefore, unless better evidence
is presented, it is reasonable to conclude that the 'decomposition'
does not take place.

II. CRYSTAL STRUCTURE OF TiNi

Prior to the single crystal study of Wang et al.[23] , it was generally
accepted, based on the powder patterns that TiNi was a B2(CsCl)-type
structure in the high temperature range. However, Wang et al proposed
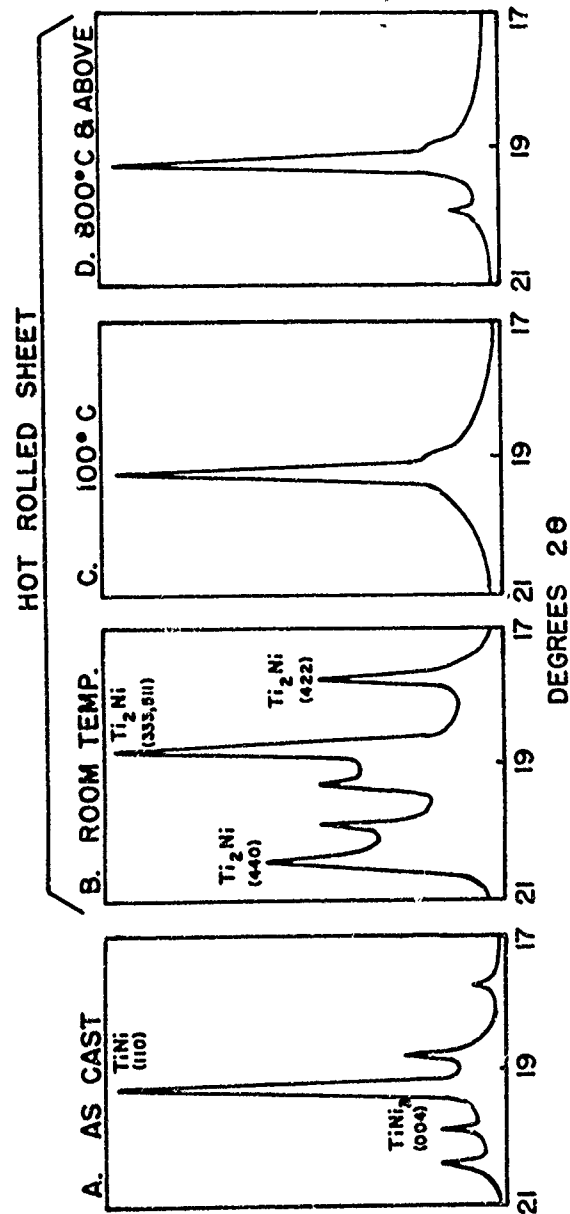
Fig. 7

Fig. 7: Partial X-ray diffractometer scans of 55.4 at.% Ni as arc-cast, and hot-rolled sheet at various temperatures.

(after Gilfrich; ref.20)

a short-range trigonal($P\bar{3}m1$) structure statistically distributed into a super structure with a = 9 Å(Fig. 6) in the temperature range, 60° to 600°C. The two conclusions are based on different methods of investigation and should be analyzed more critically as follows:

Given a three-dimensional lattice, $\bar{R}_n = n_1\bar{a}_1 + n_2\bar{a}_2 + n_3\bar{a}_3$, there exists a reciprocal lattice, $\bar{R}_s^* = h\bar{b}_1 + k\bar{b}_2 + \bar{b}_3$ such that $\bar{a}_i \cdot \bar{b}_j = \delta_{ij}$ (where i,j = 1,2,3). Further, from the Laue equations,

$$
\left.
\begin{aligned}
\bar{S} \cdot \bar{a}_1 &= h \\
\bar{S} \cdot \bar{a}_2 &= k \\
\bar{S} \cdot \bar{a}_3 &= \ell
\end{aligned}
\right\}
\quad
\begin{aligned}
&\text{where } \bar{S} \text{ is the diffraction vector of} \\
&\text{modulo } (1/\lambda)
\end{aligned}
$$

it is clear that X-ray diffraction from a crystal lattice with $\bar{a}_1$, $\bar{a}_2$ and $\bar{a}_3$ as lattice repeats will occur only at the reciprocal lattice points, $\bar{R}_s^*$. It is equally clear that the diffraction pattern from a three-dimensional crystal is also three-dimensional. However, an X-ray powder pattern is, in essence, one-dimensional data. In other words, the three-dimensional data are collapsed into one-dimension. This can be understood as follows from the Debye's formula for a powder diffraction pattern:

The observed intensity, I(s), is proportional to the square of amplitude, A(s),

$$
I(s) \propto |A(s)|^2 = \sum_n^N f_n^2 + \sum_{n \neq n'}^N f_n f_{n'} \cdot \cos 2\pi(\bar{S} \cdot \bar{r}_{nn'})
$$

The observed intensity from a powder pattern is the sum of the average of these terms or,

$$
\overline{I(s)} = \sum_n^N f_n^2 + \sum_{n \neq n'}^N f_n f_{n'} \cdot \overline{\cos 2\pi(\bar{S} \cdot \bar{r}_{nn'})}.
$$

Since, the average of the cosine term is

$$
\overline{\cos 2\pi(\bar{S} \cdot \bar{r}_{nn'})} = \int_0^\pi \int_0^{2\pi} \cos(2\pi\bar{S} \cdot \bar{r} \cdot \cos\gamma) \sin\gamma \, d\gamma \, d\theta
$$

$$
= \frac{\sin 2\pi(\bar{S} \cdot \bar{r}_{nn'})}{2\pi(\bar{S} \cdot \bar{r}_{nn'})}
$$

the observed powder diagram depends only on the length of the inter-atomic vectors and does not depend on their mutual orientations.

Without losing any generality, one can say that it is impossible to solve a three-dimensional problem unambiguously based on one-dimensional data; for a number of three-dimensional models can be proposed based on a given set of one-dimensional data. This is the fundamental weakness of the powder pattern method and the reason that the single crystal diffraction method is definitely superior.

14

A. Single Crystal Growth

For the reasons described above, it was realized by Wang et al.[22] that it was absolutely necessary to obtain single crystals of TiNi and three-dimensional data in order to gain a true understanding of the TiNi crystal structure. For an alloy as ductile as TiNi, growth of single crystals of appropriate size for X-ray diffraction proved to be extremely difficult by conventional methods. It was by a modified "strain-anneal" method[22] that TiNi single crystals of appropriate size were produced. The technique is essentially as follows:

A polycrystalline wire of TiNi was chemically etched to insure a clean surface. As in the standard "strain-anneal" method[39], strain was introduced by pulling or twisting the wire. The ends of the wire were then spot-welded to tungsten leads and vacuum sealed at 10^{-6} mm pressure into a pyrex glass tube as shown in Fig. 8. Annealing was accomplished by resistance heating by passing a controlled alternating electric current through the wire. Temperature control was achieved by varying the voltage across the wire by means of a variable auto-transformer. A single crystal of TiNi was successfully grown when the temperature was raised and lowered a few dozen times in a cyclic manner. The effect of this cycling on single crystal growth was found to be most effective in the range in which thermal expansion and contraction of the wire was most sensitive to temperature changes.

B. TiNi-I, TiNi-II and TiNi-III

1. The diffusionless Transformation Near Room Temperature.

The preliminary investigation of the single crystals of TiNi was based on Laue photographs (Figs. 9-a, 9-b, 9-c and 9-d). In Fig. 9-a, the specimen was essentially polycrystalline while in Fig. 9-b, a single crystal of TiNi is indicated. This Laue photograph also shows 'asterism' associated with the diffraction spots. However, upon heating to above the transition temperature, T_c(in this case approximately 36°C) the 'asterism' disappeared instantaneously and the pattern became one of normal discrete Laue diffraction spots. The appearance and disappearance of Laue-asterism was readily reversible with the temperature change and was directly associated with diffusionless transformation. The absence of major changes in the diffraction pattern, or the relative intensities as the whole, in transversing T_c indicates that the crystal lattice as the whole remains nearly the same in the two states.

"Laue-asterism" has been known to result from mildly deformed single crystals with the presence of 'curved' or broken up lattice domains which may be local in character or spread over a large region[40]. In particular, the Laue photographs (Fig. 10) of an aluminum single crystal before and after shear[41] can be compared with those from TiNi(Figs. 9-b, 9-c). It is obvious that the TiNi crystal structure undergoes a mild distortion upon cooling below the critical temperature. This was the first indication that the transition occuring in TiNi close to room temperature is not a crystallographic transformation, but is

Fig. 8

NOLTR 72-4

tungsten leads . glass tubing

TiNi wire

autotransformer
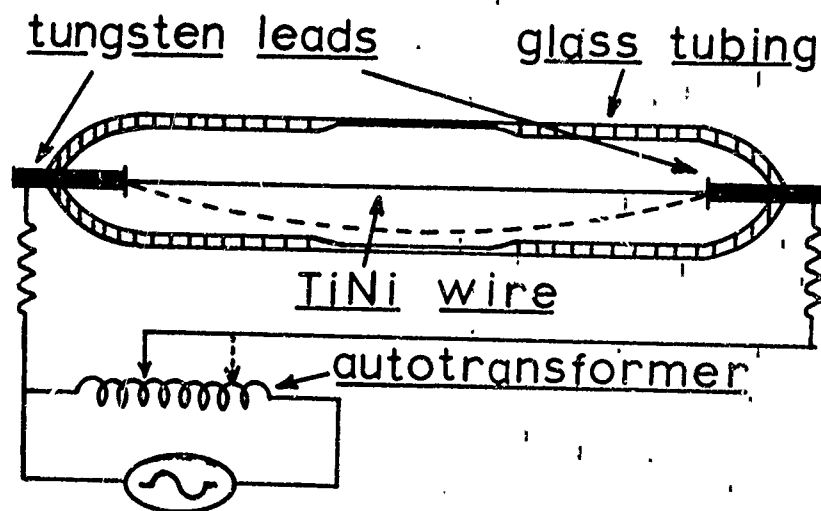
(after Wang et al.; ref. 22)

Fig. 8; Schematic diagram of the setup for growing
single crystals of TiNi; solid lines show the low vol-
tage condition when the TiNi wire is under strain ;
broken lines show the high voltage condition when the
TiNi wire is under minimum strain. Cycling is carried
out alternating between these two conditions. The middle
section of the glass tubing is thinned in order to allow
more efficient transmission of X-rays.

Fig. 9

polycrystalline wire

(a)

S.C.;at R.T.

(b)

S.C.; 40°~600°C

(c)

S.C.; above 700°C

(d)

(after Wang et al; ref. 23)

Fig. 9; Laue photographs(using Mo unfiltered radiation);
(a) TiNi poly-crystalline wire., (b) TiNi single crystal
wire at R.T.,(c) 40° through 600°C and (d) above 700°C.

Fig. 10

(b)

(a)

(after Burgers and Lebbink; ref. 41)

Fig. 10.; Laue photographs of an aluminum single crystal rod; (a) before deformation, (b) after a shear of 0.4(asterism clearly visible).

18

a crystallographic distortion and thus a second-order transformation.
We shall now elaborate on the differences between crystallographic
transformation and crystallographic disto ion.

Phase transformations between different crystal modifications are
fundamentally different from between the liquid and gaseous states.
The liquid and gaseous states are distinguished from one another by
a greater or smaller interaction between their molecules, whereas
different crystal modifications are qualitatively different from one
another in their internal symmetry. Therefore, each symmetry pro-
perty exists or does not exist, appears or disappears with a sudden
jump, not gradually. This is to say that in each state, the matrix
will have either one symmetry or the other but not something in-between.
With this understanding, a crystallographic transformation is the
transformation between two thermodynamic states, $\Phi_1(P,T)$ and $\Phi_2(P,T)$
with distinct crystal modifications. At the transition point, the
chemical potentials of the two phases are equal: $\mu_1(P,T, C_1) = \mu_2$
(P,T, C_2) where C_1 and C_2 represent the crystal modifications of
the two states. In each state, the point matrix will have either one
of the symmetry or the other such that the transformation, $C_1 \longrightarrow$
C_2 is discontinuous. Therefore, two-dimensional interface('habit
plane') exists between the two crystallographic modifications. Thermo-
dynamically, such a transformation is first order and is accompanied
by a latent heat which is equal to the difference in entropy between
the two crystal modifications multiplied by the temperature at which
the transformation takes place.

$$\mu_1 = E_1 - TS_1 + PV_1 = \mu_2 = E_2 - TS_2 + PV_2$$

$$(E_2 - E_1) - T(S_2 - S_1) + P(V_2 - V_1) = 0$$

$$Q = T \cdot \Delta S$$

where μ – thermodynamic potential
E – internal energy
S – entropy
V – volume

Crystallographic distortion differs from crystallographic transfor-
mation because of the absence of any discontinuous change in the
arrangement of the atoms in the crystal. However, there is an abrupt
change of symmetry in the sense that even a small arbitrary displace-
ment of the atoms from their initial symmetric positions is sufficient
to produce an abrupt change in the symmetry of the lattice. For ex-
ample, at high temperature, $BaTiO_3$ has a cubic lattice with a unit
cell as shown in Fig. 11. As the temperature is lowered to its
critical temperature($120°C$), Ti and O atoms begin to shift relative
to the Ba atoms along one edge of the cube and the lattice becomes
tetragonal. Further cooling results in a further shift of atoms and
thus a continuous change in the atomic arrangement. Thus, during the
crystallographic distortion, the matrix changes continuously and homo-
geneously in such a manner that the two crystal modifications are
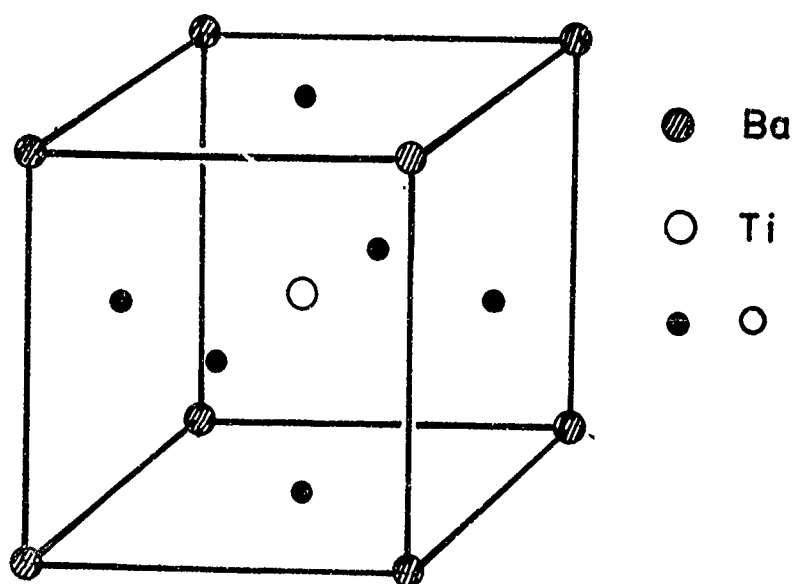
Fig. 11

BaTiO₃

Fig. 11; Crystal structure of BaTiO₃ .

indistinguishable. On the other hand, during crystallographic trans-
formation, two crystal modifications are in equilibrium and distinct
from one another.

The absence of any discontinuity of state in crystal distortion cata-
gorizes this type of phase transformation as second-order. Following
thermodynamic arguments for second-order phase transformations[42] ,
order-disorder parameter exists which determines the degree of the
atomic displacement from the original crystal symmetry. This parameter
equals zero ($\gamma=0$) for no displacement, and maximum displacement
corresponds to $\gamma=1$. The absence of discontinuity of states results
in the absence of latent heat or volume change at the transition point.

2. The Transformation Involving Diffusion at 600° to 700°C

Heating the crystal above 600° ∿700°C produces a definite change in
the relative intensities of the diffraction spots(compare Figs. 9-c
to 9-d). This change is not accompanied by a change of diffraction
angles and is therefore attributable to replacement disorder†. This
reasoning is elaborated below.

By neglecting surface effect, an ideal single crystal can be expressed
mathematically in term of its electron density as:

$$\rho_c(r) = \rho(r)*[Z(r) \cdot \sigma(r)]$$

> where $\rho(r)$ - electron density within the unit cell.
> $\sigma(r)$ - 'form factor' which defines the exterior
> shape of the crystal.
> $Z(r) = \Sigma\delta(r - r_n)$, a Dirac(delta) function with
> $r_n = n_1a_1 + n_2a_2 + n_3a_3$ such that
> $\delta(r) = 0$ when $r-r_n \neq 0$
> $\delta(r) = \infty$ when $r-r_n = 0$
> moreover, $\int\delta(r-r_n)dV_r = 1$.

Through the use of the faltung(convolution) theory, the reciprocal
space, $A(s)$ to the real space, $\rho_c(r)$ can be expressed as:

$$A(s) = \int\rho_c(r)\exp(-2\pi i\bar{s}\cdot\bar{r})dV_r \quad = \int\rho(r)*[Z(r)\cdot\sigma(r)]\exp(-2\pi i\bar{s}\cdot\bar{r})dV_r$$

$$= F(s) \cdot R(s).$$

> where $F(s) = \text{transf}[\rho(r)] = \sum_i f_i\exp(2\pi i\bar{s}\cdot\bar{r}_i)$
> $R(s) = \text{transf}[Z(r)\cdot\sigma(r)]$
> $= Z(s)*\Sigma(s)$
> $= 1/V_c \Sigma\delta(s - r^*)$

---

† Replacement disorder results when atomic sites remain unchanged but
the atomic sequence of occupation of these sites becomes disordered.
Displacement disorder results when the atomic sequence of occupation
remains unchanged but atom sites are displaced and thus spatially
distorted.

therefore,

$$I(s) \propto |A(s)|^2 = |F(s)|^2 + |R(s)|^2.$$

Thus, it is obvious that the X-ray diffraction data from a crystal consists of two parts: 1) F's), the intensity which determines the electron density distribution within the unit cell and 2) R(s), which is expressed in term of positions and shapes of diffraction spots. This is the part which yields information on the fundamental lattice repeats, and the shape of the crystal.

This understanding, combined with experimental evidence, led to the conclusion that two transitions exist in 51 at.% Ni of TiNi; one at 600° ~ 700°C(with diffusion) involving replacement order-disorder and one at 40°C(diffusionless) involving displacement order-disorder. Following the notation of Wang et al[23], the three distinct thermodynamic states of TiNi are designated as:

TiNi-I   Between 700°C up to the m.p.(1310°C)

TiNi-II   Between 40°C up to about 600°C

TiNi-III   Below 40°C to about -90°C

(TiNi-IV   Below -90°C)

These three states(or four states) as predicted by Wang et al[23],were corroborated by the internal friction data of Hasiguti and Iwasaki[29] as shown in Fig. 12.

C. The TiNi-II Structure

Further investigation of TiNi single crystals with a precession camera showed the diffraction symmetry to be m3m both above and below the 40°C transition. Typical procession photographs showing undistorted reciprocal lattices taken at various temperatures are given in Figs. 13-a, 13-b, 13-c and 13-d. The TiNi-II pattern shown in Fig. 13-a consists of a set of diffuse streaks and a set of regular diffraction spots(inter-connected with solid lines). Disregarding the streaks, the diffraction spots alone indicate a CsCl-type diffraction pattern; i.e., the fundamental reflections, h + k + ℓ = 2n are strong and the super-reflections, h + k + ℓ = 2n + 1 are weak. This combined with a measured lattice constant, a = 3.01 Å, Appears to confirm the previous reports [12][7] based on the powder patterns that TiNi has a CsCl-type structure. However,the streaks disappeared and re-appeared reversibly at the TiNi-II ⇌ TiNi-III transition. Simultaneously, a set of weak reflections appeared and disappeared. Furthermore, the lattice repeat of these weak reflections(inter-connected by dotted lines in Fig. 13-b) is exactly three times that of the 3 Å lattice

Fig. 12
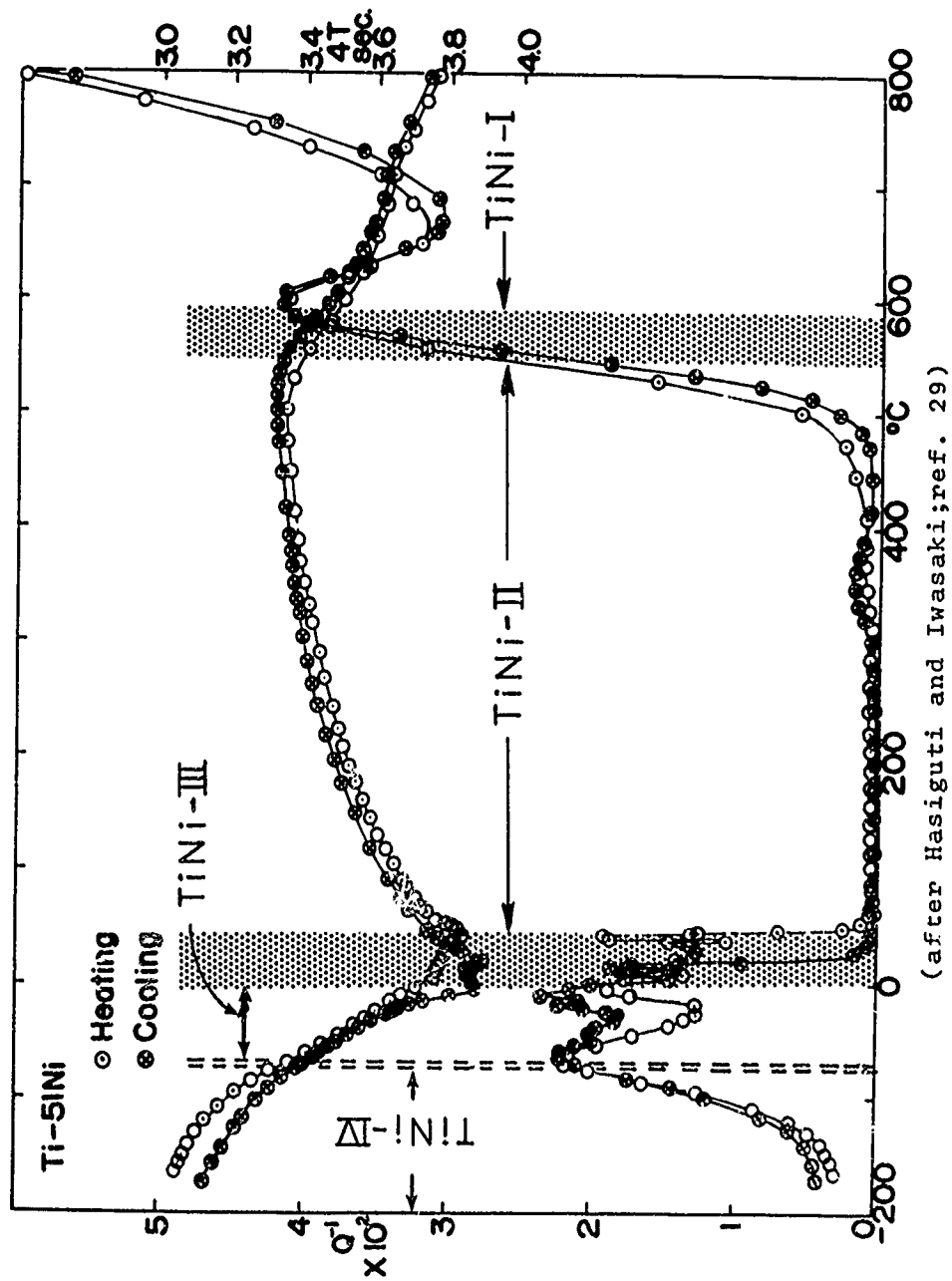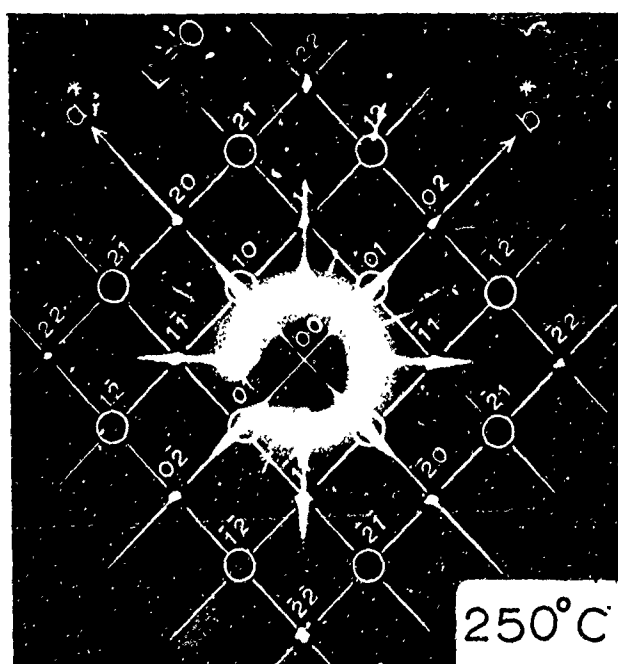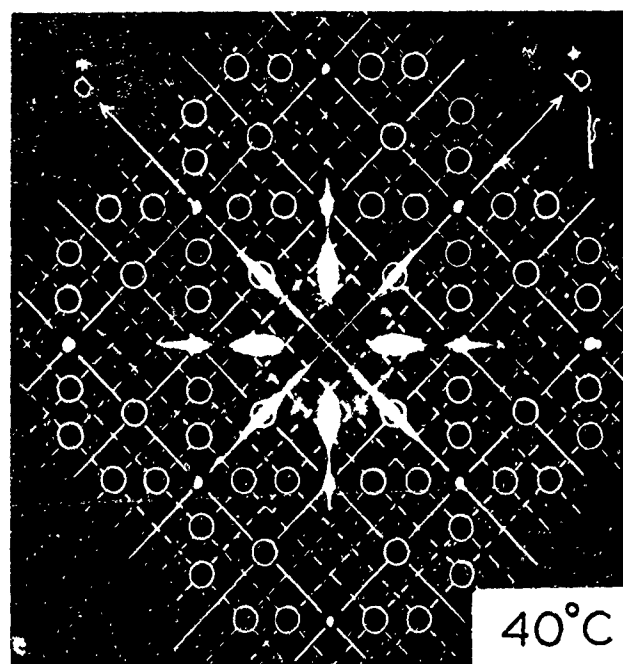

Fig. 12.; Internal frictions and elastic moduli in the temperature range from -170°C to 800°C of a TiNi specimen which was annealed at 800°C for 2 hrs. and furnace cooled.
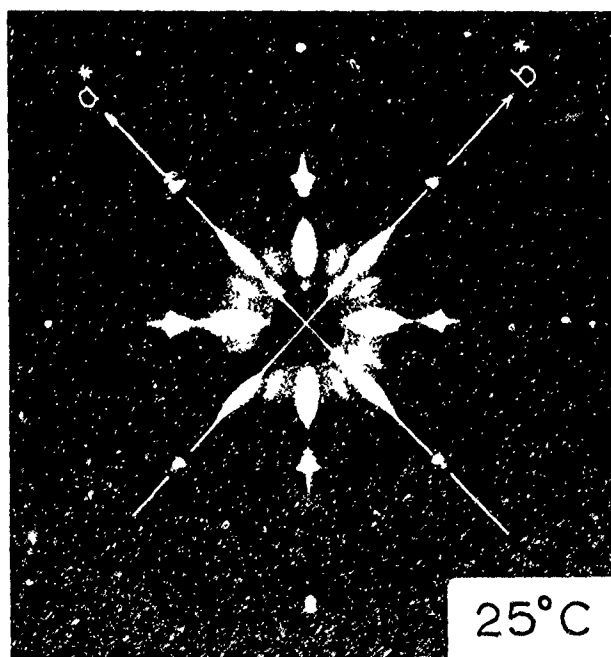
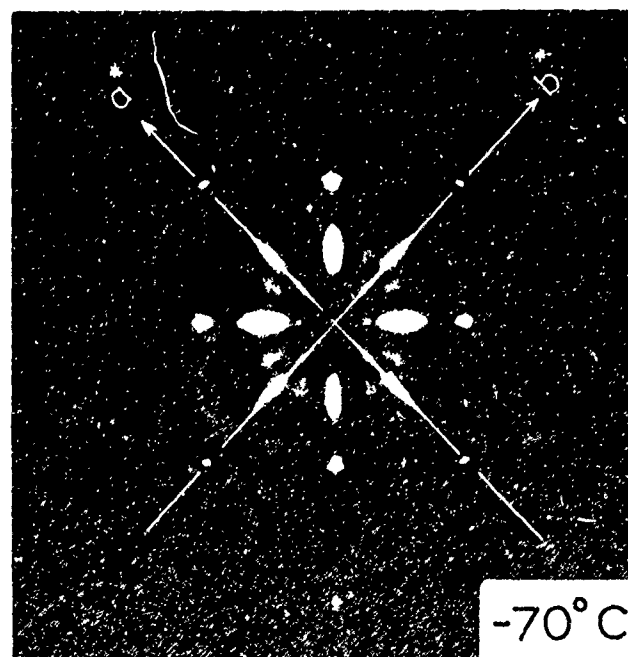(after Hasiguti and Iwasaki;ref. 29)

Fig. 13

(a)
250°C

(b)
40°C

(c)
25°C

(after Wang et al.;ref. 23)

(d)
-70°C

Fig. 13.; Zero layer(C* = 0) precession photographs
of a TiNi single crystal at various temperatures.

such that the two lattices have a sub- and super-lattice relationship to one another.

These observations imply that the TiNi crystal structure is not a simple CsCl-type, but has a 9 Å super-lattice which transforms from a disordered to an ordered state in going from TiNi-II to TiNi-III at the 40°C transition. Further, it is observed that the streaks in the TiNi-II pattern(Fig. 13) are directed toward the reciprocal lattice origin. To understand the nature of these streaks, it is best to refer to the fundamental Laue equations which govern the nature and position of reflections.

$$\bar{S} \cdot \bar{a}_1 = n_1 \ , \quad \bar{S} \cdot \bar{a}_2 = n_2 \ , \quad \bar{S} \cdot \bar{a}_3 = n_3$$

where $\bar{S}$ is the diffraction vector with $|\bar{S}| = (2\sin\theta)/\lambda$ and
n_1, n_2 and $n_3 = 0, \pm 1, \pm 2, \pm 3$ -------

In vector notation, it is obvious that each of the Laue equations describes a set of parallel planes perpendicular to vector $\bar{a}_i$ with an inter-planar spacing of $1/|\bar{a}_i|$. That is, if only one of the three Laue conditions is satisfied, diffraction in reciprocal space is a set of planes; if only two conditions are satisfied, diffraction in reciprocal space is a set of lines. Only when all three conditions are simultaneously satisfied will diffraction occur at diescrete reciprocal lattice points. Inasmuch as the interplanar distances described by the three Laue equations are equal to $\lambda/|\bar{a}_i|$, the reciprocal lattice constants, $\bar{b}_1$, $\bar{b}_2$ and $\bar{b}_3$ will vary proportionally and simultaneously with the wavelength, λ , used. This is illustrated experimentally by the 'white radiation streaks' produced by a continuous wavelength spectrum. Conversely, it is easy to see that the same effect can be produced with monochromatic X-rays if the lattice constants $\bar{a}_1$, $\bar{a}_2$, and $\bar{a}_3$ vary proportionally and simultaneously. Since the 40°C transition is diffusionless, a cooperative displacement of atom positions within interatomic distances is expected. This fact, together with the alternate reason described for the 'white radiation streaks', led to the following conclusion.

For a cubic structure like TiNi, atomic displacements will cause the lattice constants to elongate or shorten simultaneously with equal magnitudes only if such cooperative displacements take place on the {111}planes. This suggests that the atomic arrangement in the {111} planes is unique, with reference to either interatomic distances or arrangement of atomic species. Based on these considerations, the conditions which the crystal structure of TiNi-II must satisfy are:

1. The structure must be centrosymmetric.
2. The overall atomic composition ratio, Ti:Ni must be 1:1.
3. The atomic arrangement of the {111} planes must be unique.
4. The structure must show a sub-(3 Å) and super-(9 Å) lattice relationship in which the sublattice is ordered while the superlattice is disordered.
5. The diffraction symmetry obtained from such a structure must be cubic, m3m.

25

A B2(CsCl)-type structure is composed of two interpenetrating simple cubic lattices(one interconnecting cube-corners), the other cube-centers) which are referred hereafter as the (0) and (1/2) lattices. A crystal structure meeting the requirements described above can be constructed based on a linear atomic sequence, $-(Ni-Ti-Ti)_n-$ for the (0) lattice and $-(Ti-Ni-Ni)_n-$ for the (1/2) lattice as shown in Fig. 6. The crystal structure constructed in this manner meets conditions, 1, 2 and 3 in that it is centrosymmetric with an overall Ti:Ni atom ratio equal to one and the atomic arrangement on (111) plane is unique, i.e., alternating layers of Ti and Ni. However, the structure is rhombohedral and not cubic and does not yield m3m diffraction symmetry as required by experimental evidence. The 9 Å super-lattice is not disordered; thus part of condition 4 is not satisfied. However, these inconsistencies both can be resolved by the following consideration.

A simple cubic lattice based on a linear atomic sequence, $-(B-A-A)_n-$ can have four possible orientations of the unique <111> axis as shown in Fig. 14. Since the orientation of the unique axis is the only difference among the four possibilities, the internal free energy of each of the four types should be exactly the same. Therefore, the four orientations are equally probable and are expected to be statistically distributed in the TiNi-II structure. The unique axes of these four different orientations are:

$<111>$, $<\bar{1}11>$ $<1\bar{1}1>$ $<\bar{1}\bar{1}1>$

respectively referred to common coordinates. Since these four possibilities would be inherent to both the (0) and (1/2) lattices in the TiNi-II structure, there should be 16 possible combinations of different orientations between the two lattices. However, the requirement of a unique atomic arrangement, the (111) plane eliminates the possible combinations with different orientations. This leaves only four distinct possible combinations in which the planes of unique atomic arrangement in both lattices are oriented in the same direction, therefore, there are four possible orientations for the TiNi-II structure.

Combination of these four different orientations can also be considered as fault-stacking. It is observed in Fig. 14 that the first and the fourth layer of types I and II are identical. Further, the second layer of type I is identical to the third layer of type II and conversely, the third layer of type I is identical to the second layer of type II. Therefore, if the sequence of layer stacking were designated as ABCABC for type I, the type II sequence must be ACBACB. This demonstrates the fact that disorientations in TiNi alloy can be considered as stacking faults.

In summary, the crystal structure of TiNi-II, as proposed by Wang et al.[23], is rhombohedral in short-range order but exhibits cubic diffraction symmetry because of the statistical distribution of the rhombohedral domains in the four<111> unique directions(referred to the cubic axes).
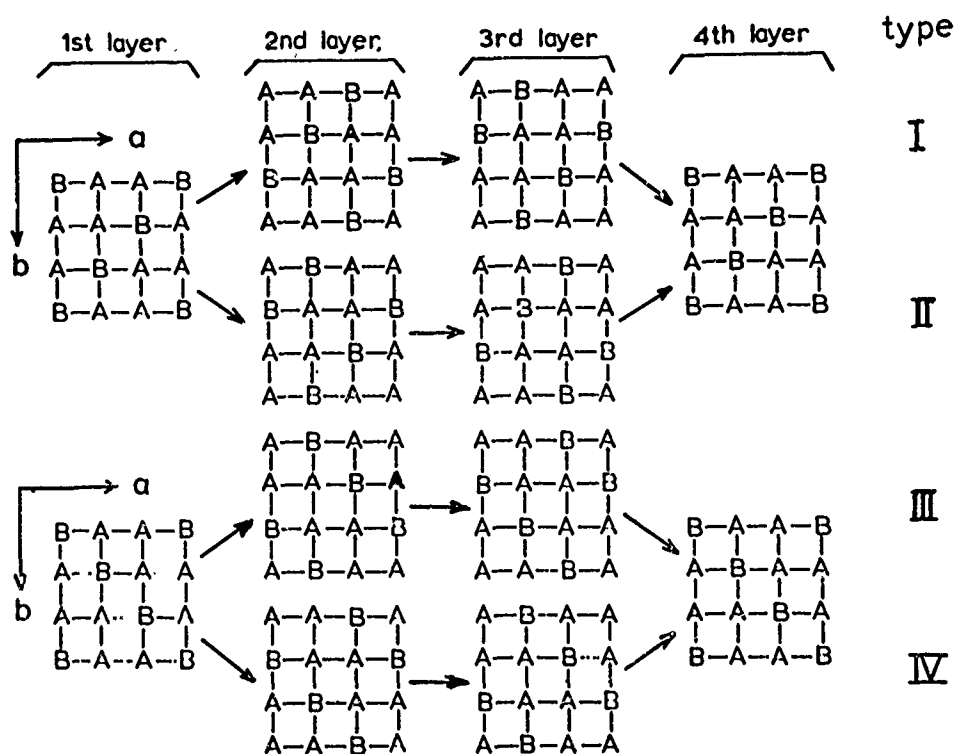
Fig. 14

(after Wang et al.; ref. 23)

Fig. 14.; The four possible orientations of a 3-dimensional lattice whose linear sequence is $-(A-A-B)_n-$.

a. The TiNi-II short-range P$\bar{3}$m1 structure.

The rhombohedral structure thus proposed was later identified by Carter[30] as belonging to space group, P$\bar{3}$m1 with three units of TiNi per unit cell as follows:

1 Ti(a);   0,   0,   0   1 Ni(b);   0,   0, 1/2
2 Ti)d)$\pm$(1/3, 2/3, Z_T)   2 Ni(d);$\pm$(2/3, 1/3, Z_N)

where $Z_T = 1/6$ and $Z_N = 1/3$.

The lattice correspondence between the B2 and P$\bar{3}$m1 structure is:

$$
\begin{pmatrix} a_1 \\ a_2 \\ a_3 \end{pmatrix}_{P\bar{3}m1}
=
\begin{pmatrix} \bar{1} & \bar{1} & 0 \\ 0 & \bar{1} & 1 \\ 1 & 1 & 1 \end{pmatrix}
\cdot
\begin{pmatrix} a_0 \\ a_0 \\ a_0 \end{pmatrix}_{B2}
$$

with $|a_1| = |a_2| = \sqrt{2}|a_0|$ and $|a_3| = \sqrt{3}|a_0|$

This relationship is illustrated in Fig. 15. The corresponding inverse matrix which gives the transformation of the P$\bar{3}$m1 indices, H;K,L into the B2 cubic indices, h, k, ℓ is:

$$
\begin{pmatrix} h \\ k \\ \ell \end{pmatrix}_{B2}
= 1/3
\begin{pmatrix} \bar{2} & \bar{1} & 1 \\ 1 & \bar{1} & 1 \\ 1 & 2 & 1 \end{pmatrix}
\cdot
\begin{pmatrix} H \\ K \\ L \end{pmatrix}_{P\bar{3}m1}
$$

Inasmuch as the H,K, L indices of P$\bar{3}$m1 are integers without restrictions, it is clear that the h,k,ℓ indices of B2 can assume one third values. In the (hk0) plane when $K = -(H + L)/2$, $h = (-H + L)/2$ and $k = (H + L)/2$ so one half indices are possible. This condition of replacement disorder presumably exists in the TiNi-II phase and produces the diffraction streaks shown in Fig. 13-a. During transformation from TiNi-II to TiNi-III, atoms shear in the <111> direction so as to create a displacement disorder in the P$\bar{3}$m1 short-range structure. This misalignment brings in the expected one-third reflections in the (hkℓ) planes. These mechanisms will be discussed in more detail in a later section.

Based on powder diffraction, Chandra and Purdy[32] (X-ray) and Scholl, Larson and Freise[33] (neutron) found that within experimental error the structure factor ratio,(SFR) of |F(200)|/|F(100)| (B2 indices) agreed with the value expected for a B2 structure. The fact led Chandra and Purdy to suggest that, if the TiNi-II complex structure is to be given credence, it must be assumed that TiNi-II phase exists sometimes as a B2-type and sometimes as the complex structure. It
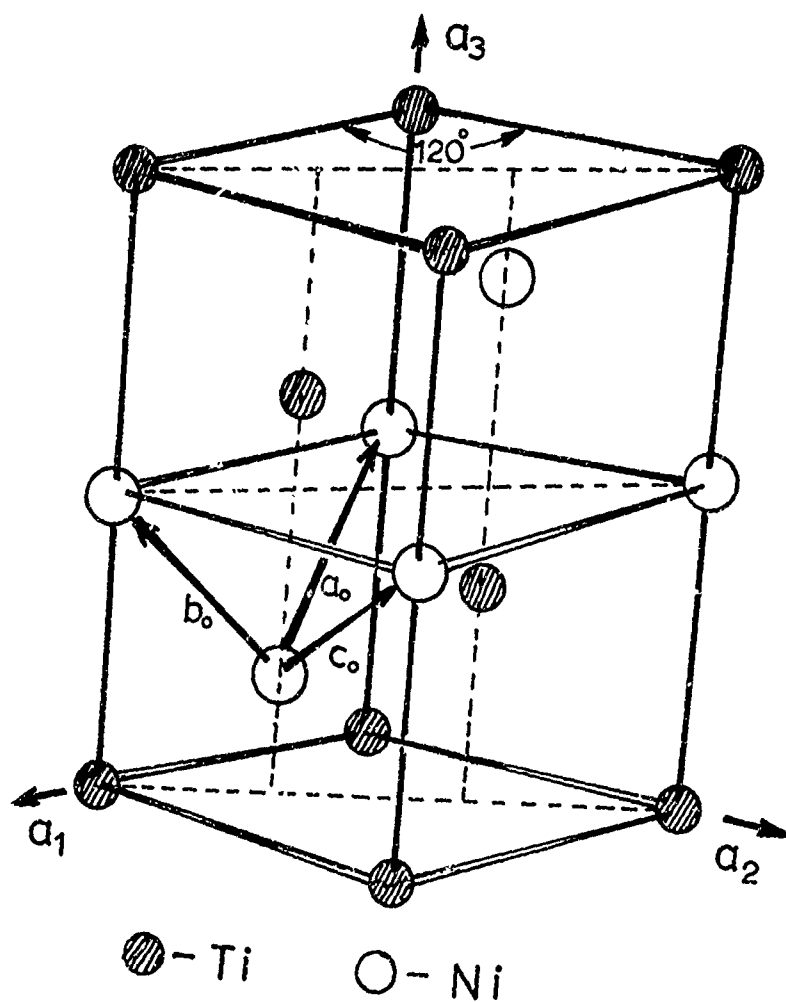
Fig. 15

⊘ - Ti   O - Ni

(after Carter; ref. 30)

Fig. 15.; The relationship of the CsCl-type structure
(indicated by a_o, b_o and c_o) to the larger hexagonal
cell of TiNi-II(indicated by a_1, a_2 and a_3

was shown by Wang et al[34] that this conclusion is not necessarily correct. From the lattice correspondence given above between the B2 and P3m1 structures, the structure factor equivalent equation can be derived.

$$F(h00) = F(\bar{H}0H)$$

$$= f_T \{1 + 2Cos2h\pi(Z_T - 1/3)\} + f_N \{Cos(h\pi)$$

$$+ 2Cos2h\pi(Z_N - 1/3)\}$$

In P3m1 there are twelve planes that are equivalent to $(\bar{H}0H)$;

$(\bar{H}0L)$, $(H0\bar{L})$, $(\bar{H}\bar{H}L)$, $(\bar{H}\bar{H}\bar{L})$, $(0HL)$, $(0\bar{H}\bar{L})$

$(H0L)$, $(\bar{H}0\bar{L})$, $(\bar{H}\bar{H}\bar{L})$, $(\bar{H}\bar{H}L)$, $(0\bar{H}L)$, $(0H\bar{L})$

Analogously, the $\{110\}_{B2}$ planes convert to eighteen equivalent P3m1 planes;

$(0\bar{1}2)$, $(01\bar{2})$, (102), $(\bar{1}0\bar{2})$, $(\bar{1}12)$, $(1\bar{1}\bar{2})$

$(0\bar{1}\bar{2})$, (012), $(\bar{1}02)$, $(10\bar{2})$, $(1\bar{1}2)$, $(\bar{1}1\bar{2})$

$(\bar{2}10)$, $(2\bar{1}0)$, (110), $(\bar{1}\bar{1}0)$, $(1\bar{2}0)$, $(\bar{1}20)$

The calculated structure factors and their structure factor ratios for both B2 and P3m1 are compared in Table 2(X-ray) and Table 3 (neutron). These calculations show that the fact that the observed intensity ratios, I(200)/I(100) and I(110)/I(100) from both X-ray and neutron diffraction happen to agree with those expected for a B2(CsCl)-type structure can neither prove the existence of the B2 structure nor disprove the existence of the complex structure proposed by Wang et al[23]. This is to say that additional data are required to prove a B2 structure. These additional data may come in the form of a) aboslute intensity measurements or b) measurements of relative intensities of all the symmetry-independent reflections within the reflection sphere. Absolute intensity measurements are obviously difficult, particularly in the presence of diffuse streaks. Powder patterns could be used to measure the relative intensities of all the symmetry-independent reflections only if TiNi powder were available. Unfortunately, because of the high ductility and low friability of TiNi alloy, it is virtually impossible to prepare TiNi powder by conventional methods. All X-ray and neutron powder diffraction patterns obtained to this point for TiNi came from bulk specimens and thus may be inaccurate due to preferred orientation. Of course this was the reason the authors[32,33] were forced to limit their comparison of the intensity ratios to I(200)/I(100) alone. This shortcoming was eventually overcome by Buehler and Wang[45] who obtained TiNi powder for the first time in the following manner.

A TiNi electrode(6 cm dia. and 8 cm long) was cast. The method of casting a large ingot of TiNi is due to Buehler and has a U.S. patent pending. This electrode was spun at high speed inside a vacuum chamber ($\sim 10^{-6}$mm) while being heated to its melting point, about 1310°C. Under these conditions, fine particles of TiNi spun off the

X-RAY DIFFRACTION

(hkℓ)	(HKL)	Sinθ/λ	F(H̄K̄L̄)	$\|F\|^2$	M	$M\|F\|^2$	$\Sigma M\|F\|^2$	SFR(B2 indices) P3̄m1	-B2(CsCl)
(100)	(1̄01)	0̄.166	⁻6.5	42.3	⁻6	253.8	} 1,267.8	$\|F(200)\|/\|F(100)\|$ 5.9	4.8
	(1̄01)	0.166	-13.0	169.0	6	-1,014.0			
(200)	(2̄02)	0.332	85.8	7,362.0	6	44,172.0	} 44,172.0		
	(202)	0.332	0	0	6	0			
(110)	(01̄2̄)	0.235	105.3	11,088.1	6	66,528.6	} 133,077.2	$\|F(1̄1̄0)\|/\|F(1̄00)\|$ 10.2	7.9
	(012)	0.235	0	-0	.6	0			
	(2̄10)	0.235	105.3	11,088.1	6	66,528.6			

(after Wang et al.; ref. 37)

Table 2.; Calculated structure factors(for X-ray) for various families of
HKL(P3̄m1) planes equivalent to (100), (200) and (110) planes of the CsCl-
type. Comparison of the calculated SFR for the P3̄m1 with that of the CsCl-
type.

NEUTRON DIFFRACTION

(hkℓ)	(HKL)	Sinθ/λ	F(HKL)	$\|F\|^2$	M	$M\|F\|^2$	$\Sigma M\|F\|^2$	SFR(B2 indices) P3̄m1	B2(CsCl)
(100)	(Ī01)	0.166	1.37	1.88	6	11.28	} 56.34	$\|F(200)\|/\|F(100)\|$	
	(101)	0.166	-2.74	7.51	6	45.00		=0.67	= 0.5
(200)	(2̄02)	0.332	2.07	4.28	6	25.68	} 25.68		
	(202)	0.332	0	0	6	0			
(110)	(0Ī2)	0.235	2.07	4.28	6	25.68	} 51.36	$\|F(110)\|/\|F(100)\|$	
	(0Ī2̄)	0.235	0	0	6	0		= 0.95	= 0.71
	(2̄10)	0.235	2.07	4.28	6	25.68			

(after Wang et al.;ref. 37)

Table 3.; Calculated structure factors(for neutrons) for various families of HKL(P3̄m1) planes equivalent to (100), (200) and (110) planes of the CsCl-type. Comparison of the calculated SFR for the P3̄m1 with that of the CsCl-type.

electrode and collected as powder. The powder was then sieved to
provide a sample with particle sizes between 44 to 70 microns.
X-ray diffraction was used to confirm that the powder sample was the
same as the bulk material.

With the TiNi-II crystal structure established, it is possible to
interpret both the 700°C and the 40°C transitions. The 700°C transi-
tion is, as reasoned before, a diffusion involved replacement order-
disorder transition. Therefore, TiNi-I(700°C to its melting point)
is essentially a replacement-disordered B2-type structure, therefore
a bcc. Upon transformation from TiNi-I to TiNi-II, the atomic se-
quence, $-(A-B-B)_n-$ forms in the resulting P$\bar{3}$ml structure in the
following manner proposed by Carter . The mechanism depends upon
the presence of thermally generated vacancies in the B2 structure.
If a nearest neighbor atom moves into a vacancy site, in effect, the
vacancy has moved along a body diagonal. If the vacancy continues
to move in the same direction, the result is the same as if a linear
-Ti-Ni-Ti-Ni- atomic chain had moved along the body diagonal a dis-
tance of $\sqrt{3}(a_o/2)$, where a_o is the cubic unit cell edge as shown
in Fig. 16.

   b. Atomic shear direction at the 40°C transition.

Inasmuch as the 40°C transition is diffusionless, and 'martensitic'
in nature, the atoms undergo a cooperative shear. In order to ascer-
tain the direction of this shear, Wang et al[23] performed a partial
Fourier synthesis including only the super-reflections(encircled
reflections in Fig. 13-b). This Fourier shows only those atoms which
actually participated in cooperative movements during the 40°C tran-
sition.

Based on the theory of diffraction, the electrons of a crystal are
responsible for its diffraction spectra, and conversely the electron
density can be calculated by a Fourier synthesis, once the diffraction
spectra and their phases are known. This is expressed mathematically
as follows:

$$\rho(\bar{r}) = 1/V \sum F(\bar{H})\exp(2\pi i \bar{H} \cdot \bar{r})$$

   where $\bar{H}$ is the diffraction vector expressed in terms of
   h,k, ℓ, the Miller indices and V is the unit cell volume.

When a structure is composed of a sub- and super-structure, the sub-
structure is defined[46] as that part of the electron density which
conforms to the sub-structure period; whereas the super-structure
is that portion of the electron density which does not conform to
the sub-structure period. With this definition, it is easy to see
that the 9 Å repeat created during the 40°C diffusionless atomic shear
is equivalent to a super-structure. Since the super-reflections are
caused by the super-structure, a Fourier synthesis based on super-
reflections alone should ield a scaled down electron density of the
super-structure. In the TiNi case, it should yield the positions of
atoms which participated in shearing. However, in the TiNi case, the
Fourier synthesis is hampered in two ways; a) symmetry-independent
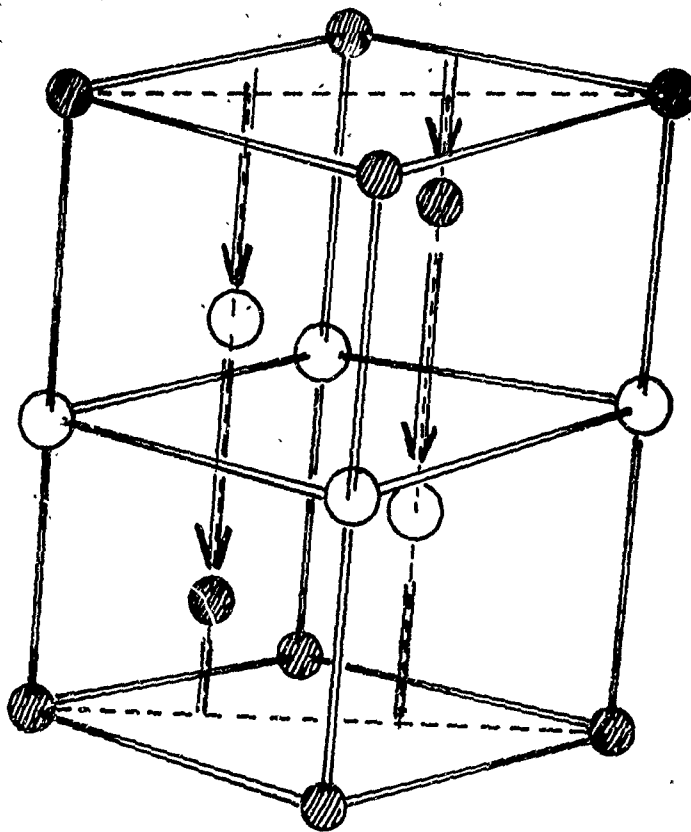
Fig. 16

(after Carter; ref. 30)

Fig. 16.; Arrows points to the atoms which moved $a_3/2$ in order to affect the transformation.

reflections are too few in number and b) phases of the super-reflections are unknown. In order to circumvent these difficulties, Wang et al[23] resorted to a graphic method which is based on the close relationship between the distribution of atoms and the Miller indices of the observed reflections, e.g., the intense 200 reflection implies an atomic separation of $a_0/2$. In this manner, atomic position which satisfy all the super-reflections can be found by plotting the graph shown in Fig. 17. In this plot, 13 nodes can be detected along the diagonal. These 13 nodes can be rationalized by referring to the (110) plane shown in Fig. 18. If atoms were to shear in the <111> direction as shown by arrows, 13 nodes would be created just as shown in Fig. 17. This conclusion was later supported by the electron diffraction work of Marcinkowski et al[34] who also found the direction of shear to be in the <111> .

III. MECHANISM OF TiNi MARTENSITIC TRANSFORMATION

A. Structure of TiNi-III('Martensite')

By assuming atoms to shear in the <111> direction and assuming an 'inhomogeneous' model of shear, Wang[47] worked out a detailed transformation-mechanism from a B2(CsCl)-type to a triclinic(P$\bar{1}$) structure. Followed by a sub-micro twinning, a final structure(P1) is obtained as follows:

Mechanical twinning is thought to be achieved by homogeneous shear which conforms to the macroscopic observation. Homogeneous shear is completely defined[48,49] by K_1, the twin plane; K_2, the second circular section; n_1, the direction of shear and n_2, the axis of the principal zone. In addition, S, the shear plane and s, the crystallographic shear are used. Homogeneous shear has been accepted as the atomic mechanism of mechanical-twin formation for A2(bcc)-type structure. The basic unit of shear is (1/6)[111] and the displacement of a row of atoms is proportional to its distance from the twin plane, K_1 with the factor sequence, (FS), 0-1-2-3-4---- as in Fig. 19-a. In contrast to the homogeneous shear model, the inhomogeneous shear model has a FS, $-(0-1-\bar{1})_n-$ where $\bar{1}$ indicates shearing in the reverse direction, as shown in Fig. 19-b. The homogeneous and in-homogeneous shear models are therefore the two atomic mechanisms through which a reflection-twin can be achieved in an A2 structure.

Although a B2(CsCl)-type structure has an A2(bcc) configuration†, the mechanical twin-elements for an A2(bcc) structure, when applied to a B2-type structure, do not produce a reflection-twin, regardless of whether a homogeneous or inhomogeneous shear model is used. The homogeneous model leads to a tetragonal structure with P4/mm symmetry whereas the inhomogeneous model leads to a trigonal structure with P$\bar{3}$m1 symmetry as shown in Fig. 20. Therefore, mechanical-twinning of a B2 structure must be explained by a different mechanism than that used for an A2 structure.

† 'Configuration' here means the structure in which atomic ordering has been ignored.

Fig. 17

NOLTR 72-4
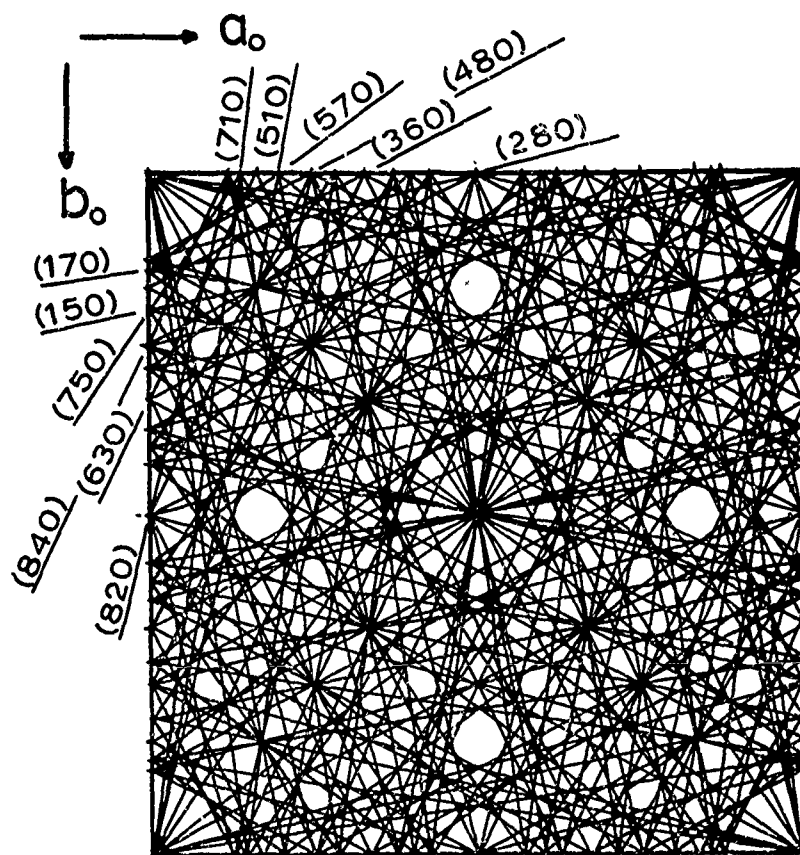
(after Wang et al.; ref.23)

Fig. 17.;A two-dimensional Fourier projection cal-
culated from the (150),(170),(280),(480),(360) and
(570) super-reflections observed in Fig. 13-(b);13
nodes are observed along the diagonal of the square.

Fig. 18

NOLTR 72-4

◆—◆ :Ti–Ti distance(in metal) ≈ 2.89 Å

●—● ; Ni–Ni distance(in metal) ≈ 2.49 Å
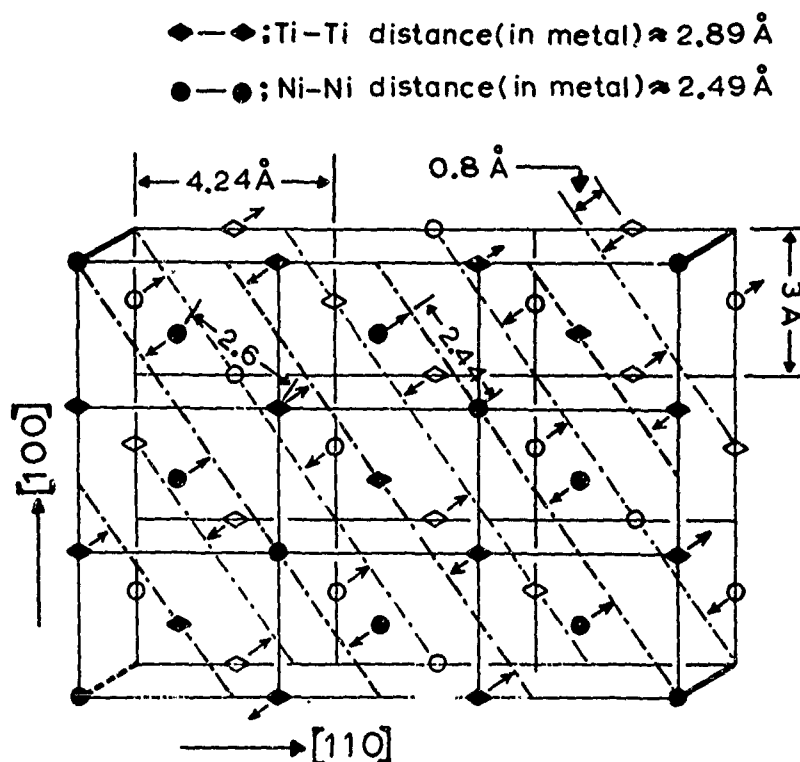
(after Wang et al.; ref. 23)

Fig. 18.;The (1$\bar{1}$0) plane of the TiNi-II structure whose orientation is shown in Fig. 6. The approximate directions of the atomic shear as indicated by arrows is in 111 of the CsCl structure. The dotted lines indicate the possible final positions of the atoms.

Fig. 19
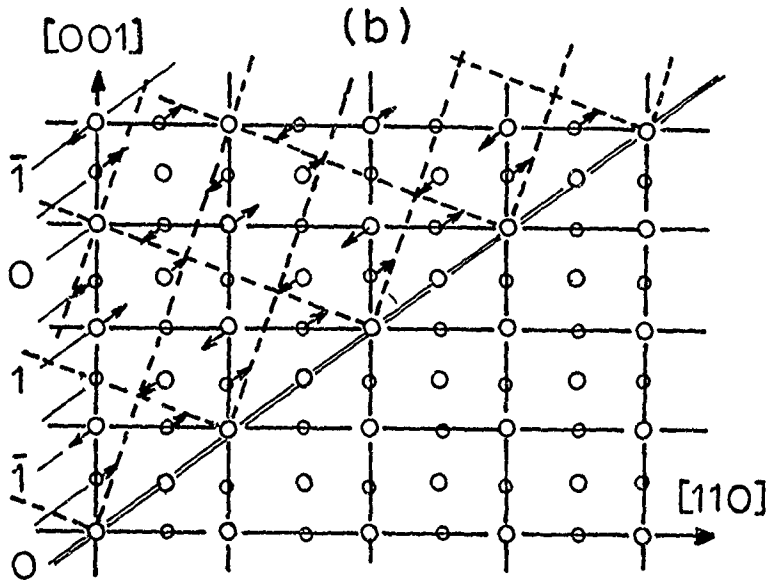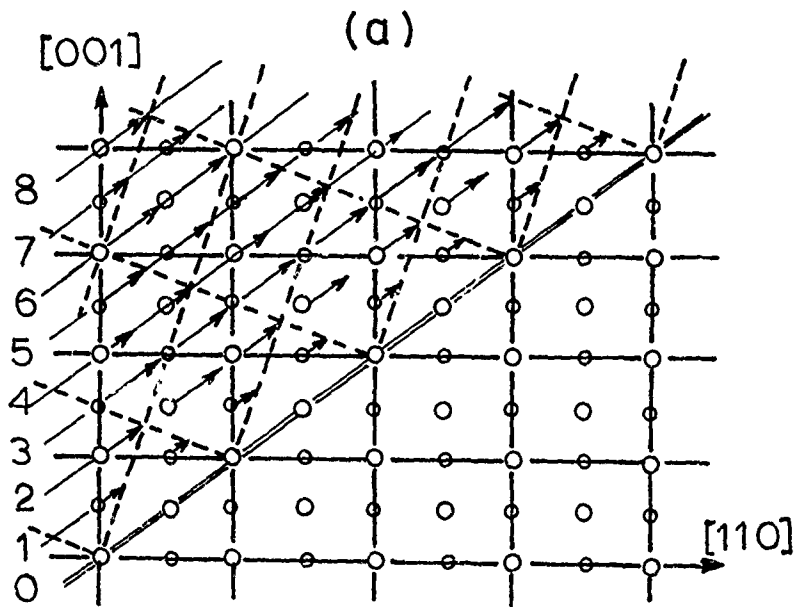
(after Wang; ref. 47)

Fig. 19.;(a) Homogeneous(simple) shear on the (1$\bar{1}$0) plane of an A2(bcc) structure leading to a twin(dotted line). (b) Inhomogeneous shear model on the (1$\bar{1}$0) plane of an A2(bcc) structure leading to a twin(dotted line).

38
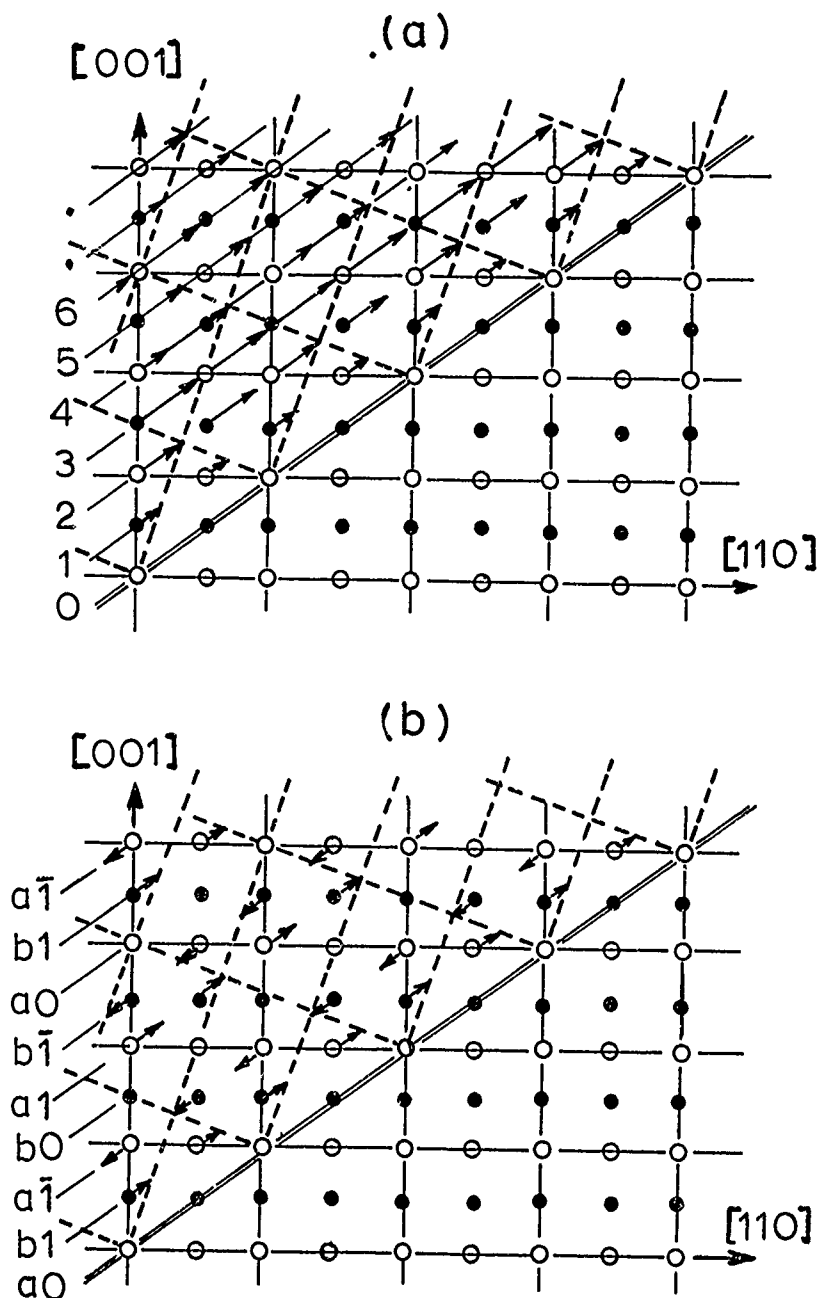
Fig. 20

(after Wang; ref. 47)

Fig.20.; (a) Homogeneous(simple) shear on the (1$\bar{1}$0) plane of a B2(CsCl) structure leading to a tetragonal structure with P4/mmm symmetry. (b) Inhomogeneous shear on the (1$\bar{1}$0) plane of a B2 structure leading to a trigonal structure with P$\bar{3}$m1 symmetry.

Nevertheless, because the basic unit of shear, (1/6)[111], in the A2 structure is based on the requirement that the shear vector, $\bar{T}$, must be the least of all possible vectors giving rise to the twinned state[50] the following conclusion is possible. So long as the structure under consideration has an A2 configuration and so long as the shear movement are within interatomic distances and cooperative(such as those found in martensitic transformations), the basic unit of the shear vector will be (1/6)[111] and the shear will be inhomogeneous. Transformation-twinning of a B2-type structure satisfies these conditions, and the B2 $\longrightarrow$ P$\bar{1}$ transformation is described below.

1. Triclinic(P$\bar{1}$) structure.

Let us assume that the shear vector is aligned in the <111> direction throughout the following discussion. Then, three of the six {110} planes,(1$\bar{1}$0), (10$\bar{1}$), (0$\bar{1}$1) will be parallel to the shear vector and the other three,(110), (101) and (011) will not . These two distinct groups of planes will be referred to hereafter as the parallel and the nonparallel planes. With a FS such as $-(0\text{-}1\text{-}\bar{1})_n-$ taking place exclusively on the (1$\bar{1}$0) plane, there are two ways to construct a 3-dimensional structure. Either the b0 rows of atoms fall between the a1 and a$\bar{1}$ rows of atoms(which leads to a structure with P$\bar{3}$m1 symmetry) or the b0 rows of atoms fall immediately adjacent to the a0 rows of atoms(which leads to a structure with P$\bar{1}$ symmetry). In the former case, the shear movements throughout the lattice as a whole are inhomogeneous and non-cooperative; in the latter case, they are inhomogeneous but cooperative. Inasmuch as martensitic transformations involve cooperative shear of atoms, only the latter case need be considered.

In Fig. 21-a, the relationship between the unit cell constants of the P$\bar{1}$ structure and those of the B2 structure is shown. The vertical view along the [100] direction of the B2 structure shows subsequent planes of atoms with 0,1 and $\bar{1}$ cooperative shears along the (0$\bar{1}$1) plane(Fig. 21-b). The triclinic structure thus derived belongs to space group, P$\bar{1}$, and has six atoms per unit cell as follows:

Atom A; 1(a);   0,   0,   0

         2(i); $\pm$ X $\pm$ Y $\pm$ Z

         (with X = 1/2, Y = 1/6, Z = 1/3)

Atom B; 1(e);   1/2,   1/2,   0

         2(i); $\pm$ X, $\pm$ Y, $\pm$ Z

         (with X = 0, Y = 1/3, Z = 1/3)

The lattice correspondence between the two structure is

$$
\begin{pmatrix} a_1 \\ a_2 \\ a_3 \end{pmatrix}_{P\bar{1}} = \begin{pmatrix} 0 & 1 & 1 \\ 1 & 0 & 0 \\ 0 & 1 & \bar{2} \end{pmatrix} \begin{pmatrix} a_0 \\ a_0 \\ a_0 \end{pmatrix}_{B2}
$$

Fig. 21

(after Wang et al; ref 47)

Fig. 21.; (a) The b0 row of atoms falls immediately adjacent
to the a0 row of atoms. The unit cell constants of the transformed
structure goes from the a layer to the b layer.
        (b) Planes of cooperatively shearing atoms along the
(0$\bar{1}$1) plane. (projection along <100>)

41
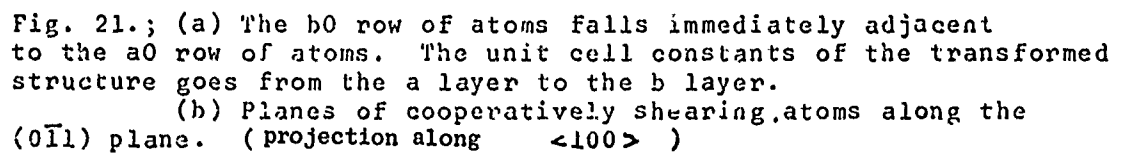
with $\alpha = 90°$, $\beta = 108.4°$ and $\gamma = 90°$ for the $P\bar{1}'$ structure.

Two distinct modes of twinning and one mode of trilling are possible in the course of the B2 $\longrightarrow$ P$\bar{1}$ transformation. The first mode of reflection-twinning(Mode-I) arises from the fact that there are two ways in which the b0 rows of atoms can be placed adjacent to the a0 rows of atoms; either along [100] or along [010]. These two choices are equivalent to the b axes of the P$\bar{1}$ structure being parallel to [100] or [010] of the B2 structure. The twin plane for Mode-I twinning is therefore $(1\bar{1}0)$ of the B2 structure and $(11\bar{1})$ of the P$\bar{1}$ structure(Fig. 22-a). The second mode of twinning(Mode-II) arises from the fact that within the inhomogeneous model described above, two types of FS are possible; $-(0-1-\bar{1})_n-$ and $-(0-\bar{1}-1)_n-$. In a 2-dimensional structure, the $-(0-1-\bar{1})_n-$ FS leads to a bcc lattice(Fig.23-a), whereas the $-(0-\bar{1}-1)_n-$ FS gives an oblique lattice(Fig. 23-b). The two structures are distinctly different and appear to have no relationship to one another. In extending to 3-dimensional structure, the two types remain distinct if each b0 row of atoms falls between an a1 and a$\bar{1}$ row of atoms. However, if the b0 row of atoms falls next to the a0 row of atoms as shown in Fig. 21-a, the two structures are actually reflection twins of one another. This can be visualized in the following manner.

If the FS, $-(0-1-\bar{1})_n-$ operates exclusively on the $(1\bar{1}0)$ plane, the projected structure on the $(1\bar{1}0)$ plane and on the other two parallel planes, $(10\bar{1})$ and $(0\bar{1}1)$, will be A, B and C as shown in Figs. 24-a, 24-b and 24-c. The projected structure B is actually the structure based on the other FS, $-(0-\bar{1}-1)_n-$. That is, both FS actually coexist in the P$\bar{1}$ structure but in different orientations. Mode-II twinning is therefore generated when both FS exist simultaneously on one of the $(1\bar{1}0)$-type parallel planes. The twin plane for Mode-II twinning is therefore $(0\bar{1}1)$ of the B2 structue and (001) of the P$\bar{1}$ structure as shown in Fig. 22-b.

A combination of Mode-I and Mode-II twinning results in an overt P3m symmetry and therefore a trilling as shown in Fig. 25. One more possible twinning occurs when a crystal of B2 structure is already growth-twinned prior to the transformation. In this case, the two twinned domains can simultaneously undergo shearing and yet leave the twin-plane unchanged as shown in Fig. 26.

Using the TiNi powder obtained by Buehler and Wang[45] and the mechanism of the B2 $\longrightarrow$ P$\bar{1}$ transformation described above, Wang, Pickart and Alperin[51] proceeded to establish the TiNi-III structure.

Experimentally, an X-ray powder diffraction pattern was obtained with a Picker Horizontal Diffractometer using Cu Kα radiation. Temperature control was effected by use of a semiconducting thermo-electric element. The element was soldered onto a copper block whose temperature was maintained constant by an internal water-flow. A chromel-alumel thermo-couple was soldered to the surface of the thermo-electric element directly adjacent to the sample. A power supply capable of delivering 5 amps. at 2 volts was used to power the thermo-electric element. In

Fig. 22

NOLTR 72-4

(a)

[010] [100]

(b)

[010] [001]
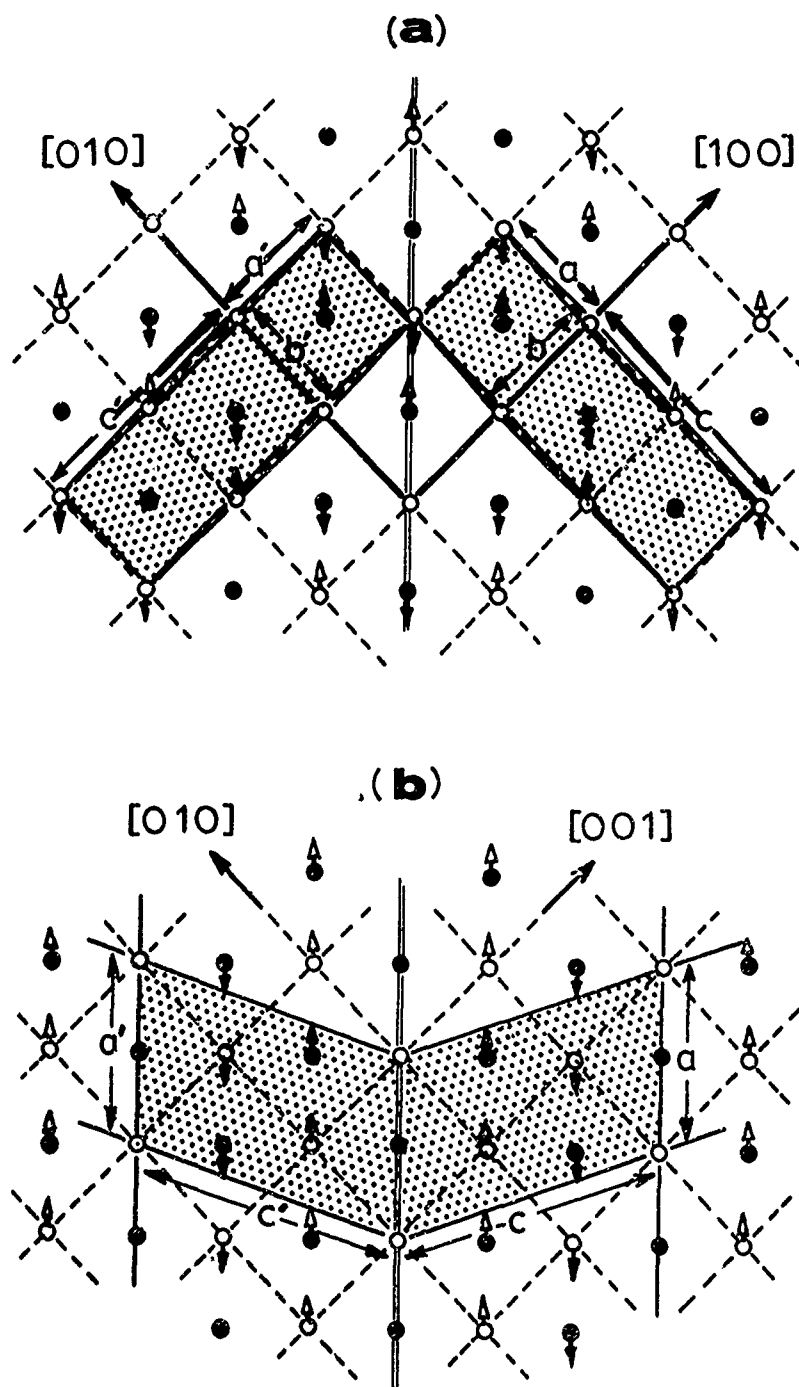
(after Wang et al.; ref.51)

Fig. 22.; (a) Mode-I twinning along the (1Ī0) plane of
a B2 structure;(open arrows are shear in <111> ; solid
arrows are shear in <ĪĪĪ> . (b) Mode-II twinning along
the (1Ī0) plane of a B2 structure.
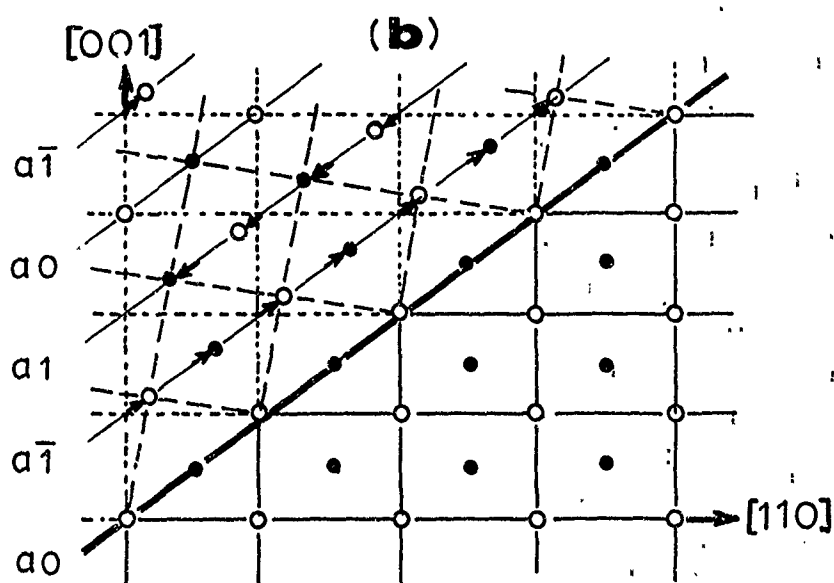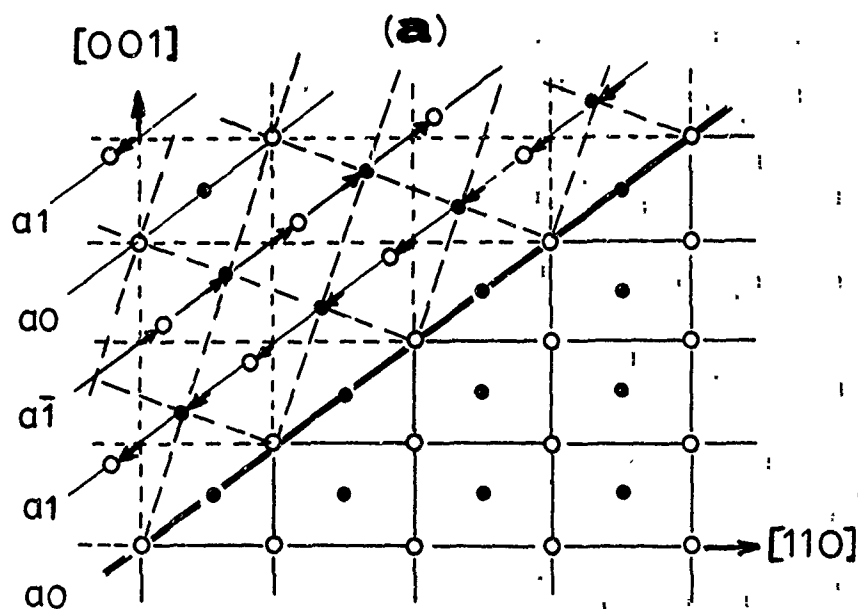
Fig. 23

(after Wang.; ref. 47)

Fig. 23.; The transformed structure based on the
-(0-1-$\bar{1}$)$_n$- factor sequence (a) and the structure
based on the -(0-$\bar{1}$-1)$_n$- factor sequence - (b).

Fig. 24
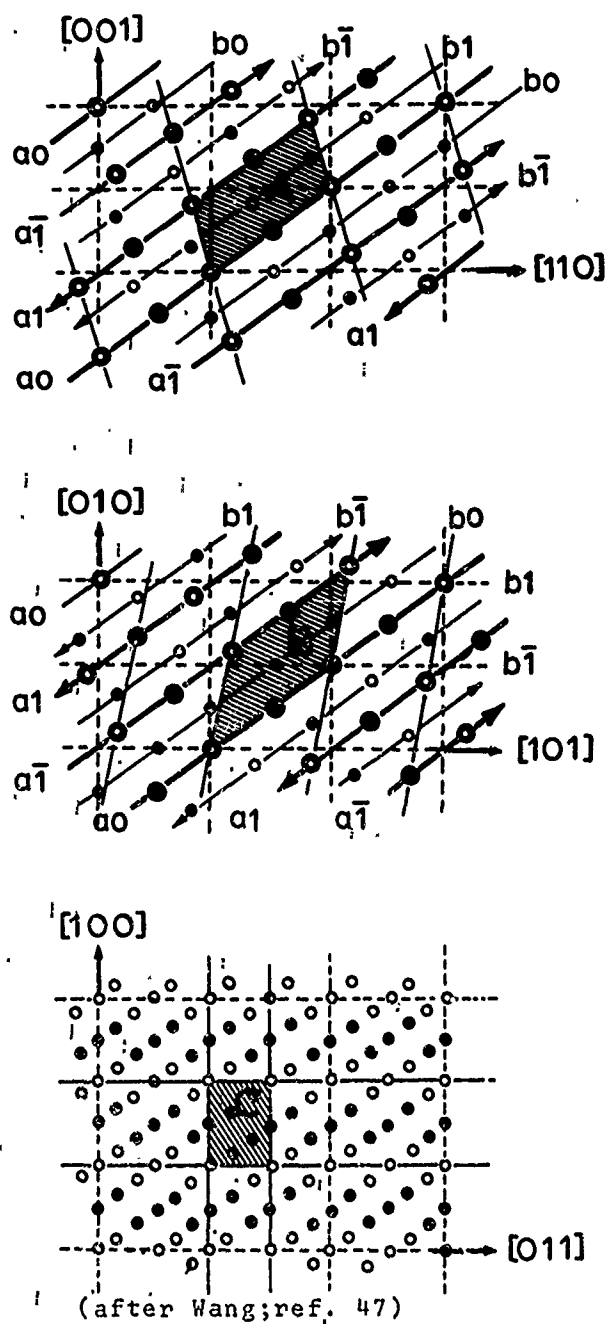
(after Wang;ref. 47)

Fig.24;The structures,A,B and C projected
onto the (1$\bar{1}$0),(10$\bar{1}$) and (0$\bar{1}$1) parallel
planes(double circles are the a layer;
single circles are the b layer).
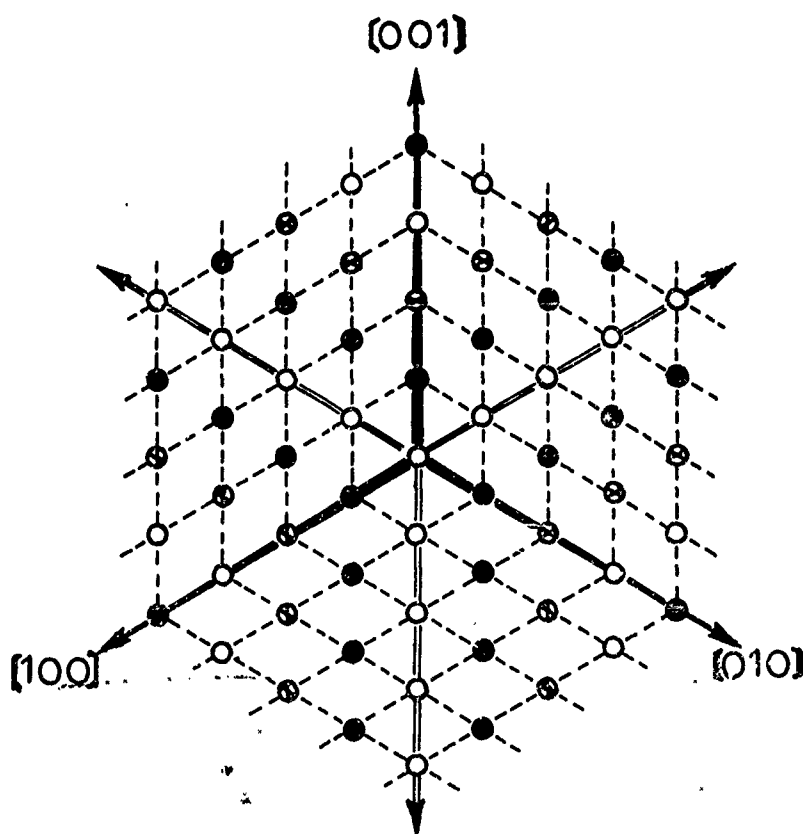
Fig. 25

(after Wang.; ref. 47)

Fig. 25.; Trilling produced by the coexistence of
two modes of twinning.(solid lines are Mode-I
twinning; open lines are Mode-II twinning; atoms.
shear vertically to the paper; ●-downward, ⊗ -
upward and O - stationary).

Fig.26

(after Wang.; ref. 47)
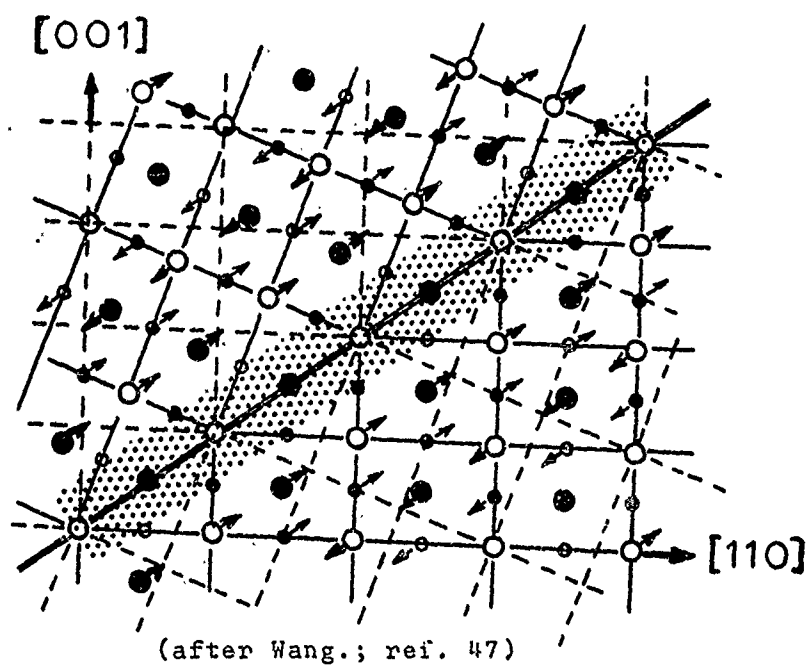
Fig. 26.; Twinned crystal in the B2 structure
(solid line) remains twinned after a transfor-
mation shear(dotted line). (Large circles are
the a layer and small circles are the b layer;
open lines are the twin plane).

this manner, the sample temperature could be varied from, -20°C to
80°C simply by varying the current and its flow-direction(the flow-
direction determines whether sample temperature is higher or lower
than the reference temperature). The whole assembly was enclosed in
a vacuum chamber equipped with a beryllium window. Powder patterns
were obtained at the intervals of 3° 4°C between -10° to 80°C, and
in critical areas, at one degree centigrade intervals.

Low and high temperature neutron diffraction patterns were obtained
with the reactor at National Bureau of Standards(Gaithersburg,
Maryland). For work between 4°K and R.T., a standard low temperature
large diameter aluminum cryostat was used. Six runs were made in this
temperature range. For temperatures between R.T. and 80°C, patterns
were obtained approximately at 5°C intervals. In all cases, a
crystal monochromated beam of $\lambda = 1.11$ Å was used.

A few initial assumptions made by Wang et al[51] were:

    a. The structure of TiNi-II is B2-type.

    b. During the transition from TiNi-II to TiNi-III, an inhomo-
geneous but cooperative atomic shear takes place in the <111>
direction, as established earlier in the single crystal study of
Wang et al[23], but without distortion of the original lattice.

    c. A factor sequence, $-(0\text{-}1\text{-}\bar{1})_n-$, is present in $(1\bar{1}0)$ plane.

Under these conditions and with the shear-vector,(1/6)[111] completed,
a new structure(Structure A) with space group $P\bar{1}$ as shown in Fig.
27-a is obtained. Crystallographic data and the calculated powder
patterns of Structure A for both X-ray and neutron diffraction are
given in Table 4. When FS, $-(0\text{-}\bar{1}\text{-}1)_n-$ is present in $(1\bar{1}0)$, Structure
B(Fig. 27-b) a reflection-twin of Structure A is obtained. It can
be shown that the powder pattern of Structure B is identical to that
of Structure A. Neither structure, however, is acceptable as the
'martensite' because the calculated powder pattern has far fewer
reflections than are observed within a given 2θ range.

    2. Triclinic(P1) structure.

The fact that Structures A and B are reflection-twins of one another
and that shear-strain can be minimized by the formation of fine-twins
(e.g., as small as a few atomic layers) allows the following postulate
to be made. If Structure A and Structure B were to intertwin with
one another on a sub-micro scale as shown in Fig. 27-c, a new struc-
ture whose c axis is twice that of Structure A or B will result.
Structure C is non-centrosymmetric and belongs to space group P1.
Crystallographic data and the calculated powder pattern of Structure
C are given in Table 5. It is observed that there is a general
agreement, particularly with regard to the number of reflections in
a given 2θ range, between the calculated and the observed patterns
for both X-ray and neutron diffractions.

Observed reflections with high intensities for both X-ray and neutron

Fig. 27

structure A

structure C

structure B

(a)

(b)

(c)
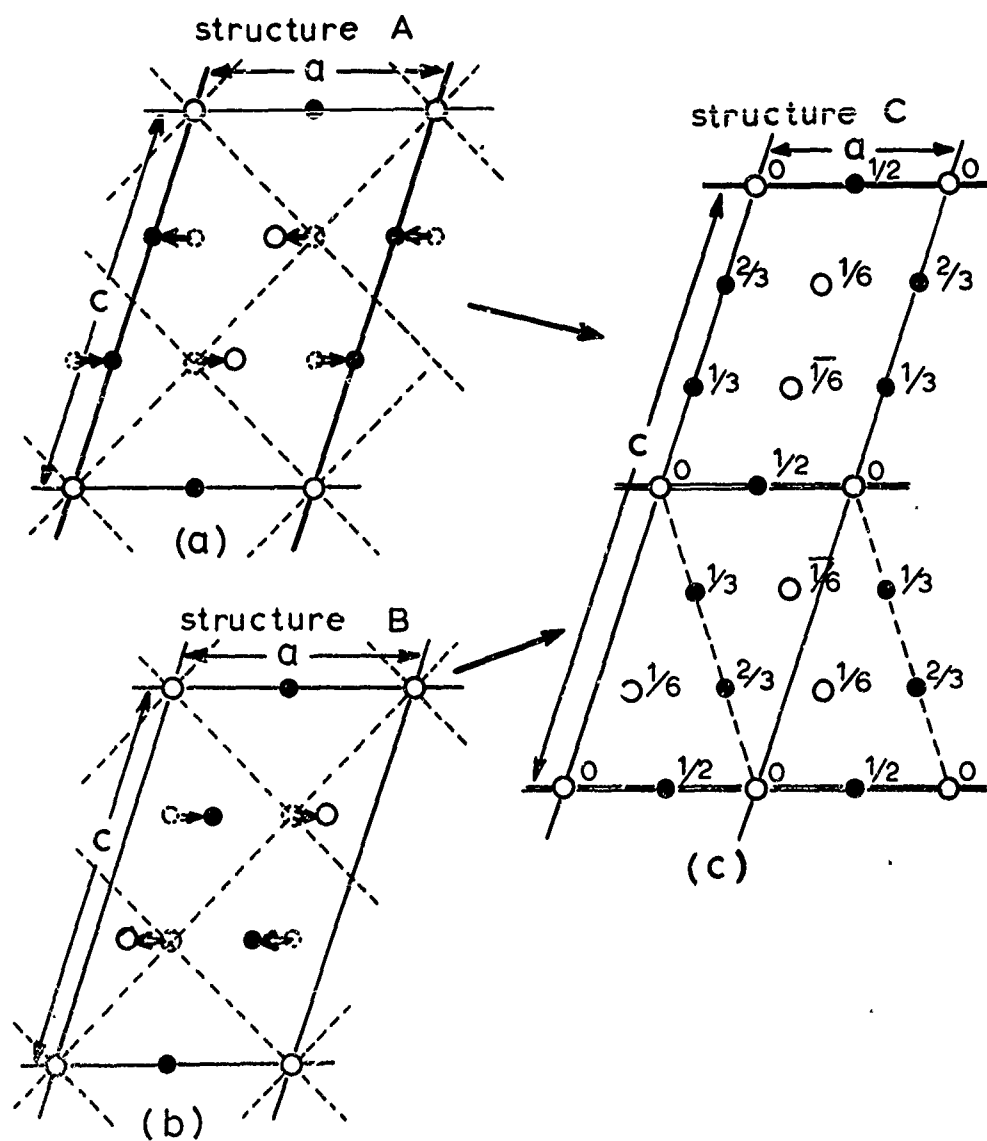
(after Wang et al.; ref. 51)

Fig. 27; Structures A, B and C. In (a) and (b), dotted lines and dotted circles indicate the B2 lattice and their atomic positions respectively(open circles at y = 0; solid circles at y = 1/2). Arrows show projected shear-vectors. In (c), double lines represent twin-planes.

Table 4

NOLTR 72-4

Triclinic(P1); Structures A or B.

Lattice Constants:
a = 4.24, b = 3.00, c = 6.70 Å; α = 90°, β = 108.4°, γ = 90°

Atomic Positions:

| Ti: | 0, | 0, | 0 | Ni: | 1/2, | 1/2, | 0 |
| ±(| 5/6, | 5/6, | 2/3) | ±(| 1/3, | 1/3, | 1/3) |

h	k	l	X-ray(1.54 Å) 2θ	I_c	h	k	l	Neutron(1.11 Å) 2θ	I_c
-1	1	0	37.36	209	1 0 0 / -1 0 1 }			15.86	25
1 1 1 / -1 -1 2 / 0 0 3 }			42.60	423	0 1 0 / 1 0 1 / -1 0 2 }			21.32	33
-2	0	2	45.06	119	0 -1 1 / 0 1 1 }			23.60	11
2 0 1 / -1 -1 3 }			51.76	154	0 -1 2 / -1 0 3 }			29.48	12
0	2	1	63.68	76	1 1 1 / -1 -1 2 / 0 0 3 }			30.34	9
0	-2	2	69.20	30	-2 -1 1 / 0 -1 3 / 0 1 3 }			37.40	12

(after Wang et al; ref. 51)

Table 4.; Crystallographic data and calculated X-ray and neutron powder diffraction patterns for the P1̄ structure (Structure A or B). Claculated intensities are based on

$I_c(hkl) = k \cdot M \cdot Lp \cdot F_c(hkl)$, where k = proportionality

constant, M = multiplicity factor, Lp = Lorentz and polarization factor. Planes with calculated relative intensities less than 10 in X-ray and less than 6 in neutron diffraction patterns are not listed.

Table 5

NOLTR 72-4

Triclinic(P1); Structure C.

Lattice Constants:
a = 4.24, b = 3.00, c = 13.4 Å; α = 90°, β = 108.4° and γ = 90°

Atomic Positions:

T1:				N1:		
0,	0,	0		1/2,	1/2,	0
0,	0,	1/2		1/2,	1/2,	1/2
1/2,	1/6,	1/6		0,	2/3,	1/6
1/2,	5/6,	1/3		0,	1/3,	1/3
5/6,	5/6,	2/3		1/3,	1/3,	2/3
1/6,	1/6,	5/6		2/3,	2/3,	5/6

h	k	l	X-ray(1.54 Å) 2θ	I_c	h	k	l	Neutron(1.11 Å) 2θ	I_c
-1	1	1 }	36.66	172	-1	0	1	15.04	22
0	1	3 }			0	1	0		
0	-1	3 }			0	1	0 }	21.32	90
					1	0	2 }		
-1	1	0 }	37.36	248	-1	0	4 }		
-1	-1	2 }							
-1	1	2 }			0	1	1 }	21.92	11
					0	-1	1 }		
1	-1	1 }	39.38	80					
-1	1	3 }			1	0	3 }	25.21	11
					0	0	5 }		
1	1	2 }	42.62	1356	-1	0	5 }		
-1	-1	4 }							
0	0	6 }			-1	1	1 }	26.20	49
					0	1	3 }		
-2	0	1 }	43.22	74	0	-1	3 }		
-2	0	3 }							
					-1	1	0 }	26.68	10
2	0	0 }	45.02	214	-1	1	2 }		
-2	0	4 }							
					1	1	2 }	30.34	51
1	-1	3 }	46.78	68	-1	-1	4 }		
-1	1	5 }			0	0	6 }		
2	0	1 }	47.92	272	2	0	0 }	32.14	22
-2	0	5 }			-2	0	4 }		
					0	1	5 }		
1	-1	4 }	51.76	380					
2	0	2 }			2	0	1 }	34.02	33
-1	1	6 }			1	0	5 }		
-2	0	6 }			-2	0	5 }		
2	0	3	56.44	29	1	-1	4 }	36.66	15
					2	0	2 }		
1	-1	5	57.44	115	-1	1	6 }		

(after Wang et al; ref. 51)   Table 5.

diffraction were then fitted with calculated values by varying the lattice constants. This produced the new lattice constants:

$$a = 4.17 , \quad b = 3.11 , \quad c = 12.55 \text{ Å}$$
$$\alpha = 96.6°, \quad \beta = 105.18, \quad \gamma = 84.09°.$$

Needless to say, this set of lattice constants was not unique and other solutions were also possible. The choice of this solution over the others at this stage was based on criteria which are in keeping with the phenomenon of diffusionless cooperative atomic shear. They are:

     a. The new lattice constants should not deviate too much from those calculated from the undistorted A2 lattice.

     b. The changes in lattice constants should be predominantly in interaxial angles, ie., deviations in cell edges should be small.

     c. The new lattice should yield the best fit between the calculated and observed powder patterns both with respect to positions(2θ angle) and intensities.

In this context, it is observed that the unit cell edges changed very little compared to the changes that took place in interaxial angles. The new lattice constants gave fair agreement between the calculated and observed. In theory and in practice, where it is feasible, the final matching of powder patterns should be accomplished through a least-squares refinement by the use of a computer. However, this was not practical in this case because the number of experimental data was smaller than the number of parameters to be adjusted. Also, because the data consisted of powder patterns where some observed intensity peaks might be due to two or more unresolved reflections. As an alternative to least-squares refinement, Wang et al.[51] adjusted the atomic parameters based on the following empirical considerations:

     a. Atoms shear in approximately the <111> direction and therefore parallel to $(\bar{1}10)_{B2}$ and $(001)_{P1}$;

     b. In the TiNi-III phase, interatomic bonding is more metallic in character[31] and hence interatomic distances should approach the intermetallic distances for Ti-Ti and Ni-Ni for those atoms involved in shearing.

By assuming the Ti-Ti and Ni-Ni interatomic distances in the metallic state to be 2.89 and 2.49 Å("INTERATOMIC DISTANCES", The Chemical Society, Burlington House W1, London,1958) respectively, a set of atomic positions was assigned. This set of atomic positions was then refined one at a time by calculating a new set of powder patterns each time a new positional parameter was assigned. The final calculated X-ray and neutron diffracton patterns are given in Table 6 and graphically compared to the observed patterns in Fig. 28.

    3. Hexagonal,(P6/m) structure.

The calculated powder pattern based on Structure C(P1) agrees fairly well with the observed,but a few discrepancies remain. In the X-ray pattern, the observed peaks at $2\theta = 19.2°$ and $39.1°$ are not accounted

Table 6

NOLTR 72-4

TiNi-III ('martensite'): P1

Lattice Constants:
a = 4.17, b = 3.11, c = 12.55 Å; α = 96.06, β = 105.18, γ = 84.09°

Atomic Positions:

Ti;				Ni;		
0	0	0		.5	.5	0
0	0	.5		.5	.5	.5
.615	.160	.16666		.069	.665	.16666
.385	.840	.33333		.931	.335	.33333
.718	.840	.66666		.264	.335	.66666
.282	.160	.83333		.736	.665	.83333

h	k	l	$\sin\theta/\lambda$	X-ray(1.54 Å)		Neutron(1.11 Å)	
				2θ	I_c	2θ	I_c
0	0	1	.04140	7.32	0	5.26	0
0	0	2	.08280	14.66	0	10.54	0
-1	0	1	.12082	21.46	22	15.42	12
0	0	3	.12420	22.06	0	15.84	0
1	0	0	.12450	22.12	< 10	15.88	< 3
1	0	2	.13086	23.26	< 10	16.70	< 3
1	0	1	.14082	25.06	< 10	17.98	< 3
-1	0	3	.15191	27.06	< 10	19.42	< 3
0	1	0	.16210	28.92	< 10	20.84	48
0	-1	1	.16398	29.26	18	20.98	8
0	0	4	.16560	29.56	0	21.18	0
1	0	2	.16610	29.66	< 10	21.19	89
0	1	1	.17056	30.46	< 10	21.82	7
0	-1	2	.17588	31.44	< 10	22.52	< 3
-1	0	4	.18017	32.22	12	22.95	76
0	1	2	.18797	33.66	< 10	24.08	< 3
-1	-1	1	.19133	34.28	195	24.52	< 3
-1	-1	2	.19502	34.96	< 10	25.00	0
0	-1	3	.19597	35.14	< 10	25.00	28
1	1	0	.19648	35.24	< 10	25.20	0
1	0	3	.19691	35.32	< 10	25.26	< 3
0	0	5	.20700	37.20	0	26.56	0
-1	-1	3	.20709	37.20	38	26.58	< 3
1	1	1	.20986	37.72	36	26.94	< 3
-1	1	0	.21200	38.12	60	27.22	< 3
0	1	3	.21213	38.14	< 10	27.24	22
-1	1	1	.21246	38.22	339	27.28	9
-1	0	5	.21277	38.26	< 10	27.32	< 3
1	-1	1	.21948	39.52	76	28.20	< 3
-1	1	2	.22083	39.78	61	28.38	< 3
0	-1	4	.22204	40.00	< 10	28.54	< 3
-1	-1	4	.22621	40.88	458	29.18	15
1	1	2	.22999	41.27	434	29.43	14
1	0	4	.23106	41.70	< 10	29.72	< 3
1	-1	2	.23416	42.28	80	30.14	< 3
-1	1	3	.23626	42.68	60	30.40	< 3

Table 6
(2)

NOLTR 72-4

h	k	l	sinθ/λ	X-ray(1.54 Å) 2θ	I_c	Neutron(1.11 Å) 2θ	I_c
0	1	4	.24165	43.80	< 10	31.04	< 3
-2	0	2	.24170	43.80	342	31.15	< 3
-2	0	1	.24185	43.82	27	31.15	< 3
-1	0	6	.24801	44.92	< 10	31.96	< 3
0	0	6	.24840	45.00	478}	32.02	13
-2	0	3	.24846	45.00	54}	32.02	< 3
2	0	0	.24900	45.12	< 10	32.08	< 3
-1	-1	5	.25076	45.44	20	32.32	< 3
0	-1	5	.25224	45.74	< 10	32.52	< 3
1	0-1	3	.25479	46.22	48	32.86	< 3
1	1	3	.25531	46.32	19	32.92	< 3
-1	1	4	.25749	46.74	70	33.22	< 3
-2	0	4	.26172	47.56	< 10	33.78	< 3
2	0	1	.26258	47.72	83	33.90	10
1	0	5	.26725	48.62	< 10	34.52	6}
0	1	5	.27317	49.78	< 10	34.72	7}
-2	-1	2	.27593	50.30	< 10	35.68	35
-2	-1	1	.27808	50.72	< 10	35.96	< 3
-1	-1	6	.27932	50.98	< 10	36.12	< 3
-2	-1	3	.27995	51.10	< 10	36.20	< 3
1	-1	4	.28006	51.12	48}	36.22	< 3
-2	0	5	.28052	51.20	66}	36.28	4
2	0	2	.28164	51.42	< 10	36.44	< 3
-1	1	5	.28322	51.74	33	36.64	< 3
1	1	4	.28442	51.98	< 10	36.80	< 3
0	-1	6	.28527	52.14	< 10	37.02	22
2	1	0	.28626	52.34	< 10	37.06	< 3
-2	-1	4	.28990	53.04	< 10	37.54	< 3
2	1	1	.29998	55.04	< 10	38.90	< 3
-2	1	1	.30363	55.78	< 10	39.40	4
-2	0	6	.30383	55.82	< 10	39.42	< 3
1	0	6	.30479	56.00	< 10	39.54	< 3
2	0	3	.30516	56.08	< 10	39.60	< 3
-2	-1	5	.30518	56.08	< 10	39.60	< 3
-2	-1	2	.30529	56.10	< 10	39.62	< 3
0	1	6	.30753	56.56	< 10	39.82	13}
-2	1	0	.30759	56.82	< 10	39.84	5}
1	-1	5	.30882	56.82	100	40.10	< 3
-1	1	6	.31233	57.52	19	40.56	< 3
-2	1	3	.31247	57.54	< 10	40.58	< 3
1	1	5	.31629	58.32	37	41.10	< 3
2	-1	1	.31695	58.46	< 10	41.15	11
2	1	2	.31853	58.78	< 10	41.42	< 3
0	-2	1	.32345	59.78	< 10	42.08	< 3
0	2	0	.32420	59.92	< 10	42.18	< 3
-2	1	4	.32482	60.06	< 10	42.26	5
-2	-1	6	.32505	60.10	< 10	42.30	< 3
0	-2	2	.32797	60.70	< 10	42.70	< 3
0	2	1	.33018	61.14	< 10	43.00	< 3
2	0	4	.33120	61.18	114	43.08	< 3
2	-1	2	.33126	61.36	< 10	43.12	5

(after Wang et al; ref. 51)   Table 6.
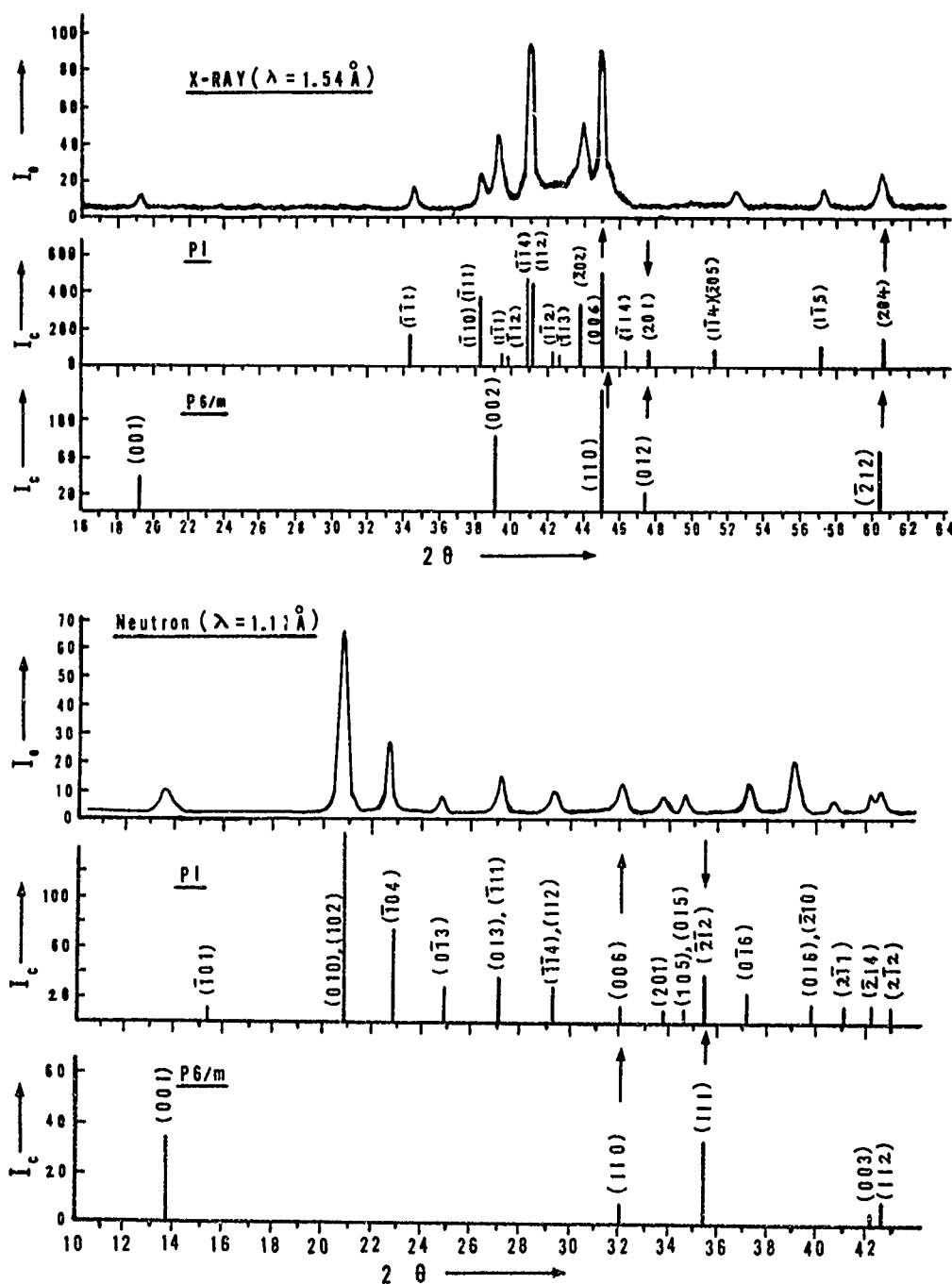
Fig. 28

(after Wang et al., ref. 51)

Fig. 28.; Observed X-ray and neutron powder diffraction patterns of P1(derived from the B2 structure) and P6/m(derived from the P3̄m1). Arrows indicate phases of the calculated structure factor of those overlapping planes between the P1 and and P6/m structures.

for by this model. The observed peak at $2\theta = 41°$ should be approximately twice as high as that at $45°$, according to the model. Experimentally, the two peaks are nearly the same. In the neutron diffraction pattern, the peaks at $2\theta = 3.6°$ and $39°$ are again not accounted for by this model. The calculated 212 reflection at $2\theta = 35.2°$ is completely missing experimentally.

In the only single crystal work on TiNi, Wang et al[23] inferred a cubic super-structure($a = 9$ Å) based on the atomic sequence,-(A-A-B)$_n$- and a P$\bar{3}$m1 trigonal sub-structure for the TiNi-II phase. If a cooperative shear of atoms took place in $<111>_{B2}$ in the P$\bar{3}$m1 structure, the final structure would not be P$\bar{1}$ or P1 but would be hexagonal(P6/m) as shown in Fig. 29. The crystallographic data and the calculated powder pattern of this hexagonal structure are given in Table 7 and graphically shown in Fig. 28. A combination of the calculated intensities from the P1 and P6/m structures resulted in much better agreement with the observed patterns. However, this still leaves some irreconcilable discrepancies; the absence of a peak at $2\theta = 47.3°$ in the X-ray pattern and a similar absence at $2\theta = 35.3°$ in the neutron pattern.

At this point, Wang et al[51] argued that since lattice-wise there is no difference between the B2 and the P$\bar{3}$m1 structures, it is possible for the B2 and P$\bar{3}$m1 structures to coexist in one single crystal such that at transition, the single crystal, composed of both structures, shears cooperatively in the $<111>_{B2}$ direction. This means that diffraction from the B2 and P$\bar{3}$m1 structures should be combined phase-wise instead of intensity-wise.

In the X-ray diffraction pattern there are three pairs of coincident reflections; $(006)_{P1}$ and $(2\bar{1}0)_{P6/m}$ at $2\theta = 45.0°$, $(201)_{P1}$ and $(0\bar{1}2)_{P6/m}$ at $2\theta = 47.3°$, $(204)_{P1}$ and $(\bar{2}12)_{P6/m}$ at $2\theta = 60.5°$.

Phase calculations show that the first and the third pair of reflections are in phase whereas the second pair of reflections at $2\theta = 47.3°$ is out of phase with one another. In the neutron diffraction case, there are only two pairs of coincident reflections; $(006)_{P1}$ and $(2\bar{1}0)_{P6/m}$ at $2\theta = 32.0°$ and $(\bar{2}\bar{1}2)_{P1}$ and $(\bar{2}11)_{P6/m}$ at $2\theta = 35.3°$. In this case, the first pair is in phase but the second pair at $2\theta = 35.3°$ is out of phase. By assuming that the B2 and P$\bar{3}$m1 structures are present in nearly equal proportions and that phase interference exists between the P1 and P6/m structures, the absence of observable peaks at $2\theta = 47.3°$ in the X-ray and $2\theta = 35.3°$ in the neutron diffraction patterns can be reconciled. Logically, this suggests a coexistence of the B2 and P$\bar{3}$m1 structures prior to transition in the TiNi-II phase. However, if the proportions of B2 and P$\bar{3}$m1 are not equal, reflections at $2\theta = 47.3°$ in the X=ray and $2\theta = 35.3°$ in the neutron patterns are still to be expected. In fact, in an X-ray powder pattern study(based on bulk material), deLange and Zijderveld[52] observed reflection at $2\theta = 47.3°$(X-ray) in addition to the peaks observed here, thus substantiating the above explanation.
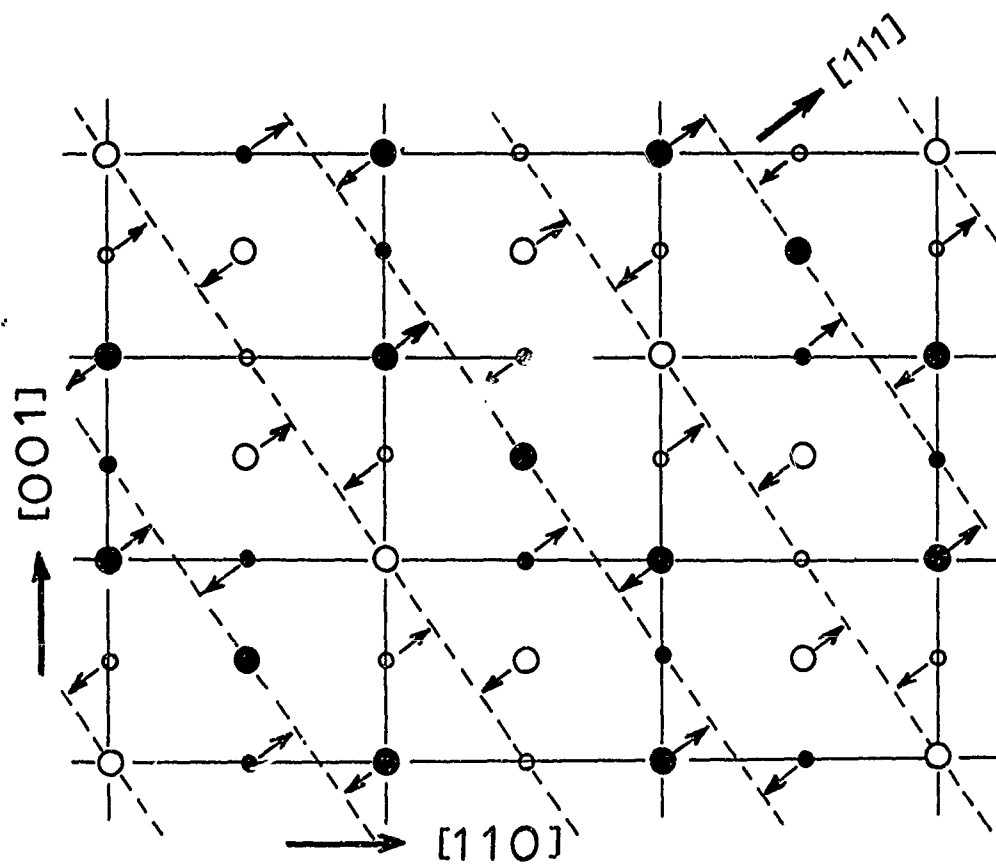
Fig. 29

(after Wang et al. ref. 23)

Fig. 29.; Starting with the P3̄ml structure, atomic shear in <111> leading to the P6/m structure is depicted.(Large circles are on one layer and small circles are on another).

Table 7

NOLTR 72-4

TiNi-III('martensite'); P6/m

Lattice Constants:
a = b = 4.02, c = 4.61 Å; $\alpha = \beta = 90°$, $\gamma = 120°$

Atomic Positions:

T1: $\begin{matrix} 0 & 0 & 0 \\ \pm(2/3 & 1/3 & 0.97) \end{matrix}$ N1: $\begin{matrix} 0 & 0 & 1/2 \\ \pm(2/3 & 1/3 & 0.45) \end{matrix}$

h	k	l (n)*	$\sin\theta/\lambda$	X-ray (1.54 Å)		Neutron (1.11 Å)	
				2θ	I_c	2θ	I_c
0	0	1	.1084	19.24	52	13.82	56
-1	1	0 (3)	.1435	25.54	0	18.34	0
-1	0	1 (6)	.1798	32.18	< 2	23.04	< 1
0	0	2	.2169	39.04	77	27.06	4
-2	1	0 (3)	.2485	45.02	42x3 = 126	32.04	4x3 = 12
-1	0	2 (3)	.2600	47.24	4x3 = 12	33.56	< 1
0	-1	2 (3)	.2600	47.24	3x3 = 9	33.56	< 1
-2	1	1 (6)	.2711	49.38	< 2	35.04	9 x6 = 54
-2	2	0 (3)	.2870	52.48	0	37.16	0
-2	2	1 (3)	.3068	56.42	< 2	39.82	< 1
-2	0	1 (3)	.3068	56.42	< 2	39.82	< 1
0	0	3	.3253	60.16	6	42.34	5
-2	1	2 (6)	.3261	60.51	12x6 = 72	42.66	2x6 = 12

(after Wang et al; ref. 51)

Table 7.; Crystallographic data and calculated X-ray and neutron powder diffraction patterns for the P6/m structure derived from P$\bar{3}$m1 structure; n - number of reflections with the same Bragg angle.
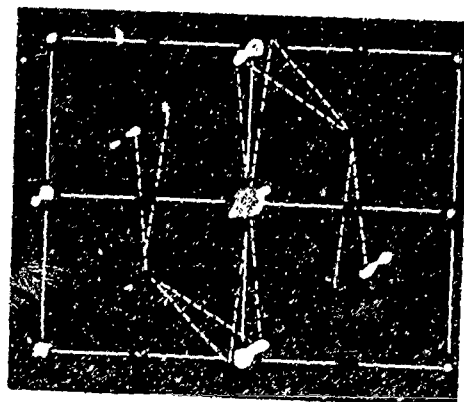
B. Electron Diffraction

The mechanism of the B2 → PĪ transformation and the proposed twinning will now be tested in light of the electron diffraction data obtained previously by other investigators. Figs. 30-a, b and c are the (110) plane electron diffraction photographs of the TiNi-III phase ('martensite') obtained independently by Marcinkowski et al.[34], Chandra and Purdy[32] and Otsuka and Shimizu[36]. It is clear that despite the fact that all were taken with the foil plane parallel to (110), the photographs are different from one another. Understandably, the authors of each paper interpreted only their own data and derived three different postulates; Chandra and Purdy in terms of phonon scattering; Marcinkowski et al, in terms of M and M' martensites; Otsuka and Shimizu in terms of precipitates.

Before analyzing these three electron diffraction patterns individually, it is well to make some comment collectively. When the shear-vector is in <111>, the six orginally equivalent {110} planes are divided into two types; Type-I, including (1Ī0), (10Ī) and (0Ī1) which are parallel to <111>, and Type-II including (110),(101) and (011) which are not parallel to <111>. When the FS is parallel to (1Ī0), further subdivision takes place among the two types. Within Type-I, (1Ī0) and (10Ī) are identical but distinct from (0Ī1). This is to say that once atomic shear takes place, the six formerly equivalent {110} planes become distinct and fall into four categories depending on the orientation of the plane relative to the shear-vector and to the FS plane. This explains immediately the possibility of obtaining different results by different groups of investigators.

As described in detail in the paper by Wang[47], twinning-II essentially is the result of two choices in FS stacking in (1Ī0) planes; along <100> or <010>. If the stacking sequence is irregular(as expected for electron diffraction specimens which are extremely thin), the disorder in the crystals is anisotropic with one degree of freedom being parallel to the electron beam, i.e., perpendicular to the foil plane. Therefore, electron diffraction data from such crystals should be interpreted in terms of a 2-dimensional structure. For this reason, projected structures are used throughout the following discussion.
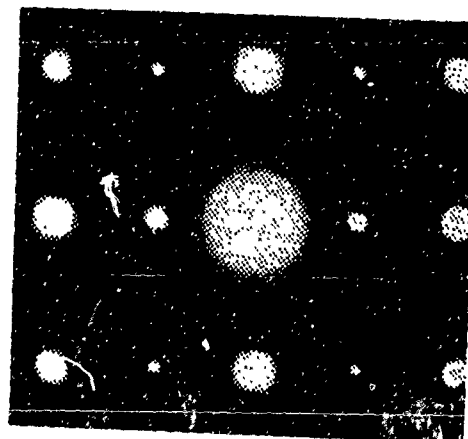
On the data from Marcinkowski et al.(ref. 34)

With the shear-vector in <111> and the FS in (1Ī0), the projected structures along (1Ī0), (10Ī), (0Ī1) after completion of shear are shown in Fig. 24. These structures are definable in terms of unit cells, A, B and C, whose reciprocal lattices, A^*, B^* and C^* are shown side by side in Fig. 31-b and compared with that of M and M' given by Marcinkowski et al.(Fig. 31-a). It is immediately obvious that there is a one to one correspondence between the M and M' martensites and the A and B structure given by Wang et al.[51]. The only difference is in the angle θ, as defined in the paper by Marcinkowski et al. This angle is larger in A and B than in M and M'. However, it is clear that this angle is entirely dependent upon the degree of shear and would be samller if the magnitude of shear was less than
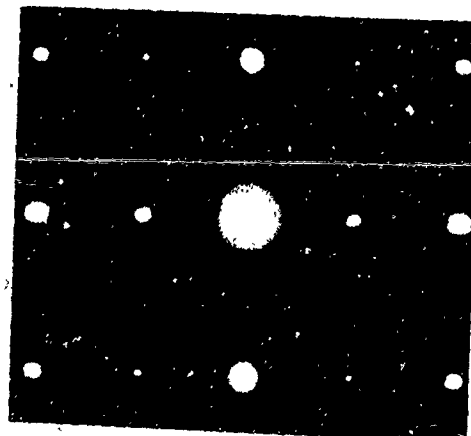
Fig. 30

NOLTR 72-4

(c)

Otsuka & Shimizu
ref. 20

(b)

Chandra & Purdy
ref. 19

(a)

Marcinkowski et al.
ref. 13

Fig. 30.; Electron diffraction pattern on the (110) plane, of TiNi-III
obtained by various investigators.

Fig. 31

(after Marcinkowski et al.ref.34)   (after Wang et al.;ref. 51)

Fig. 31.; (a) The M and M' martensites proposed by Marcinkowski et al is compared with (b) the reciprocal lattices, A*, B* and C* given by Wang et al.

the unit of shear, 1/6[111]. As demonstrated above in the X-ray and neutron diffraction patterns, the atoms in fact shear much less than 1/6[111]; therefore, the angle θ should be smaller than indicated in the A and B structures. Inasmuch as Structure C actually gives a reciprocal lattice identical with that of the B2-type, it is possible to mistake Structure C for a B2 structure. The mechanism proposed by Marcinkowski et al. for arriving at the M and M' martensites was restricted to 2-dimensional case and was essentially a 'simple' shear model. This may fail in the 3-dimensional case as was pointed out by Wang et al.[47] . This weakness(reflected in the authors' inability to describe properly atomic movements out of the 2-dimensional plane considered) resulted in their proposal of inhomogeneous and non-cooperative movements of atoms in the third dimension. This also is, in part, responsible for the authors' erroneous conclusion that the martensites M and M' are not reflection-twins of one another. Based on these observations, it can be concluded that in this particular experiment the shear-vector happens to lie in the foil plane and is lined up along a unique <111> direction.

On the data from Chandra and Purdy(ref. 32)

The data obtained by Chandra and Purdy consists of two parts. The first part, ill-defined diffuse maxima along the reciprocal planes (112)* and (11$\bar{2}$)*, are essentially in the same lattice framework as those obtained by Marcinkowski et al. except that they occur in both directions. Therefore, it can be concluded that these ill-defined maxima resulted from that portion of matrix(within the 'selected' area) whose shear-vector was parallel to the foil plane but aligned in both of the two possible directions <111> and <$\bar{1}\bar{1}$1>. It is believed that the coexistence of these two possible shear-vectors and their subsequent interaction with one another, is responsible for the diffuse nature of these reflections. The second part, well-defined peaks at 0,0,1/2; 0,0,3/2 etc., are completely different and cannot be accounted for by A*, B*, or C*. Attention therefore is directed to the projected structures on the (110), (101) and (011) non-parallel planes as shown in Fig. 32. These structures are describable in terms of D, E, and F whose reciprocal lattices, D*, E* and F*, are shown in Fig. 33. It is clear that these structures cannot account for the well-defined peaks. However, D, E and F are free of twinning. When D and E form twins by Twinning-II(as described by Wang[47]), a new structure $\bar{D}$ results as shown in Fig. 34-a. The reciprocal lattice, $\bar{D}$*(Fig. 35) then will account for the well-defined peaks. In other words, within the 'selected' area, there was yet another portion of shear-vectors that were not aligned parallel to the foil plane.

In summary, in the experiment of Chandra and Purdy, the shear-vectors at least within the 'selected' area, were distributed in all four possible <111> directions. This is in sharp contrast to the experiment of Marcinkowski et al. in which the shear-vectors were all aligned in one unique <111> direction. In light of this contrast, it is interesting to note the distinct manners in which the specimens were prepared by these two groups of investigators.
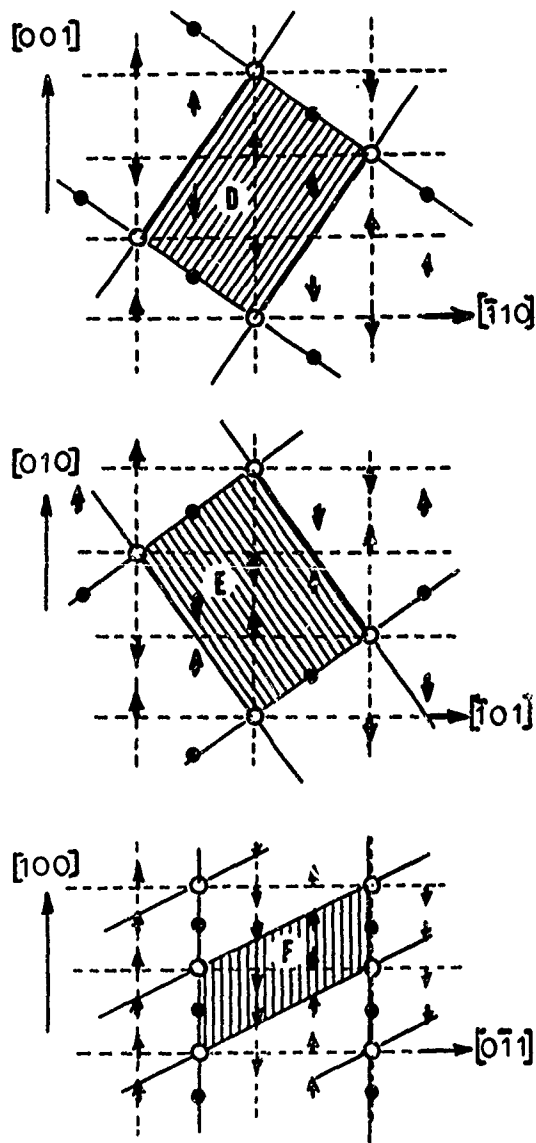
Fig. 32

Fig. 32; Projected 2-dimensional structures on the (110),(101) and (011) non-parallel planes represented in terms of the D,E and F unit cells. Atoms that remain fixed are represented by circles whereas atoms that are involved in shear are indicated with arrows. The shear-vector is projected onto the plane of the paper.
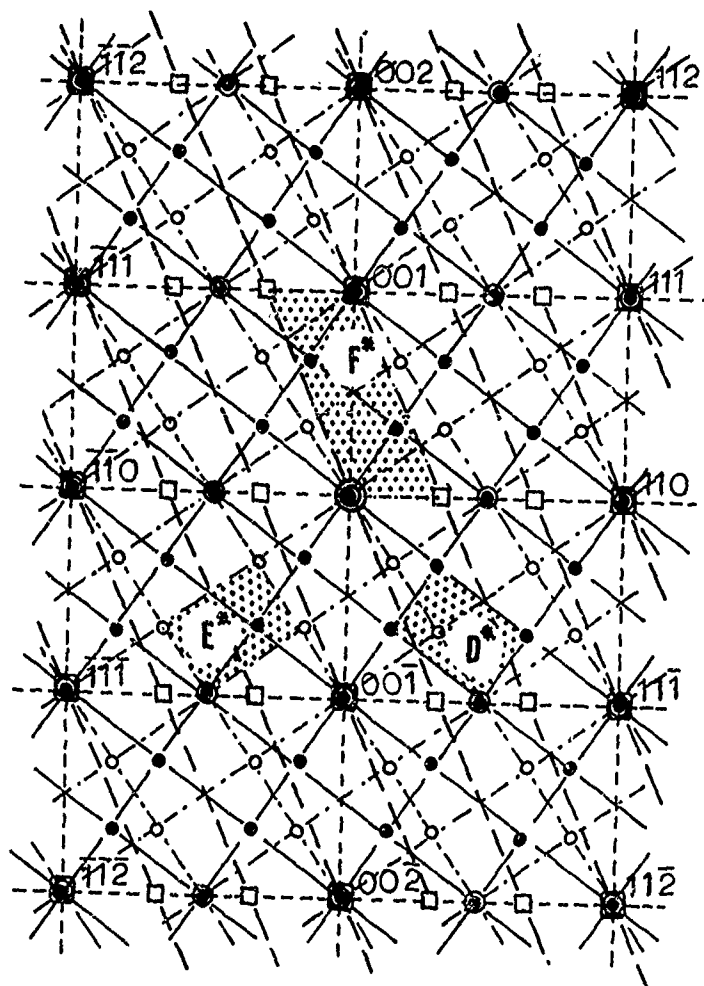
Fig. 33

(after Wang et al.;ref. 51)

Fig. 33.; Reciprocal lattices of D,E and F
represented in terms of D*, E*,and F*.

Marcinkowski et al. - "Thin strips about 0.004 inch thick were rolled from a button; intermediate softening at 850°C was necessary between successive passes through the rolls."

Chandra and Purdy - " Thin foils suitable for electron microscopy were prepared by electro-polishing spark-cut sections of bars or rolled sheet."

It was suggested by Wang et al[51] that in the process of rolling, Marcinkowski et al inadvertently lined up the shear-vectors in a unique direction; whereas Chandra and Purdy, through spark-cutting made the shear-vectors(which were once aligned in a unique direction by the process of rolling) disperse in all possible directions.

On the data from Otsuka and Shimizu(ref. 44)

The data from Otsuka and Shimizu is completely different from both that of Marcinkowski et al. and that of Chandra and Purdy. Since, the existence of Twinning-II will not affect the projected structures on parallel planes, all possible structures for parallel planes are theoretically exhausted by A, B and C as described above. The data of Otsuka and Shimizu therefore, must correspond to one of the non-parallel planes with twinning. This possibility is realized in terms of unit cell $\bar{F}$ which results from a twinning of the F structure as shown in Fig. 34-b. The reciprocal lattice, $\bar{F}^*$(Fig. 35) indeed satisfies the data obtained by these authors. Therefore, in this experiment, within the 'selected' area, the shear-vectors must be aligned in a unique direction which is not parallel to the foil plane.

In this manner, it has been shown by Wang et al[51] that the very mechanism which successfully quantitatively explains both the X-ray and neutron powder diffraction patterns also qualitatively satisfies the three independe^t _ _ of electron; diffraction data. Clearly, any interpretatic.. c. a. electron diffraction pattern of the TiNi-III phase must be made with prior knowledge of the orientational relationship be. 'een the diffra .ion geometry, the shear-vector, and the FS plane.

C. 'yi..nce Added in Proof of the Mechanism and the Structure

Earl1.r, in their investigation of the TiNi transition, deLange and Zijderveld[52] obtained pole-figures both under tension and compression for five reflections(excluding the 110 reflection of the B2 structure) within the 2θ range 35° through 50° for Cu Kα1 radiation(Fig. 36). The reflection (2θ = 45.1°), according to the structural model given in this paper , is the $(006)_{P1}$ plane. As shown in Fig. 35, $(006)_{P1}$ is the only plane, among the five planes investigated by deLange and Zijderveld, which is parallel to both the shear-vector and the twin-plane. Because of this unique property, the No. 6 pole-figure given by these authors for both tension and compression are of interest in that they can clarify the transformation mechanism
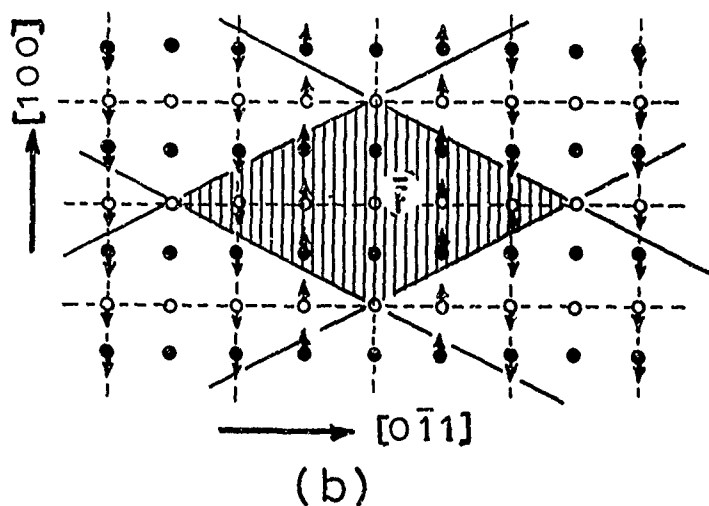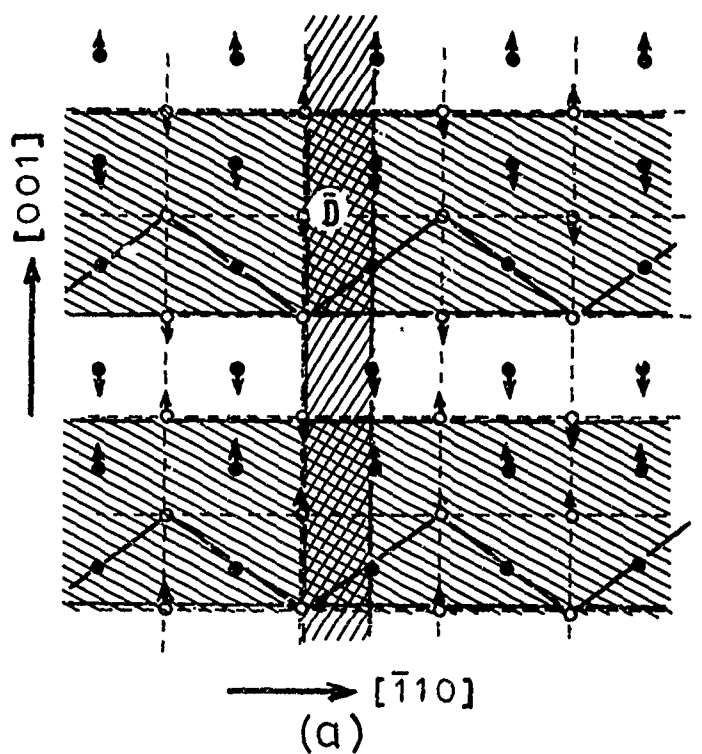
Fig. 34

(after Wang et al.; ref. 51)

Fig. 34.; (a) Twinning of D and E results in a struc-
ture, D̄. (Horizontal dotted lines indicate twin-planes;
arrows show projected shear-vectors). (b) Twinning of the
F structure resulting in structure, F̄.·

66
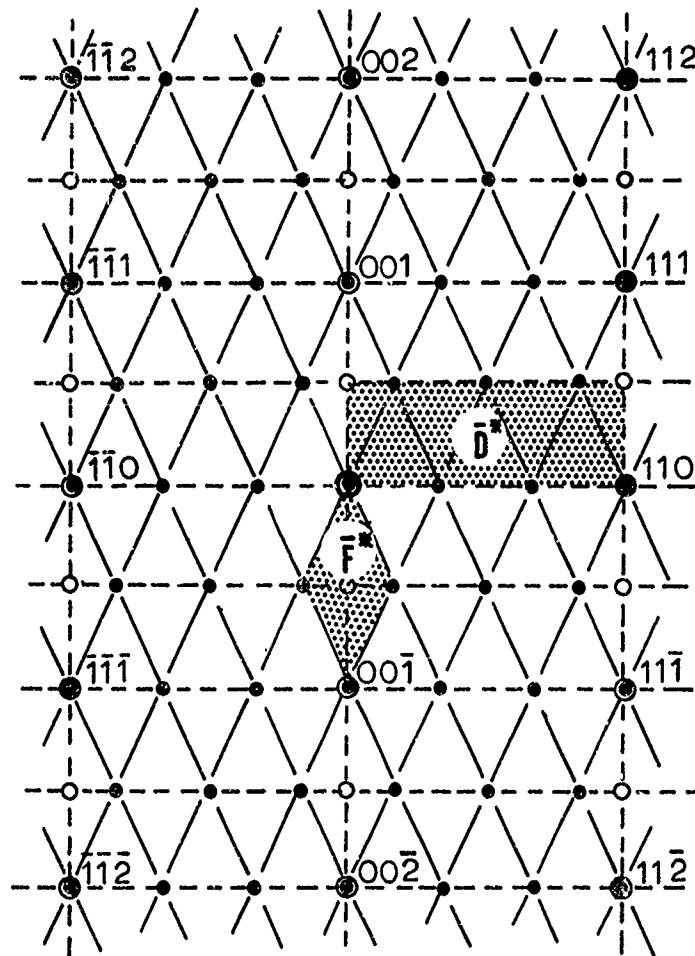
Fig. 35
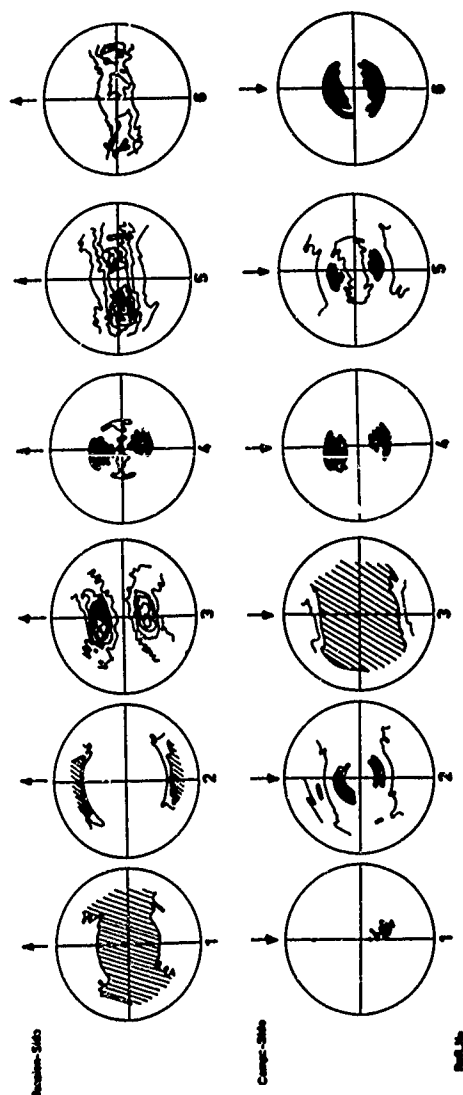

(after Wang et al.; ref. 51)

Fig. 35.; Reciprocal lattices of $\bar{D}$ and $\bar{F}$ represented in terms of $\bar{D}^*$ and $\bar{F}^*$.

Fig. 36

(after de Lange and Zijderveld; ref. 52)

Fig. 36.; Ple-figures of the tension and compression side of specimen 2. The numbers 1 to 6 refer to the six reflections in Fig. 43.(Fe Kα radiation).(The sign of the stress is indicated by arrows).

proposed.

Assume a single crystal of TiNi with (110) parallel to the force-direction as shown in Fig. 37. Under tension, atomic shear will take place on (110) such that the resulting $(006)_{P1}$ planes will be parallel to the force direction. The pole-figure should then show a dominant reflection in the direction perpendicular to the force. On the other hand, under compression, atomic shear will take place in $(0\bar{1}1)$ and lead to $(006)_{P1}$ being perpendicular to the force-direction. The pole-figure then should show reflections dominantly in the force-direction. These results are in complete agreement with the actual pole-figures obtained by these authors as shown in Fig. 37. At this point, a word of caution is in order. According to the mechanism of transformation and the P1 structure given, atoms shear in the $(00\ell)_{P1}$ plane and in the $\langle hh0 \rangle_{P1}$ direction. This immediately implies that the structure factors,

$$F(hk\ell) = \sum_i f_i \exp\{2\pi i(hx_i + ky_i + \ell z_i)\} \quad \text{and therefore,}$$

$$I(hk\ ) \propto |F(hk\ell)|^2$$

of the (hhℓ) and (00ℓ) type reflections will remain nearly constant regardless of the magnitude of shear. Experimentally, reflections, (114) and (112) at $2\theta = 41°$ and (006) at $2\theta = 45°$ fall into this category. These two sets of X-ray diffraction reflections are the two most intense peaks observed. Due to their high intensity, they have been used to monitor the kinetics of the transformation[52][53]. However, it should be clear that for the reasons presented here, these two sets of reflections are poor reflections to use in monitoring the kinetics of the transformation.

IV. NATURE OF THE TiNi MARTENSITIC TRANSITION

A. Transport and Thermodynamic Property Changes

1. Heat Capacity

The unusually high heat of transition associated with the TiNi transition was first pointed out by Wang et al.[23]. In fact, this was one of the features of the TiNi transition described as unique by these authors in comparison with other known martensitic transformation[44]. Meanwhile Wasilewski et al[54] reported the heat of transformation to be 370 20 (cal/g.mole) based on calorimetric measurements and differential thermal analysis. Following this report, Dautovich et al[55] also reported a calorimetric study and gave a heat of transition in excess of 310 (cal/g.mole) in support of the finding of Wasilewski et al. While Wasilewski et al. claimed the transition to be first-order, Dautovich et al. gave no definite concusion as to the order of the transition.

In order to determine whether the TiNi transition is a first order or

Fig. 37

tension
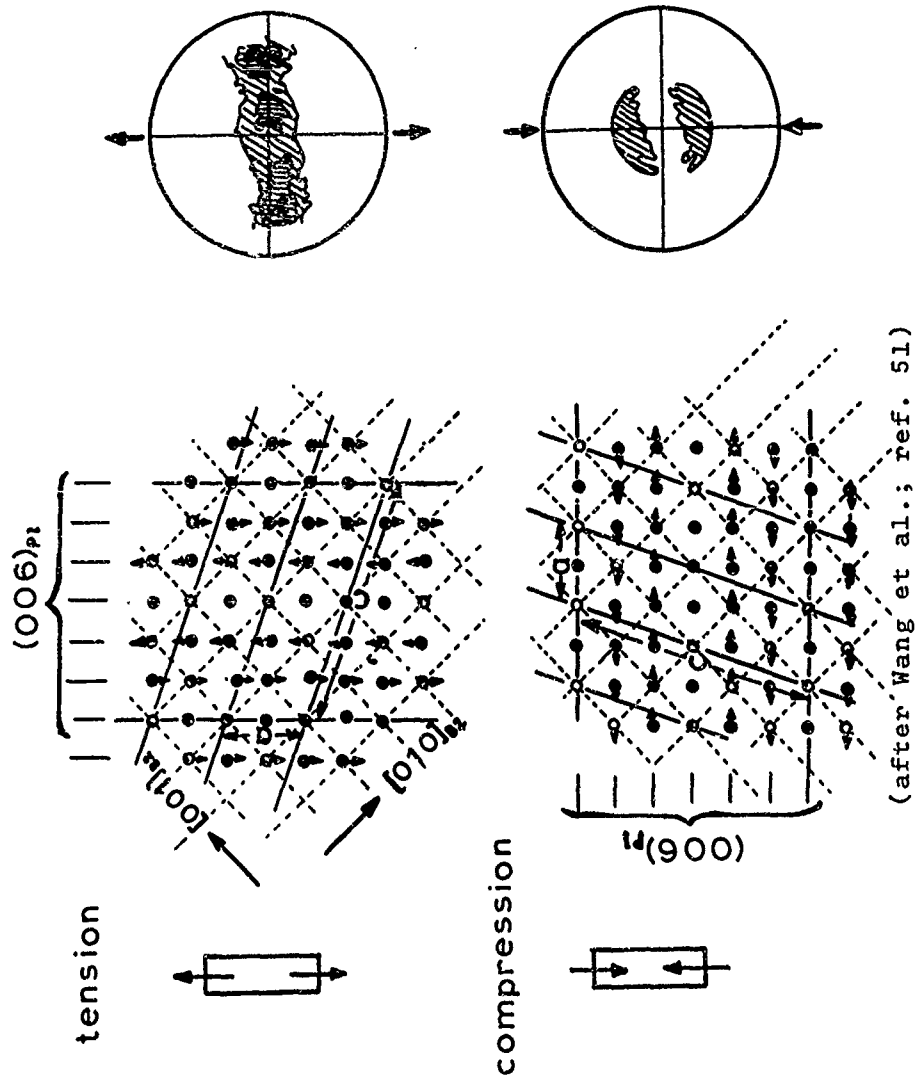
compression

(after Wang et al.; ref. 51)

Fig. 37; Relationship between the internal structure and the force-direction based on the mechanism proposed. The internal structure is then compared with the pole-figure for $(006)_{P1}$ obtained by deLange and Zijderveld(ref. 52).

higher order, Berman et al.[56] undertook yet another calorimetric study near the martensitic transition temperature. Unlike the method of differential thermal analysis used by Wasilewski et al.[54] , the method utilized by Berman et al. did not employ continuous-heating Instead, the sample is brought to thermal equilibrium at increments of a few degrees. In this maner, higher-order transiton can definitely be differentiated from the first order.

The thermodynamic classification of transitions is based on the order of the lowest derivative of Gibb's free energy, G which shows a discontinuity at the transition temperature. If the values of this function are G_1 and G_2 for the two forms concerned, the transition temperature is defined as that temperature at which $G_1 = G_2$. In a derivatives of G with respect to temperature and pressure;

$$\left|\frac{\alpha \Delta G}{\alpha T}\right|_P \quad = \; - \; \Delta S \qquad\qquad \left|\frac{\alpha \Delta G}{\alpha P}\right|_T \; = \; \Delta V$$

In a second order transition, the entropy and volume are continuous, but their derivatives(e.g., the specific heat and the compressibility) are not. It follows that the enthalpy is also continuous; thus, the transition has an anomalous specific heat, but no latent heat. A second order transition in a solid solution implies not only a vanishing latent heat of transition, but also continuity of composition. While these thermodynamic property changes are good indications, in practice great care is required to distinguish between latent heats and anomalous specific heats as pointed out by Berman et al.[56] . Fortunately, in the solid state another physical parameter, based on symmetry, can be used to distinguish the order of the transition. This has been discussed in terms of "Crystallographic transformation" vs. "Crystallographic distortion" in the earlier section.

The measurements by Berman et al. covered the temperature range, 25° through 218°C with the transition occuring at around 90°C. Their experimental results are summarized in Fig. 38 from which Berman et al. derived the following conclusions:

    a. Between 24° to 61°C, the specific heat is a linear function of temperature,

$$C_p = 48.211 + 0.075797(t) \qquad \text{where t is in centigrade.}$$

conforming to an approximation of the Kopp-Neuman rule, i.e., the molar heat capacity of the compound is the sum of the molar-heat capacities of Ni and Ti in this instance. From compiled heat capacities of Ni and Ti, the values calculated for TiNi are 51.09 (J/deg.mole) at 25°C and 51.6 (J/deg.mole) at 40°C, compared with the observed values of 50.11 and 51.24 (J/deg.mole) respectively. This additivity indicates that the heat effect of the transition is minimal in this region.

    b. From 61° to 113°C, there is a higher-order transition with a maximum heat capacity at about 87°C.

Fig. 38

NOLTR 72-4
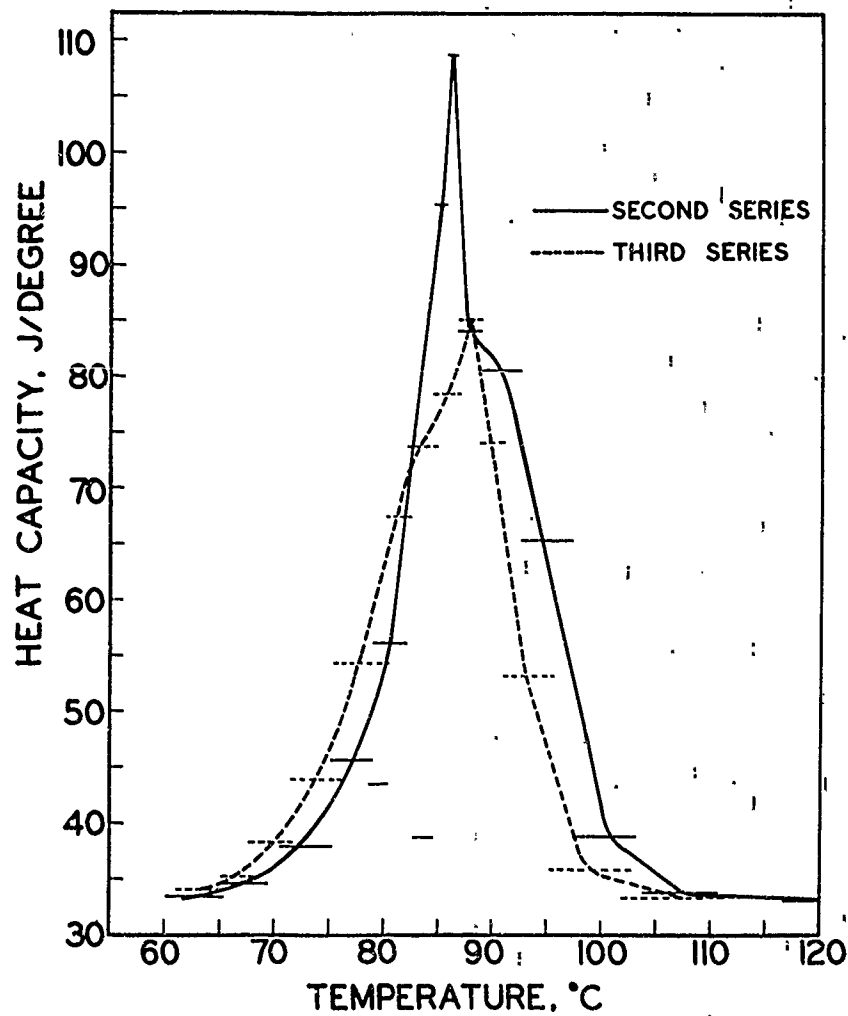
(after Berman et al. ref. 56)

Fig. 38.; Average heat capacity of sample plus
calorimeter vs. temperature. (Solid lines
connect experiments of second series; broken
lines connect experiments of third series).

c. From 113° to 145°C the heat capacity is describable as,

$$C_p = 47.406 + 0.19667(t)$$

and from 145° to 218°C as
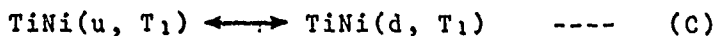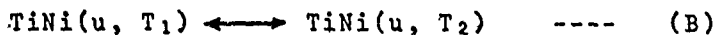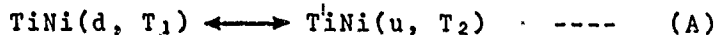
$$C_p = 64.437 - 0.168509(t) + 0.00048679(t)^2.$$

In the 113° to 218°C range, the specific heat is nearly a linear function of temperature, but slightly below the sum of the molar-heat capacities of Ni and Ti. The value calculated by the additivity rule for TiNi is 54.8 (J/deg.mole) at 127°C, compared with the observed value of 49.90 (J/deg.mole). The effect from the transition is therefore again considered to be minimal in this region. Berman et al. observed variations in thermal properties of the alloy depending upon its thermal history as did Wang et al.[31]. Because of this uncertainty, Berman et al.[36] could set only a lower limit for the heat of transition, H = 4,150 (J/mole).

Later, in 1968 Wang et al.[31] reported the measurements on the following properties: electrical resistivity, Hall coefficient, magnetic susceptibility, sound wave attenuation and differential thermal analysis. In order to meaningfully correlate and interpret the data from these measurements, the authors obtained data from alloys with identical transition temperatures and thermal histories. This was accomplished by performing all measurements on alloy specimens from a single melt having a composition of about 51 at.% Ni and a transition temperature near 60°C. One of the unique mechanical characteristics of TiNi is its 'memory' effect; a TiNi wire deformed below the transition temperature will recover its original shape immediately upon heating above the transition temperature . Thermodynamically, this can be considered in three steps:

$$TiNi(d, T_1) \longleftrightarrow TiNi(u, T_2) \quad \text{----} \quad (A)$$

$$TiNi(u, T_1) \longleftrightarrow TiNi(u, T_2) \quad \text{----} \quad (B)$$

$$TiNi(u, T_1) \longleftrightarrow TiNi(d, T_1) \quad \text{----} \quad (C)$$

where u, denote 'undeformed' and d, denotes 'deformed, with T_1 and T_2 being the temperatures above and below the transition temperature range respectively.

Since (B) is the sum of (A) and (C), we have for the state function enthalpy,

$$\Delta H_B = \Delta H_A + \Delta H_C \qquad \text{as} \quad \Delta H_C \neq 0$$

$$\Delta H_B \neq \Delta H_C$$

Since both the deformed and undeformed TiNi wires undergo diffusionless shear movements yet have different heats of transformation, $(\Delta H_A \neq \Delta H_B)$, the shear mechanism in the strained sample(which results in shape recovery) must differ from that which involves no shape recovery. For this reason, Wang et al.[31] made measurements on

73

specimens which were not only free of deformation but also free of sustained tensile and compression stresses.

2. Electrical Resistivity

Previously, based on single crystal diffraction work, Wang et al.[23] showed the existence of a diffusion-involved transition in the 600° ∿ 700°C range. Above this transition TiNi-I exists as a replacement disordered bcc, while below this transition TiNi-II exists as a combination of B2 and P3ml in equilibrium. This contention was proved by Wang et al.[31] from the series of electrical resistivity measurements described below.

The electrical resistivity curve obtained from an alloy annealed at 610°C for seven days then furnace cooled to room temperature, is shown in Fig. 39. The electrical resistivity curves of the alloy annealed at various temperatures,(700°, 800° and 900°C) for similar time periods followed by an oil quench are also shown in Fig. 39. There was a definite overall increase in the resistivity of the alloy as the annealing temperature was raised. This is exactly what is expected from the fact that the ratio of TiNi-I to TiNi-II increases as the annealing temperature is increased. Inasmuch as TiNi-I, presumably does not undergo the unique 'Martensitic' transition, it is also reasonable that the triangular form of the resistivity curve, a manifestation of the 'martensitic' transition, becomes progressively smaller(area-wise) and less prominent as the annealing temperature is raised. Further, the fact that the triangularly shaped electrical resistivity curve is not due to a simple hysteresis effect is proved in the following manner.

Experiments show that the cooling path, M_S - $M_S^!$ and the heating path, $M_S^!$ - A_S are irreversible, i.e., in a given heating(or cooling) cycle, if the heating(or cooling) process is halted and the direction of the cycle reversed to cooling(or heating), the resistivity curve does not retrace its original path. In fact, in reversing to cooling from heating, $M_S^!$ - A_S, the resistivity curve takes a path whose slope is intermediate between those of $M_S^!$ - A_S and A_S - M_S; in reversing to heating from cooling, M_S - $M_S^!$, the resistivity curve is always displaced toward A_S. In contrast, A_S - M_S is reversible. In this connection, it is important to point out that the triangular shape and the irreversible nature of the resistivity curve are totally independent of the rate of heating or cooling. Further, as long as thermal cycles are carried beyond the temperature range, $M_S^!$ - A_S without reversing the thermal cycling direction(within the temperature range, $M_S^!$ - A_S on heating and M_S - $M_S^!$ on cooling), the triangular portion of the curve will remain unaltered. This type of thermal cycling is referred to by Wang et al.[31] as 'complete' cycles and the other type(about to be described) as 'incomplete' cycles.

If the thermal cycling direction is reversed within the two 'irreversible' temperature ranges, e.g., thermal cycling between 10° and 50°C, the triangular form of the resistivity curve is altered. After six such 'incomplete' cycles, the resistivity curve shown in Fig. 40-b

Fig. 39

Fig. 39; Effect of annealing temperatures on the electrical resistivity of TiNi(51 at.% Ni) at and around the 'martensitic' transition temperature.

Fig. 40

(after Wang et al.; ref. 31)

Fig. 40.; Effect of 'incomplete' cycles on the electrical
resistivity of TiNi(51 at.% Ni) at and around the 'martensitic'
transition temperature; cycling direction is indicated by arrows
(a) without 'incomplete' cycling,(b) after six 'incomplete' cycl-
ing and (c) after several hundred 'incomplete' cycles.

Fig. 40

NOLTR 72-4

(after Wang et al.; ref. 31)

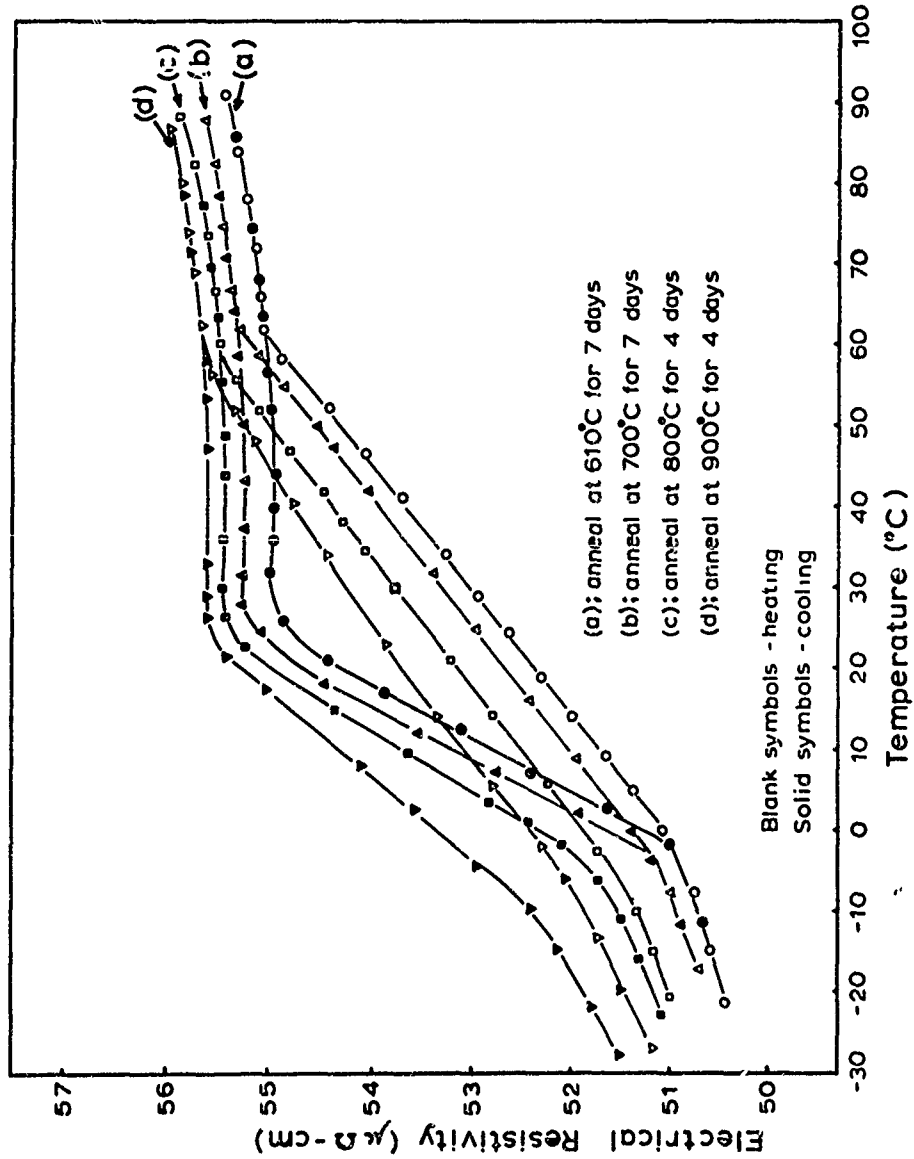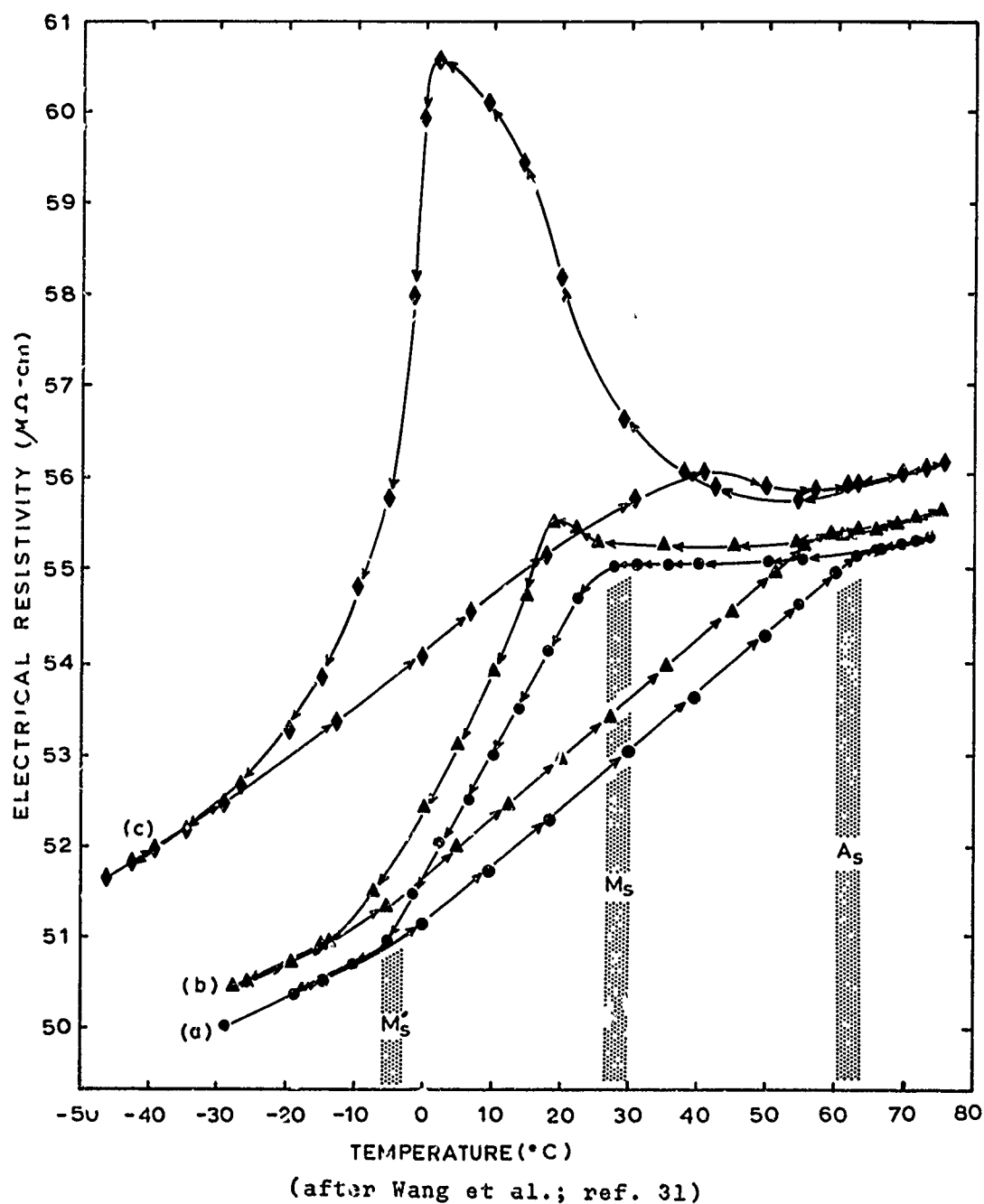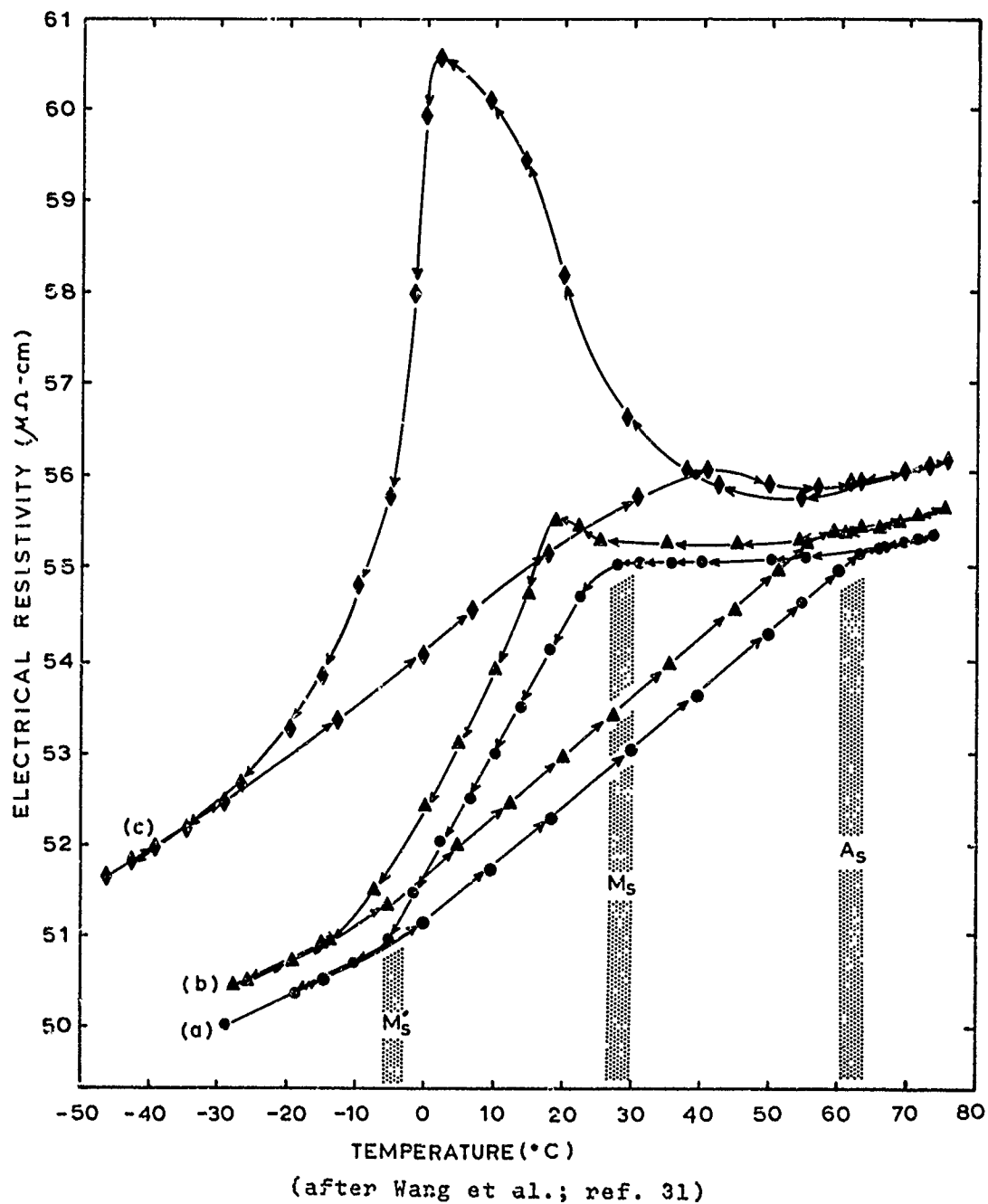Fig. 40.; Effect of 'incomplete' cycles on the electrical
resistivity of TiNi(51 at.% Ni) at and around the 'martensitic'
transition temperature; cycling direction is indicated by arrows
(a) without 'incomplete' cycling,(b) after six 'incomplete' cycl-
ing and (c) after several hundred 'incomplete' cycles.

was obtained. A few hundred 'incomplete' cycles yields a resistivity curve with a large peak in the cooling half of the cycle such as that shown in Fig. 40-c, which is what was reported originally as the resistivity curve of TiNi over the transition temperature range by Dautovich and Purdy[24]. Hence, the resistivity curve of the alloy can assume any intermediate form from that of Fig. 40-a to that of Fig. 40-c depending upon the number of 'incomplete' cycles applied to the alloy. This implies that a properly annealed alloy stored in a laboratory cabinet will continue to change in resistivity because of room temperature fluctuations which are, in effect, un-intentional 'incomplete' thermal cycles. The argument that the resistivity change may be due to 'aging' is refuted by the fact that a resistivity curve like Fig. 40-a remains the same so long as the alloy is stored below the $M_s^!$ or above the A_s temperature. Further experiments showed that a resistivity curve like Fig. 40-c can be restored to an alloy with one like Fig. 40-a only after prolonged re-annealing at 600°C or above.
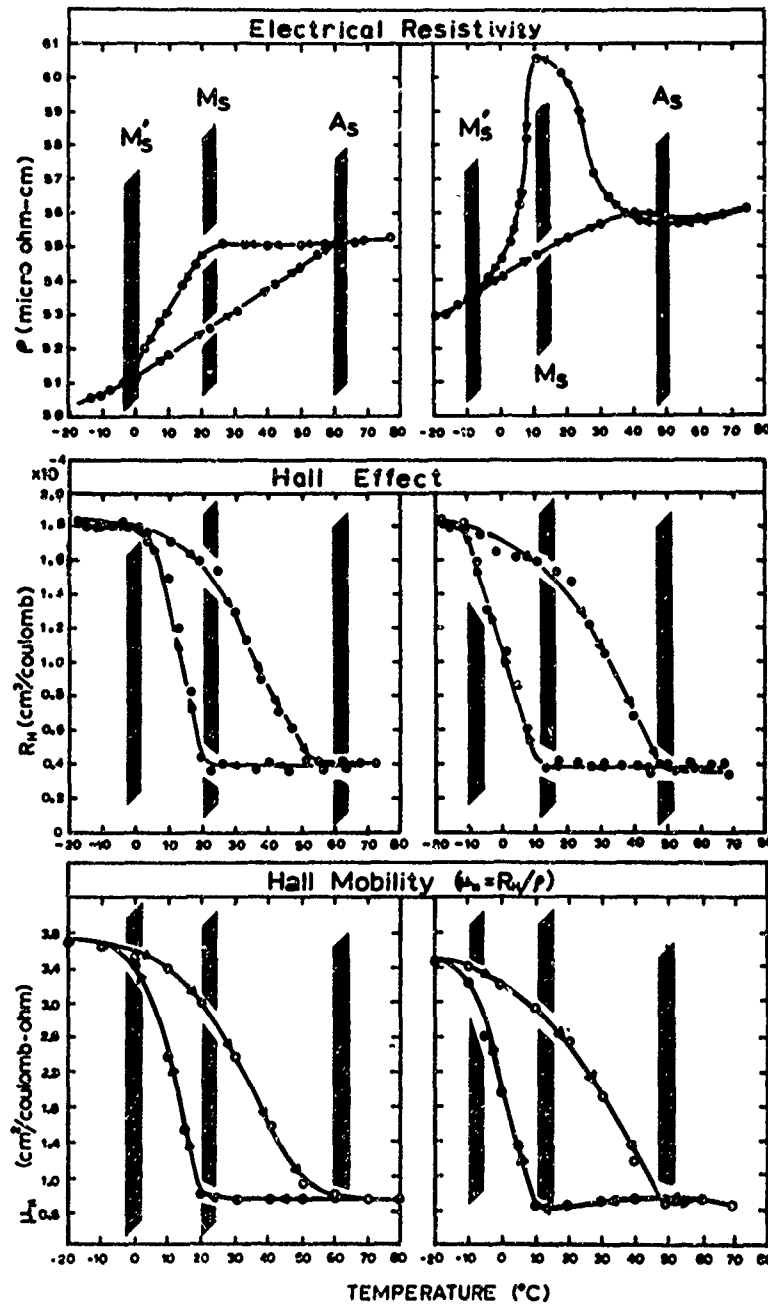
3. Hall Coefficient

The Hall coefficient and resistivity were measured concurrently using standard dc techniques. The resistivity measurements made here serve two purposes: 1) to check the original resistivity measurements, and 2) to find the correspondence between changes of the Hall effect and changes of electrical resistivity. Because of the small Hall voltage and the relatively large temperature coefficient of resistance, a three-probe configuration was used to minimize cross voltage on the Hall probes. The Hall constants measured in this manner are accurate to within ± 5% over the entire temperature range investigated. The primary current used for both the Hall and resistivity measurements was 1.1 amp. which caused no detectable resistance-heating in the sample.

The Hall coefficient (Fig. 41) showed relatively constant values of $1.8 \times 10^{-4} (cm^3/C)$ below the $M_s^!$ temperature and $0.4 \times 10^{-4} (cm^3/C)$ above the A_s temperature for both 'complete' and 'incomplete' cycles. However, in both cases, within the $M_s^!$ to A_s temperature range, the existence of a triangular form whose vertices coincide with the A_s, M_s and $M_s^!$ temperatures is definite and significant. The shifting of the triangular form to a somewhat lower temperature is similar to what was observed in the resistivity data. But, within experimental error, there is no difference between the two Hall coefficient curves obtained from 'complete' and 'incomplete' cycles. The Hall mobility, calculated from the observed electrical resistivity and Hall coefficient and based on the relationship, $\mu_H = c \cdot R_H/\rho$ is given in Fig. 41.

4. Magnetic Susceptibility

Measurements of the magnetic susceptibility were made, based on the Faraday-Curie principle[57], using an Ainsworth automatic vacuum chemical balance[58]. The apparatus was calibrated using palladium whose susceptibility was taken to be $5.4 \times 10^{-9} (emu/gm)$. For one gram of material whose magnetic susceptibility is of the order of

77

Fig. 41

Fig. 41; Electrical resistivity, Hall coefficient and calculated Hall mobility of 'complete and 'incomplete' thermal cycled specimen; 'complete' thermal cycled on the left and 'incomplete' thermal cycled on the right.

10^{-6}(emu/gm), the ideal differential sensitivity for the instrument is about 1×10^{-8}(emu/gm). However, because of room vibration, magnetic field fluctuations etc., the actual sensitivity is about $\pm 5 \times 10^{-8}$(emu/gm).

Previously, the magnetic susceptibility of TiNi in the low temperature region was shown by DeSavage and Goff[59] to be temperature independent and interpreted as due to Pauli spin susceptibility. This is confirmed in an experiment of Wang et al.[31] . The magnetic susceptibility, as summarized in Fig. 42, shows a constant value, 2.1×10^{-6} (emu/gm), below the M_s temperature and 3.0×10^{-6}(emu/gm) above the A_s temperature. Between these two temperatures the data shows the familiar triangular form, but again there is no difference(within experimental error) between 'complete' and 'incomplete' cycles.

5. Sound-velocity Changes

Measurements of sound-velocity changes in TiNi at and around its transition temperature were first made by Bradley[60] . The measurement method was a pulse technique in which sound-velocity was gauged by a two crystal, ultasonic velocimeter. The pulse height was 200 V with a pulse width of 0.7 seconds. These results showed a considerable difference between the heating and cooling halves of thermal cycles, reminiscent of the effect observed in the resistivity curve from 'incomplete' cycles. Wang et al.[31] extended Bradley's experiment by measuring sound-velocity changes both after 'complete' and 'incomplete' cycles. The results obtained from these two extreme cases are shown in Fig. 42 and demonstrate a definite difference.

6. Differential Thermal Analysis

As stated above, DTA and calorimetric measurements had been made[54,55,56] but exclusively on heating cycles. Subsequent measurements by Wang et al.[31] covered not only both cooling and heating cycles but also the two extreme cases of 'complete' and 'incomplete' cycles. The results, summarized in Fig. 42 show practically no difference between the two extreme cases except that the heat of transition in cooling is associated with the irreversible step, $M_s - M_s'$.

B. Correlation of Electrical Resistivity vs. X-ray Diffraction

As described above, the electrical resistivity curve shows a single step on heating and two steps on cooling. The fact that this is not due to a hysteresis effect has been stressed. Parallel to this, is the X-ray evidence obtained by Wang et al.[23,51] that:

1. The TiNi-II $\rightleftharpoons$ TiNi-III martensitic transition proceeds by continuous cooperative shear movement of the atoms. This is supported by calorimetric evidence that the transition is of order higher than first.

2. The TiNi-III martensite consists sub-micro twinned structures.

79
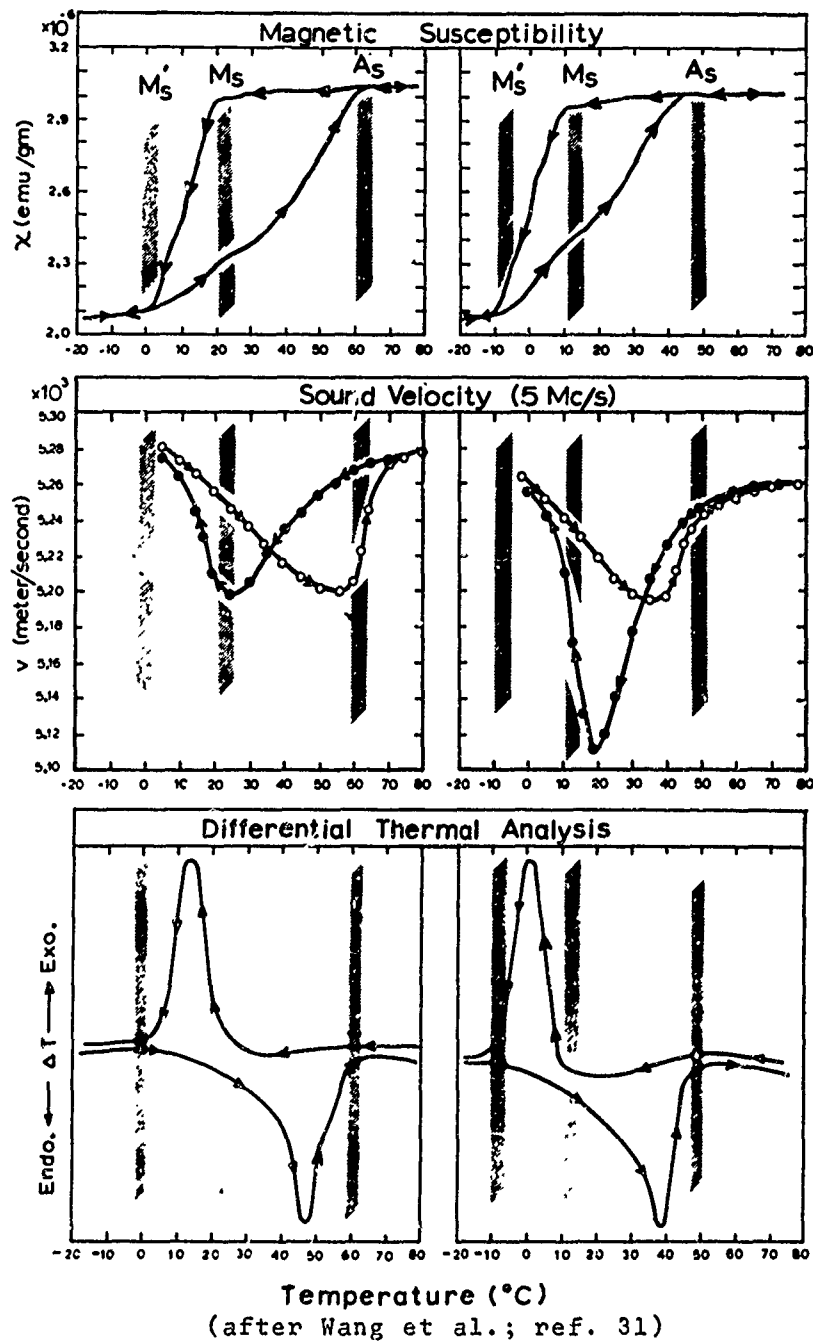
Fig. 42

Temperature (°C)
(after Wang et al.; ref. 31)

Fig. 42; Magnetic susceptibility, sound-velocity change and differential thermal analysis of the 'complete' and 'incomplete' thermal cycled specimen; 'complete' cycled on the left and 'incomplete' cycled on the right.

3. As summarized in Fig. 43, there is no difference (except for some temperature hysteresis) between the cooling and heating cycles insofar as the TiNi-III(P$\bar{1}$) pattern is concerned. There is, however, a definite difference between cooling and heating cycles for the $(110)_{B2}$ reflection. On cooling, the $(110)_{B2}$ peak splits into two definite peaks before its disappearance, whereas on heating there is no such splitting at any stage. This splitting is understood in term of atomic shear in $<111>_{B2}$, creating, in the process, two types of $\{110\}_{B2}$ planes; planes that are parallel and planes that are not parallel to the shear-vector, $<111>_{B2}$. The mechanism requires the d spacing of these two types of (110) planes to be somewhat different. This results in splitting of $(110)_{B2}$ reflection during the initial stage of transformation. Therefore, the two-step electrical resistivity curve on cooling is interpreted in the following manner.

First step(A_s - M_s); the lattice relaxes and distorts into a new lattice as shown in Fig. 44, leaving the atomic coordinates unaltered. This is the step which is responsible for the $(110)_{B2}$ splitting.

Second step(M_s - M_s'); cooperative atomic shear takes place, leaving the lattice more or less constant, as the temperature passes through the M_s' temperature into the TiNi-III martensite.

However, on heating, restoration of the lattice to that of the B2-type structure and reverse cooperative atomic shear apparently takes place in one single step, M_s' - A_s which results in no splitting of the $(110)_{B2}$ reflection. In this context, it should be noted that the heat of transition(based on the differential thermal analysis) actually corresponds to the two irreversible steps, M_s - M_s' on cooling and M_s' - A_s on heating in which atomic shear presumably took place. During an 'incomplete' cycle, the atomic shears are expected to be cooperative but less homogeneous because an increase in twinning results in an increase in the density of sub-micro twinning.

Existence of twinning in an alloy matrix(particularly in the sub-micro range) will interfere with electron flow and affect the mean relaxation time, τ, and the effective mass of an electron m^*. This results in a rise in electrical resistivity. The rise in the resistivity curve at the end of step, A_s - M_s in an 'incomplete' cycle is in keeping with such an interpretation. Thus, the greater the degree of sub-micro twinning, the higher the peak in the resistivity curve between A_s and M_s. Further support of this conclusion comes from the finding of Cross et al[51] that the mechanical 'memory' effect is more pronounced the larger the peak in the electrical resistivity curve on cooling. The reason here is that a higher density of micro-twinning(therefore, a higher resistivity peak) means less strain energy and thus a more pronounced 'memory' effect. While the model proposed here is only qualitative, it is substantiated by other physical changes described below.
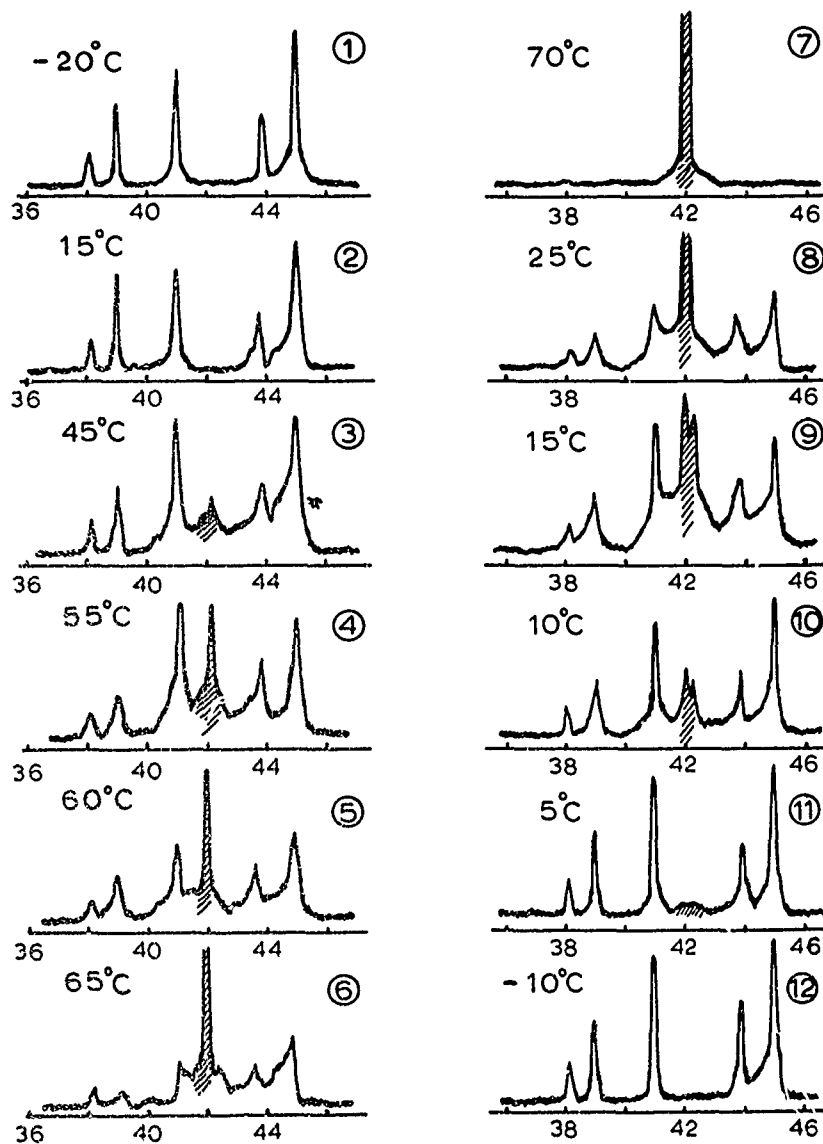
Fig. 43

(after Wang et al.; ref. 51)

Fig. 43.; X-ray powder patterns obtained at points ① through ⑫ corresponding to the points indicated on the resistivity curve(Fig. 40). (The shaded peak is the 110 reflection of the B2 structure.

Fig. 44

same lattice constants;
new atomic
coordinates.

$a = 4.24$ Å
$b = 3.00$ "
$c = 13.40$ "

$\alpha = 90°, \beta = 108.4°, \gamma = 90°$

(A_S)

$a = 4.17$ Å
$b = 3.11$ "
$c = 12.55$ "

$\alpha = 96.06°, \beta = 105.18°, \gamma = 84.09°$

(M_S)

(M'_S)
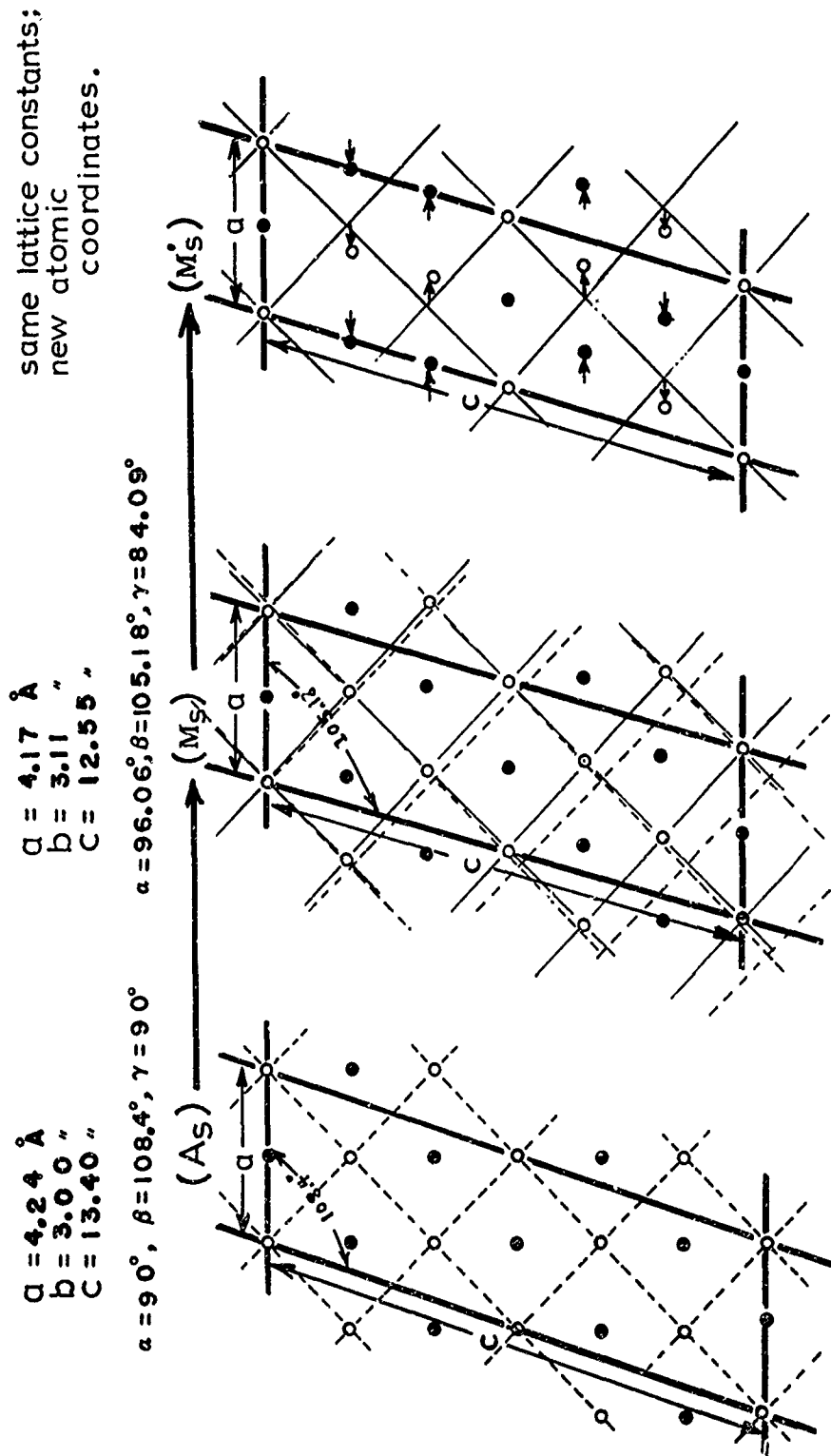
(after Wang et al.; ref. 51)

Fig. 44.; Mechanisms of transformation corresponding to steps, A_S-M_S and $M_S-M'_S$ on cooling; A_S-M_S corresponds to relaxation(distortion) of the lattice whereas $M_S-M'_S$ corresponds to shearing of atoms.

The model proposed here necessarily leads to the conclusion and prediction that atomic-arrangement insensitive properties should not differ for 'complete' or 'incomplete' cycles; whereas atomic-arrangement sensitive properties should behave in much the same way as the electrical resistivity.

Classical free electron theory predicts a Curie-type manetic contribution by conduction electrons to the magnetic susceptibility.

$$\chi = n\ \mu_B /\ k_B \cdot T$$

where it is assumed that an electron has associated with it a magnetic moment of one Bohr magneton, μ_B. However, this is in conflict with the experimental observation that the susceptibility of most normal non-ferromagnetic metals is independent of temperature. Pauli[62] showed that application of a Fermi-Dirac distribution would correct the theory as follows. Most conduction electrons in a metal have zero probability of reacting to an applied magnetic field because the states with parallel spin are already occupied. Only electrons within a range of about $k_B \cdot T$ at the top of the Fermi distribution have a chance to react with the field. Thus, only a fraction, T/T_F of the total number of electrons contribute to susceptibility. Hence, the Pauli spin susceptibility.

$$\chi_p = (n\ \mu_B / k_B \cdot T)\ (T/T_F) = n\mu_B / k_B \cdot T_F$$

which is temperature independent.

The magnetic susceptibility of TiNi is temperature independent and therefore can be interpreted as due to conduction electrons and thus a Pauli spin susceptibility. This catagorizes the magnetic property as one which is insensitive to atomic-arrangement. Experimentally, as shown in Fig. 42, within experimental error, no difference is observed between magnetic susceptibility obtained from 'complete' and 'incomplete' cycles.

Since sound waves involve vibrations of the atoms (or molecules) with respect to the ideal lattice, crystal imperfections (manifestations of atomic arrangement) have been found to affect sound transmission[63]. Sound velocity changes therefore can be categorized as atomic-arrangement sensitive property and should differ for 'complete' and 'incomplete' cycles. The results shown in Fig. 42 again confirm this prediction.

C.   Characterization of the TiNi Band Structure

In summary, Hall coefficient, magnetic susceptibility and heat capacity changes did not show noticible differences between 'complete' and 'incomplete' cycles. We shall now analyze this result as follows.

Let x, y and z be the three principle directions in Cartesian coordinates. A current flowing under the influence of an electric field,

$\bar{E}_x$(in the x direction) consists of carriers with average velocity, $\bar{V}_x$. A magnetic field $\bar{H}_z$(in the z direction) perpendicular to $\bar{E}_x$ will force electrons to deflect in the $\bar{V}_x \times \bar{H}_z$ direction. This deflection will continue until sufficient space-charge builds up to just balance the magnetic field. This transverse electric field, $\bar{E}_y$(in the y direction) characterizes the Hall effect. Hall coefficient R_H, is defined such that,

$$\bar{E}_y = \bar{R}_H \bar{J}_x \bar{H}_z \qquad \text{where } J_x \text{ is the current in the x direction.}$$

Indeed, this relationship can be expressed in terms of a motion equation as follows:

$$dV_y/dt + V_y/\tau = e/m^*(E_y - V_x H_z)$$

Since for d-c measurements, $dV_y/dt = 0$; the above equation of motion can be expressed in terms of mobility $\mu = e\tau/m^*$ and the applied field, H_z as,

$$V_y = \mu(E_y - \mu E_x H_z) \qquad \text{where } V_x \text{ is taken to be } \mu E_x \text{ by neglect-}$$
$$\text{ing second order terms such as } V_y E_x.$$

Since the current in the y direction must be zero, for a multiple band structure,

$$V_{y_1} + V_{y_2} + V_{y_3} \quad \dots\dots = 0$$

$$\text{where } 1,2,3,\dots\dots \text{ indicate the electron}$$
$$\text{velocity for different bands.}$$

Therefore, for the general case,

$$E_y = E_x H_y \left\{ \frac{\Sigma \mu_i^2 n_i}{(\Sigma_i \mu_i \cdot n_i)^2} \right\}$$

and the corresponding Hall coefficient is,

$$R_H = E_y/J_x H_z = \left\{ \frac{\Sigma \mu_i^2 n_i}{ec(\Sigma_i \mu_i \cdot n_i)^2} \right\}$$

It is easy to see that for an electronic structure with one electron and one hole band, the Hall coefficient will be

$$R_H = \left\{ \frac{\mu_h^2 n_h - \mu_e^2 n_e}{ec(\mu_h n_h + \mu_e n_e)^2} \right\}$$

For a single band, electronic structure, the Hall coefficient becomes totally independent of τ and m^* and thus dependent only on n, the density of carriers.

Experimentally, the Hall coefficient showed relatively constant values of 1.8×10^{-4} and $0.4 \times 10^{-4} (cm^3/C)$ above and below the A_s temperature for both 'complete' and 'incomplete' cycles. However, in both cases within the M_s' to A_s temperature range, the existence of a triangular form whose vertices coincide with the A_s, M_s and M_s' temperatures is definite and significant. Although a shift of the triangular form, $A_s-M_s-M_s'$ to a lower temperature(similar to what happened in the resistivity data) was noted in 'incomplete' cycles, within experimental error, there is no difference between the two Hall coefficient curves; from 'complete' and 'incomplete' cycles. This is to say that the peak which appeared in the cooling half of the resistivity curve from 'incomplete' cycles was not matched by a corresponding change in the Hall coefficient. Indeed, this experimental fact is the key to successful interpretation of physical property changes in TiNi which subsequently led to an understanding of the nature of the 'martensitic' transition.

In general, both the electrical resistivity and the Hall coefficient can be shown[64] to be functions of three parameters, effective mass of the electron, m^*, mean relaxation time, τ, and effective number of carriers, n. As shown above, the Hall coefficient becomes a function of n alone when and only when

 1. the band structure is a single band or
 2. the band structure is such that one of the bands dominates over the others by virtue of its electron or hole mobility.

This is to say that the band structure of TiNi must be regarded as either a simple single positive band or one positive band which dominates over the others, at least in the temperature range being considered.[†] An immediate consequence of this conclusion is that the Hall coefficient change, ΔR_H across the transition temperature range, $M_s' - A_s$ can be considered as primarily due to an actual change in the effective number of hole carriers, Δn_h.

V. "COVALENT" TO "CONDUCTION" ELECTRONIC STATES CHANGE DURING THE TiNi-II to TiNi-III TRANSITION

A. Uniqueness of the TiNi Martensitic Transition

The overt physical characteristics of TiNi and their changes as a function of temperature at and around the martensitic transition are:

 1. Below the transition temperature range(TTR), TiNi-III is ductile and yields with ease to plastic deformation; the lower the temperature, the easier the plastic deformation. Conversely, above the TTR, TiNi-II is mechanically stiff and hard.
 2. This drastic change in hardness as a function of temperature

---

† It is of interest to note that based on transport data obtained between $3°$ and $300°k$, excluding the unique transition temerature range, Goff(ref. 65) also regards the band structure of TiNi as a single standard transport band.

is also apparent in the acoustic damping character of TiNi. The
acoustic damping capacity of TiNi-III is approximately ten times
higher than that of TiNi-II.

3.   The transition is accompanied by a 'memory' effect; if a
wire or a sheet of this alloy is deformed below the transition
temperature, it will regain its original shape when heated above the
transition temperature.

4.   In returning to its original shape, the alloy can exert a
considerable force. For example, a 20 mil wire elongated by 5 or
6 % of its original length as TiNi-III, on heating and returning to
its original length as TiNi-II, it will lift a 4 to 5 kilogram of
weight.

5.   The 'memory' effect and recovery force are completely in-
dependent of the deformation mode(compression or tension), the in-
ternal matrix composition(single crystal or polycrystalline) and
the shape of the alloy.

Along with these overt physical characteristics, the following
changes of internal physical properties were also observed in going
from TiNi-III to TiNi-II(see Figs. 41 and 42).

a.   The interatomic distances present in TiNi-III are closer to
the distances expected from known metallic radii than those present
in TiNi-II.

b.   The number of effective hole carriers increases. This con-
clusion is based on the assumption of a single simple transport
band and the relationship, $R_H = 1/n$.

$$\Delta n = 1.66 \text{ atom}^{-1}$$

c.   The Pauli spin paramagnetic susceptibility increases

$$\Delta \chi = 0.9 \times 10^{-6} \text{gm}^{-}$$

d.   Energy is absorbed by the system

$$\Delta E = 2.43 \times 10^{20} \text{ eV} \cdot \text{gm}^{-1}$$

e.   The bulk modulus increases

$$\Delta K = 2.3 \times 10^{11} \text{ dynes. cm}^{-2}$$

f.   The Hall mobility decreases

$$\Delta \mu_H = 2.8 \quad \text{cm}^2 \cdot \text{coul}^{-1} \cdot \text{ohm}^{-1}$$

Although there are no well-defined characteristics associated with
every martensitic transformation, the following features neverthe-
less are often observed in martensitic transformations[66].

1) Athermal transformation.

2) Crystallographic transformation. Thus, the transformation is
first order with coexistence of 'parent' and 'martensite' separated
by a two-dimensional 'habit' plane.

3) No diffusion or interchange of atoms occurs during the transi-
tion; therefore, the martensites inherit their composition.

4) The activation energy for growth of the martensite is effectively zero, i.e., the propagation rate of the transformation is fast and independent of temperature.

In light of these characteristics, the TiNi transition can be catagorized as 'martensitic' but unique in the following ways.

·i) It is a seond-order transformation, a crystallographic distortion accompanied by an unusually large heat of transformation[56].

ii) Being a seond-order transformation, it has a sixty degree centigrade transition temperature range in which neither TiNi-II nor TiNi-III exist[31], but through which TiNi-II gradually transforms (distorts) into TiNi-III or vice versa.

iii) Considerable force accompanies the 'memory' effect. The 'memory' effect has also been observed in the indium-thalium[67], copper-aluminum[68] and gold-cadmium[69] systems but without force.

B. Characteristics of "Covalent" vs. "Conduction" Electrons

The characteristics of 'covalent' vs. 'conduction electrons described below are not necessarily mathematically precise. In fact, each item represents some degree of chemical and physical intuition based on experience. This is based on the belief that in this, as in most theoretical chemistry and physics, the form in which the mathematics is cast depends almost inevitably, on experimental results.

1. 'Covalent' bonded electrons are strongly pair correlated whereas 'conduction' electrons have only weak pair correlation.

2. 'Covalent' bonded electrons are directional(spatially) and their stability critically depends on interatomic distances. On the other hand, 'conduction' electrons are non-directional and their stability does not depend as critically on interatomic distances.

3. 'Covalent' bonded electrons are identifiable with a group of atoms in their immediate vicinity because they are under the 'influence' of atomic orbitals. 'Conduction' electrons are totally free frcm the 'influence' of atomic orbitals and thus are simultaneously shared by all atoms in the system.

4. Thus, the Pauli exclusion principle and Fermi-Dirac statistics apply independently to these two distinct groups of electrons.

5. Because of the facts given in 3 and 4, 'covalent' electrons have no Fermi-surface whereas 'conduction' electrons have well-defined Fermi-surfaces.

6. Consequently, the two electronic states are thermodynamically distinct and a transfer from one state to the other ccnstitutes a definite thermodynamic transformation. In contrast, the transformation from one conduction band to another band does not constitute a thermodynamic transformation.

7. Holes cannot substitute for electrons in forming 'covalent' bonds but 'holes' can freely substitute for electrons in 'conduction' bands.

C. Experimental Evidence in Support of the "Covalent"⇌"Conduction" Electronic Transformation

Based on the principles of the band and valence theories as well as the distinction between 'covalent' vs. 'conduction' electrons given above, experimental evidenc. now can be tested both qualitatively and quantitatively in light of the 'covalent' ⇌ 'conduction' electronic states transformation.

Qualitative Experimental Evidence

a. Since 'holes' cannot substitute for electrons in forming 'covalent' bonds, 'conduction' electrons should decrease in number in going from TiNi-III to TiNi-II, When the bond structure is a single positive band as in TiNi, a decrease in 'conduction' electrons should result in an increase in the number of 'holes' and a decrease in the Hall(positive) coefficient.

Experimentally, the positive Hall coefficient is decreased

$\Delta R_H \simeq 1.4 \times 10^{-4}$ cm^{3}C^{-1}

b. Since 'holes' contribute to the Pauli spin paramagnetic susceptibility exactly in the same manner as electrons[70] , an increase in the number of holes should produce an increase in spin paramagnetic susceptibility.

Experimentally, the magnetic susceptibility is increased

$\Delta \chi \simeq 0.9 \times 10^{-}$ emu· gm^{-1}

c. Thermodynamically, it is a phase transformation.

Experimentally, it is shown by Berman et al.[56] to be a second order transition with a heat of transition,

$\Delta H \simeq 4,150$ J·mole^{-1}

d. Due to the Fermi-surface change, the bulk modulus, the second derivative of the total energy, should change,

Experimentally, the bulk modulus is increased

$\Delta k_f \simeq 2.3 \times 10^{11}$ dynes· cm^{-2}.

e. Inasmuch as the stability of a 'covalent' bond is related to restricted interatomic distances, the acoustic damping capacity in TiNi-II is expected to be low. Conversely, in the TiNi-III phase, where 'conduction' electrons are predominant, the interatomic distances are much less rigid, a property which should produce a high acoustic damping capacity.

Experimentally, the acoustic damping capacity of TiNi-III is approximately ten times that of TiNi-II[29][60].

f. The atomic radii for atoms in the 'covalent' bonded state and in the 'metallic' bonded state are known to be considerably different.

> Experimentally, in TiNi-II, the Ti-Ni interatomic distance is close to the 'covalent' bonded distance, whereas in TiNi-III, the Ti-Ni interatomic distance, is closer to the sum of the 'metallic' radii[23].

g. By ignoring the virial theorem(inoperative or weakly operative in this case), the potential energies of 'covalent' vs. 'conduction' electrons are considered to be approximately the same. Therefore, the total energy of the system should depend largely on the kinetic energy of the electron. Quantum mechanically, the smaller the space(confinement) in which electrons are allowed to roam, the higher the kinetic energy. Thus, in going from TiNi-III to TiNi-II, absorption of energy by the system is expected.

> Experimentally, energy is absorbed in going from TiNi-III to TiNi-II and vice versa.

Quantitative Experimental Evidence

a. Heat of Transition.
As shown in Fig. 42, the anomalous heat capacity change is associated with the two irreversible paths, $M_s - M_s'$(on cooling) and $M_s' - A_s$ (on heating), and there is no difference between the DTA curves for 'complete' and 'incomplete' cycles. This implies that the major portion of the anomalous heat capacity change could not be due to a change in atomic arrangement, and therefore could not be due to phonon spectrum changes. Logically, this leaves electrons as the major cause for the anomalous heat capacity changes observed.

The fact that the TiNi-II $\rightleftharpoons$ TiNi-III transition is second order (Berman et al.[56]) made it possible to focus attention on the problem as one of order-disorder. Following Bragg and Williams[71], we shall consider a binary alloy AB, in which lattice sites occupied by A atoms are designated as α and those occupied by B atoms as β. Let the total number of atoms(also the total number of sites) be n. We shall further designate the fraction of α sites occupied by A atoms as r and the fraction of β sites occupied by B atoms as $(1 - r)$. Then, the Bragg-Williams order(long range) parameter S may be written as,

$$S = \frac{p - r}{1 - r}$$ where p is the probability that an α position is occupied by an A atom.

When order is complete, p is unity therefore, S is unity. When disorder is complete(the arrangement of replacements is random), only a fraction r of the replacements will be in the positions of order. Therefore, $p = r$ and $S = 0$. Further, a parameter V is defined as the increase in potential energy due to one replacement moving from an ordered to a disordered position. Any such replacement

spends part of its time in an α position and part in a β position. At a given moment, $(rnp)\alpha$ positions will be occupied by other replacements and so also will $rn(1-p)\beta$ positions. The replacement being considered, thus will have open to it $(rn - rnp)\alpha$ positions and $\{(1-r)n - rn(1-p)\}\beta$ positions. By Boltzmann's relation,

$$\left\{\frac{p}{1-p}\right\} = \left\{\frac{\text{Number of available } \alpha \text{ positions}}{\text{Number of available } \beta \text{ positions}}\right\}\exp(V/kT)$$

$$= \left\{\frac{r(1-p)n}{(1 - 2r + rp)n}\right\} \exp(V/kT)$$

Solving this equation for p and substituting in $S = (p-r)/(1-r)$, we find,

$$S(V,T) = 1 - \left\{\frac{\{4r(1-r)(e^x - 1) + 1\}^{1/2} - 1}{2r(1-r)(e^x - 1)}\right\}$$

where $x = V/kT$.

when $r = 1/2$, the relation simplifies to

$$S(V,T) = 1 - 2\{\exp(x/2) - 1\}/\{\exp(x) - 1\}$$
$$= \{1 - \exp(-x/2)\}/\{1 + \exp(-x/2)\}$$
$$= \tanh(x/4).$$

Now, in the dependence of V upon S and T, it is readily seen that $V(S,T) = 0$ for $S = 0$(complete disorder), $V(S,T)$ is a maximum, V_0 for $S = 1$(complete order), and V is not likely to be appreciably dependent upon temperature. Therefore, the relation is assumed to be linear.

$$V = V_0 S, \quad dV/dT = 0.$$

For $r = 1/2$(at equilibrium), the two functions reduces to

$$S_e = \tanh(V/4kT) \simeq V/4kT \text{ (when } V/4kT \text{ is small)}$$
$$V = V_0 S \text{ gives } S_e = V/V_0, \text{ hence,}$$

$4kT_c/V_0 = 1$ or $T_c = V_0/4k$ gives the degree of order S_e,

characteristic of the temperature, T_c.

Based on the reasoning derived above, the anomalous heat capacity changes during an order-disorder transition in which $r = 1/2$ is calculated in the following manner.

Let us suppose that the degree of order changes slightly from S to $S + dS$ owing to a decrease in temperature, $- dT$. The number of atoms in positions of order changes from rnp to $rn(p + dp)$. Since,

$S = (p-r)/(1-r)$, $dp = (1-r)dS$. Each atomic interchange decreases the potential energy of the whole structure by $V = V_0 S$. Hence, the evolution of energy due to increase in order is given by

$$dE = V_0 S(nr)dp = V_0 nr(1-r)SdS.$$

The evolution of energy between two states of order S_1 and S_2 is therefore

$$V_0 nr(1-r)(S_1^2 - S_2^2)/2$$

and the total amount for the change from disorder to order(i.e., S changes from 1 to 0) is

$$V_0 nr(1-r)/2.$$

For $r = 1/2$, the total energy change is

$$dE = 4kT_c n/8 = nkT_c/2,$$

function totally dependent upon the number of particles involved, namely n.

Now, the number of electrons(particles) involved in the TiNi transition has been obtained directly from the Hall coefficient change, based on the single transport band inference as described above[31].

$$R_H(A_s) = 1.8 \times 10^{-4} \ cm^3 coul^{-1} \quad vs.$$

$$R_H(M_s') = 0.4 \times 10^{-4} \ cm^3 coul^{-1}.$$

Therefore, the effective number of carriers per cubic centimeter in the two states are:(the density of TiNi alloy being 6.45 $gm \cdot cm^{-3}$)

$$n(A_s) = 1/R_H(A_s) \times 1.6 \times 10^{-19} = 1.56 \times 10^{23}(cm^{-3})$$
$$= 2.14 \ atom^{-1}$$

$$n(M_s') = 1/R_H(M_s') \times 1.6 \times 10^{-19} = 0.35 \times 10^{23}(cm^{-3})$$
$$= 0.48 \ atom^{-1}.$$

Therefore, the number of particles (electrons) involved in the transition is

$$\Delta n = n(A_s) - n(M_s') = 1.21 \times 10^{23} cm^{-3}$$
$$= 0.18 \times 10^{23} \ gm^{-1}$$
$$= 20 \times 10^{23} \ mole^{-1}$$
$$= 1.66 \quad atom^{-1}.$$

By substituting this number, Δn, in the Bragg-Williams equation, we obtain

$$\Delta E = (\Delta n)kT_c/2 = \{(20 \times 10^{23}) \times 1.38 \times 10^{-23} \times 333\}/2$$

$$= 4,595 \quad J \cdot mole^{-1} \quad \text{compared with the experimental value}[56] \text{ of}$$

$$4,150 \quad J \cdot mole^{-1}.$$

b. Bulk Modulus Changes

The validity of the change in the number of effective carriers, Δn, at the TiNi transition was further tested by Pace and Saunders[72] based on the observed change in bulk modulus. By measuring the ultrasonic attenuation(both longitudial, V_ℓ and shear V_s waves) at and around the TiNi transition temperature range, Pace and Saunders obtained the bulk modulus changes by the relationship

Bulk modulus, $K = (3\rho V_\ell^2 - 4\rho V_s^2)/3$

Poisson's ratio, $\sigma = 0.5(\rho V_\ell^2 - 2\rho V_s^2)/(\rho V_\ell^2 - \rho V_s^2)$.

These experimental results are summarized in Fig. 45 and have been used to check against the change in the number of 'hole' carriers based on the assumption:

1. The large change in the number of free carriers will be reflected in the binding forces and thus in the elastic properties.

2. The total energy of a system, of which the second derivative with respect to strains gives the elastic constants[73] , may be expressed in the Wigner-Seitz cellular method as a sum of terms which can be calculated separately. These include the Fermi energy, the energy of the lowest electronic state and the exchange and correlation terms.

3. A reasonable hypothesis is that the difference between the total energies of the two phases, TiNi-II and TiNi-III, can be attributed largely to the change of the Fermi energy.

4. The assumption is made that the s-band hole octahedra are spherical such that Fermi energy, E_f, is given by

$$E_f = (3/5)(3/\pi)^{2/3} \times (\pi^2 \hbar^2/2m)(n/\Omega)^{2/3}$$

where n is the number of free carriers per atom and r is the radius of the atomic sphere, defined so that $(4/3)\pi r^3 = \Omega$.

5. The contribution to the bulk modulus due to the Fermi energy alone is given by Jones[73] as

$$K_f = (1/9)(r^2/\Omega)(d^2E_f/dr^2).$$
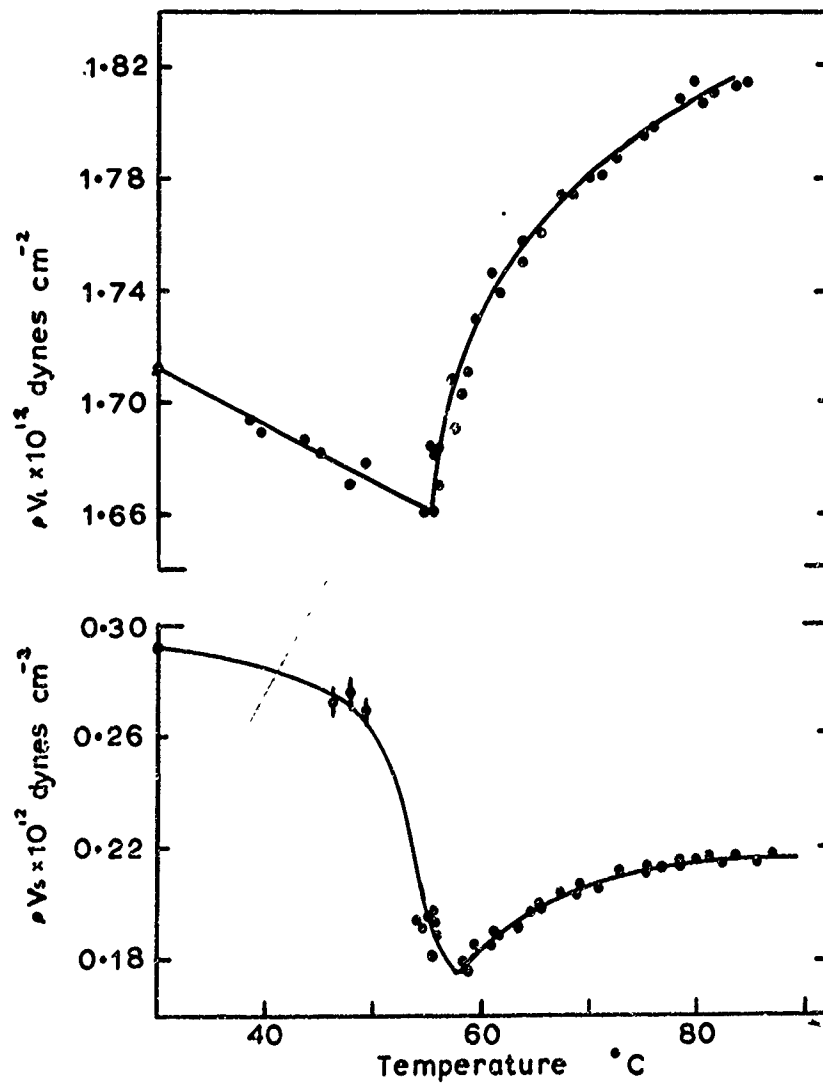
Fig. 45

(after Pace and Saunders;ref. 72)

Fig. 45; Temperature dependence of the longitudinal
and shear elastic moduli in TiNi.

Based on these assumptions and by substituting E_f and differentiating with respect to r, one obtains

$$K_f = \left(\frac{3}{20m}\pi\hbar^2\right)\left(\frac{9}{4\pi^2}\right)^{2/3}\left(\frac{n^{2/3}}{r^5}\right)$$

$$\Delta K_f = K_f(A_s) - K_f(M_s')$$

$$= \left(\frac{3\pi h^2}{20m}\right)\left(\frac{9}{4\pi^2}\right)^{2/3}\left(\frac{n(A_s)^{2/3} - n(M_s')^{2/3}}{r^5}\right)$$

With further substitution of $n(A_s) = 2.14$ and $n(M_s') = 0.48$ per atom, the bulk modulus change calculated[72] to be

$$\Delta K_f(cal.) = 3.16 \times 10^{11} \text{ dynes} \cdot cm^{-2}$$

which is in fair agreement with the experimental value,

$$\Delta K_f(exp.) = 2.3 \times 10^{11} \text{ dynes} \cdot cm^{-2}.$$

c. Pauli Spin Paramagnetic Susceptibility Change

These agreements encouraged Wang[74] to calculate the change in the Pauli spin paramagnetic susceptibility again based on the number of electrons involved in the transition, i.e., Δn. According to Pauli[62], the paramagnetic susceptibility due either to electrons or holes can be expressed as

$$\chi_{atom} = N\mu_B^2/kT_f = N\mu_B^2/E_f$$

Assuming a spherical s-hole band, as did Pace and Saunders[72], the Fermi energy is

$$E_f = (X)(Y)(Z)(n)^{2/3} = 6.12 \times 10^{-12}(n)^{2/3} \text{ erg}^2 \cdot sec^2 \cdot gm^{-1} \cdot cm^{-2}$$

$$\text{where } (X) = (3/5)(3/\pi)^{2/3} = 0.58$$

$$(Y) = (\pi^2\hbar^2/2m) = (h^2/\varepsilon m)$$

$$= 6 \times 10^{-27} \text{ erg}^2 \cdot sec^2 \cdot gm^{-1}$$

$$(Z) = (1/\Omega)^{2/3} = 17.6 \times 10^{14} \text{ cm}^{-2}.$$

Therefore, the Pauli spin paramagnetic susceptibility change is calculated as,

$$\Delta\chi_{atom}(cal.) = (\Delta n)\mu_B^2/E_f$$

$$= (\Delta n)^{1/3} \times \mu_B^2/(X)(Y)(Z)$$

$$= (1.66)^{1/3} \times (0.859 \times 10^{-40})/6.12 \times 10^{-12}$$

$$= (1.65 \times 10^{-29}) \text{ emu·atom}^- \text{ or}$$

$$= 1.8 \times 10^{-7} \text{ emu· gm}^{-1}$$

which is just about one fifth of the experimentally observed value[31]

$$\Delta\chi_{atom}(obs.) = 9.0 \times 10^{-7} \text{ emu·gm}^{-1}$$

In view of the fact that in general, the effective mass, m^*, in transition elements is much higher than the rest mass, m(as much as ten times[75]), this discrepancy can be easily reconciles by assuming a ratio, $(m^*/m) \simeq 5$. While the electronic heat capacity of TiNi itself has not been measured, the electronic heat capacities of TiFe, TiCo and TiX(where X is a combination of Fe, Co and Ni) have been measured by Starke, Cheng and Beck[76]. The electronic specific heat coefficients, thus obtained, for these compounds tend to suggest that this ratio, $(m^*/m) \simeq 5$ is reasonable for TiNi. It is of interest to note that this assumption would also reduce the bulk modulus change calculated by Pace and Saunders[72] to somewhat less than the experimental value, thus making this calculation also more reasonable.

The agreements between the calculated and observed values for those physical changes during transition; heat of transition, bulk modulus, spin paramagnetic susceptibility, are rather significant despite the number of assumptions made in their calculation. Therefore, these agreements support the original inferences by Wang et al[31], that the TiNi transition is electronic in origin, that the band structure is a single band, and that a number Δn of effective carriers undergo a thermodynamic change during the TiNi-II to TiNi-III transition.

References

1. H. Witte and H.J. Wallbaum; Ztsch. F. Metallkunde, 30, 100(1938).

2. R. Vogel and H.J. Wallbaum; Archiv F. das Eisenhuttenwessen 12, 299 (1938).

3. H.J. Wallbaum; Archiv F. das Eisenhuttenwessen, 14, 521(1941).

4. J.R. Long, E.T. Hayes, D.C. Root and C.E. Armantrout; U. S. Bur. Mines, R.I. 4463(Feb., 1949).

5. A. Taylor and R.W. Floyd; J. Inst. Metals, 80, 577(1951-52).

6. C.M. Craighead, F. Fawn and L.W. Eastwood; Battelle Memorial Inst., Second Progress Report on Contract AF 33(038)-3736 to Wright Patterson Air Force Base(1949).

7. P. Duwez and J. L. Taylor; Trans. AIME, 188, 1173(1950).

8. H. Margolin E. Ence and J.P. Nielson; Trans. AIME, 197, 243 (1953).

9. D.M. Poole and W. Hume-Rothery; J. Inst. Metals, 83, 473(1954-55).

10. D.H. Polonis and J.G. Parr; Trans. AIME, 206, 531(1956).

11. G.R. Purdy and J.G. Parr; Trans. AIME, 221, 636(1961).

12. F. Laves and H.J. Wallbaum; Naturwissen Shaften, 27, 674(1939).

13. F. Laves and H.J. Wallbaum; Ztsch. F. Kristallographie, 101, 78(1939).

14. A. Taylor and R.W. Floyd; Acta Cryst. 3, 285(1950).

15. W. Rostoker; Trans. AIME, 191, 1203(1951).

16. T.V. Phillip and P.A. Beck; Trans. AIME, 209, 1269(1957).

17. H. Stuwe and Y. Shimomura; Z. Metalk, 51, 180(1960).

18. P. Pietrokowsky and F. G. Youngkin; JAP, 31, 1763(1960).

19. W.J. Buehler and R.C. Wiley; Trans. Quart. ASM, 55, 269(1962).

20. J.V. Gilfrich; Proceedings 11th Annual Conf. on Appl. of X-ray Analysis, Denver Research Inst.(1962); Plenum Press Inc., N.Y.(1963).

21. W.J. Buehler, J.V. Gilfrich and R.C. Wiley; JAP.; 34, 1475 (1963).

22. F.E. Wang, A.M. Syeles, W.L. Clark and W.J. Buehler; JAP.; 35, 3620(1964).

23. F.E. Wang, W.J. Buehler and S.J. Pickart; JAP.; 36, 3232(1965).

24. D.P. Dautovich and G.R. Purdy; Can. Met. Quart., 4, 129(1965).

25. W. Rostoker; Trans. AIME, 194, 209(1952).

26. M.V. Nevitt; Trans. AIME, 218, 327(1960).

27. G.A. Yurko, J.W. Barton and J.G. Parr; Acta Cryst., 12, 909 (1959).

28. M.H. Mueller and H.W. Knott; Trans. AIME, 227, 674(1963).

29. R.R. Hasiguti and K. Iwasaki; J. Appl. Phys., 39, 2182(1968).

30. F. Carter; Proceeding of the Symposium on TiNi and Associated Compounds (NOLTR 68-16, U.S. Naval Ordnance Laboratory, White Oak, Maryland).

31. F.E. Wang, B.F. DeSavage, W.J. Buehler and W.R. Hosler, JAP.; 39, 2166(1968).

32. K. Chandra and G.R. Purdy; JAP.; 39, 2179(1968).

33. R. Scholl, D.J. Larson Jr. and E.J. Freise; JAP.; 39, 2179 (1968).

34. M.J. Marcinkowski, A.S. Sastri and D. Koskimaki; Phil. Mag., 18, 945(1968).

35. D. Koskimaki, M.J. Marcinkowski and A.S. Sastri; Trans. AIME, 245, 1883(1969).

36. K. Otsuka and K. Shimizu; The 62nd Annual Meet, of the Jap, Inst. Metals(1968).

37. F.E. Wang, Y.C. Cheng, K. Hu and P.H. Tsao; JAP.; 40, 1980 (1969).

38. "CONSTITUTION OF BINARY ALLOYS", edited by M. Hansen, McGraw-Hill (1958); including the 1st and 2nd supplements.

39. H.C.H. Cartenter and C.F. Elam; J. Inst. Metal; 24, 83(1920).

40. "Selected Topics in X-ray Crystallography", edited by J. Bouman, North-Holland Pub. Co. (Interscience Pub. Inc., N.Y., 1951).

41. W.G. Burgers and F.J. Lebbink; Rec. Trav. Chim., Pays-Bas, 64, 321(1945).

42. L.D. Landau and E.M. Lifshitz; "STATISTICAL PHYSICS", Pergamon Press Ltd., (Addison-Wesley Pub. Co. Inc., Mass., 1958).

43. H. Lipson and C.A. Taylor, "FOURIER TRANSFORMS AND X-RAY DIFFRACTION", G. Bell and Sons Ltd., London (1958).

44. F.S. Bowles and C.S. Barrett, Progress in Metal Physics (Pergamon Press, Inc., New York, 1952), Vol. 3; L. Kaufman and M. Cohen, ibid., Vol. 7; B. Chalmers, Physical Metallurgy (John Wiley & Sons, Inc., New York, 1959); B.A. Bilby and J.W. Christian, "The Mechanism of Phase Transformations in Metals," Institute of Monograph and Report Series, No. 18, p. 121(1955).

45. W.J. Buehler and F.E. Wang, Private Communication.

46. M.J. Buerger, Proc, Nat. Acad. Sci. U.S., 42, 776(1956).

47. F.E. Wang, "MECHANICAL-TWINNING BASED ON THE B2(CsCl)- type STRUCTURE", J.Appl. Phys. 43, 92(1972.

48. E. Schmid and W. Boas, "PLASTICITY OF CRYSTALS", London; Hughes (1950).

49. E.O. Hall, "TWINNING AND DIFFUSIONLESS TRANSFORMATION IN METALS", London; Butterworths(1954).

50.. M.A. Jaswon and D.B. Dove, Acta Cryst., 10, 14 (1957).

51. F.E. Wang, S.J. Pickart and H.A. Alperin, "Mechanism of the TiNi Transition and the Crystal Structure of TiNi-II and TiNi-III Phases", J.Appl.Phys. 43, 97(1972).

52. R.G. deLange and J.A. Zijderveld, JAP.; 39, 2195(1968).

53. W.B. Cross, A.H. Kariotis and F.J. Stimler, NASA Contract Report, Cr-1433 (September 1969), Goodyear Aerospace Corporation, Akron, Ohio.

54. R.J. Wasilewski, S.R. Butler and J.E. Hanlon, Metal Science Journal 1, 104 (1967).

55. D.P. Dautovich, Z. Melkvi, G.R. Purdy and C.V. Stager, JAP.; 37, 2512(1966).

56. H.A. Berman, E.D. West and A.G. Rozner, JAP.; 38, 4473(1967).

57. P. Curie, Ann. Chim. Phys. 5, 289(1895).

58. METHOD OF EXPERIMENTAL PHYSICS, L. Marton, Ed. (Academic Press Inc. New York, 1959).

59. B.F. DeSavage and J.F. Goff, JAP.; 38, 1337(1967).

60. D. Bradley, J. Acous. Soc. Am. 37, 700(1965).

61. W.B. Cross, A.H. Kariotis and F.J. Stimler, NASA Contract Report, CR-1433(September 1969), Goodyear Aerospace Corporation, Akron, Ohio.

62. W. Pauli, Z. Physik 41, 81 (1927).

63. W.P. Mason, "Physical Acoustics and the Properties of Solids" (Van Nostrand Co., Inc., Princeton, New Jersey, 1968).

64. J.M. Ziman, "Electrons and Phonons"(The Clarendon Press, Oxford, (1963) and "Principle of the Theory of Solids"(Cambridge University Press, Cambridge, England, 1964); C. Kittel, "Introduction to Solid State Physics"(John Wiley and Sons Inc., New York, 1968); H.M. Rosenberg, "Low Temperature Physics"(Clarendon Press, Oxford, England, 1965).

65. J.F. Goff, JAP.; 35, 2919(1964).

66. F.S. Bowles and C.S. Barrett, "Progress in Metal Physics" (Pergamon Press, Inc., New York, 1952), Vol. 3; L. Kaufman and M. Cohen, ibid, Vol. 7; B. Chalmers, "Physical Metallurgy" (John Wiley and Sons, Inc., New York, 1959); B.A. Bilby and J.W. Christian, "The Mechansim of Phase Transformations in Metals" (Institute of Monograph and Report Series, No. 8, p. 121(1955).

67. L. Guttman, J. Metals, Trans. AIME, 188, 1472(1950).

68. K. Otsuka and K. Shimizu, Act. Met. 4, 469(1970).

69. L.C. Chang and T.A. Read, Trans. AIME, 189, 47(1951).

70. A.H. Morrish, "The Physical Principle of Magnetism" (John Wiley and Sons, Inc., New York, 1965).

71. W.L. Bragg and E.J. Williams, Proc. Roy. Soc., A145, 668(1934); ibid, A151, 540(1935).

72. N.G. Pace and G.A. Saunders, Phil. Mag. 22, 73(1970).

73. H. Jones, Physica, 15, 13(1949); Phil. Mag., 43, 105(1952).

74. F.E. Wang, (1971); to be published.

75. C. Kittel, "Solid State Physics"(John Wiley and Sons, Inc., New York, 1956).

76. E.A. Starke Jr., C.H. Cheng and P.A. Beck, Phys. Rev. 126, 1746(1962).